THE PHYSICAL CONSEQUENCES OF GRAINS IN THE ATMOSPHERES OF LATE TYPE IRREGULAR AND SEMI-REGULAR GIANTS AND SUPERGIANTS

by

Mark Crandall Jennings

A Dissertation Submitted to the Faculty of the

DEPARTMENT OF ASTRONOMY

In Partial Fulfillment of the Requirements
For the Degree of

DOCTOR OF PHILOSOPHY

In the Graduate College

THE UNIVERSITY OF ARIZONA

1972

THE UNIVERSITY OF ARIZONA

GRADUATE COLLEGE

I hereby recommend that this dissertation prepared under my direction by Mark Crandall Jennings

entitled THE PHYSICAL CONSEQUENCES OF GRAINS IN THE ATMOSPHERES OF LATE TYPE IRREGULAR AND SEMI-REGULAR GIANTS AND SUPERGIANTS

be accepted as fulfilling the dissertation requirement of the degree of Doctor of Philosophy

Ray J. Weymann — Dissertation Director — Dec 18, 1971 — Date

After inspection of the final copy of the dissertation, the following members of the Final Examination Committee concur in its approval and recommend its acceptance:*

H. M. Dyck	16 Dec 1971
R E Williams	17 Dec 1971
Rodger I. Thompson	17 Dec 1971
W. F. Cooke	20 Dec 1971
Ray J. Weymann	18 Dec. 1971
P A Strittmatter	21 Jan 1972

*This approval and acceptance is contingent on the candidate's adequate performance and defense of this dissertation at the final oral examination. The inclusion of this sheet bound into the library copy of the dissertation is evidence of satisfactory performance at the final examination.

STATEMENT BY AUTHOR

This dissertation has been submitted in partial fulfillment of requirements for an advanced degree at The University of Arizona and is deposited in the University Library to be made available to borrowers under rules of the Library.

Brief quotations from this dissertation are allowable without special permission, provided that accurate acknowledgment of source is made. Requests for permission for extended quotation from or reproduction of this manuscript in whole or in part may be granted by the head of the major department or the Dean of the Graduate College when in his judgment the proposed use of the material is in the interests of scholarship. In all other instances, however, permission must be obtained from the author.

SIGNED: Mark Crandall Jennings

DEDICATION

To my parents

ACKNOWLEDGMENTS

The author wishes to thank Dr. Ray J. Weymann for his guidance, help and encouragement as director of this dissertation. Drs. H. Melvin Dyck and Robert E. Williams have given generously of their time and advice and this is gratefully acknowledged. The author is also indebted to the following people for discussions concerning various facets of this work: Drs. E. R. Capriotti, W. J. Cocke, J. Fix, A. Skumanich, R. N. Thomas, R. I. Thompson, and Mr. S. Shawl. Mr. D. F. Carbon and Mr. D. Y. Gezari have both kindly made results of their work available prior to publication.

TABLE OF CONTENTS

TABLE OF CONTENTS--Continued

LIST OF ILLUSTRATIONS

LIST OF ILLUSTRATIONS--Continued

LIST OF TABLES

ABSTRACT

The suggestion of an anti-correlation between Ca II H and K emission and observational indicators of grain material has been investigated and seems confirmed. The H and K reversals and other heavy element emission lines, especially those of ionized species, tend to vanish in stars which exhibit intrinsic polarization and infrared excesses. The high incidence of Balmer emission among polarized stars is discussed, but it is not found to be a necessary condition for polarization as has been previously suggested. It is argued that the disappearance of emission lines implies a weakening of the chromosphere usually associated with late stars and that grains are the primary agents responsible for the perturbation, either directly through cooling or by altering the density and temperature structure of the atmosphere by means of their dynamical effect.

The changes necessary to quench emission in a chromosphere are explored and it is found that a lessening of the overall temperature will suffice. The equations governing the thermodynamics of grain particles immersed in a cold plasma are derived under conditions appropriate to a stellar chromosphere. From these it is shown that a grain's internal temperature depends entirely on the local radiation temperature and that the gas cools if the grain density is sufficiently

high. The time required for cooling is found to be of the order of the time needed for the average gas particle to collide with a grain.

The hydrodynamic equations governing a two component flow are derived. The sonic point condition is obtained and shown to play an important role in determining the allowed mass loss rate. Grain driven flows are found to reproduce the observed mass loss rates, circumstellar line profiles, and infrared excesses of giants and supergiants under a set of plausible assumption and choice of parameters. The grain field is shown to be optically thick to scattering at all visible and near infrared wavelengths and the observational consequences of this are discussed. The combined results of the thermodynamic and hydrodynamic calculation are used to argue in favor of a grain perturbed chromosphere. Possibilities for future work are discussed.

CHAPTER 1

INTRODUCTION

The current realization that many late type irregular and semi-regular giants and supergiants may be surrounded by grain material of their own manufacture has followed from three lines of argument: that they are intrinsically polarized, that they exhibit infrared radiation in excess of that expected from a black body of the appropriate temperature, and that theoretical calculations indicate that solid particles may form and persist in the atmospheres of cool stars.

The first evidence of intrinsic stellar polarization was given by Grigoryan (1958, 1959a, b) who found a time variation in the mean polarization of μ Cep. Since polarization arising in the interstellar medium would not be expected to vary on a short time scale, Grigoryan correctly interpreted his observations as indicating that at least part of the observed polarization arose from the star. These observations and their interpretation were generally discounted, however, due to the low precision of the equipment. Evidence for intrinsic polarization continued to accumulate through the work of Serkowski (1965), Shakhovskoi (1963), Vardanyan (1960), and others, until in 1966

Serkowski was able to demonstrate unequivocally the existence of intrinsic polarization by observing stars at high latitudes in three colors (UBV). He found that a number of stars exhibited mean polarization many times greater than could be explained by an interstellar component, and further showed that in many cases the polarization in the ultraviolet was larger than in the yellow or blue, a phenomenon never observed for interstellar polarization. While a number of possible polarizing mechanisms have been suggested e.g., synchrotron radiation, or Rayleigh scattering by molecules. Dyck and Jennings (1971a) have shown that scattering by solid particles (Kruszewski, Gehrels, and Serkowski 1968) will explain the observed wavelength dependence of polarization for a number of stars and that for these stars Rayleigh scattering does not appear to be an acceptable alternative.

Although they were not realized as such at the time, the initial detections of infrared excesses in late stars were made by Wildey and Murray (1964) and Low and Johnson (1964) who noted deviations from black body behavior for a number of objects. In 1968 Gillett, Low, and Stein succeeded in obtaining infrared spectral scans of late stars and found a peak at approximately 10μ in some cases. However, uncertainties in the relative calibration of various spectral regions prevented their deciding whether the peak was an emission feature or resulted from an absorption feature shortward of 10μ. A subsequent

recalibration by Woolf and Ney (1969) demonstrated that the peaks were indeed emission features and that in some cases they exceeded the expected black body radiation by severalfold. These authors went on to argue that on the basis of the shape and position of the peak it could not be explained by chromospheric, molecular, or cold black body emission, but that it could be interpreted as band emission from a circumstellar distribution of mineral grains (Gaustad 1963).

The original detailed investigation into the feasibility of the production of solids in the atmospheres of stars was carried out by Hoyle and Wickramashinge (1962) who studied graphite formation in carbon stars and concluded that it was indeed possible. More recently Fix (1970) and Gilman (1969) have considered static grain creation in oxygen rich stars and have found that minerals of the type advocated by Woolf and Ney (1969) are saturated relative to their constituents. Fix (1971) has made a preliminary examination of the formation process in the dynamic case, i.e., within a moving convective cell, and concludes that grains form, and are of a size indicating subsequent expulsion from the star by radiation pressure.

In view of the body of evidence favoring the presence of grains in or about many late type stars the author undertook to study the expected consequences of such a state and the results of that study are presented in the following discussion.

CHAPTER 2

THE BEHAVIOR OF Ca II H AND K AND OTHER EMISSION LINES IN THE PRESENCE OF GRAINS

In 1969 Dyck and Johnson, in an attempt to reconcile the low temperatures needed for the production of polarization agents in late type stars with the well-known and ubiquitous Ca II H and K emission (Joy and Wilson 1949, Wilson and Bappu 1957 hereafter referred to as WB), which is taken to be indicative of high temperatures (Jefferies and Thomas 1959, Athay and Skumanich 1968), reexamined the existing polarimetric and spectroscopic data of a number of irregular and semi-regular variables. Basing their discussion on ten objects, they reported a correlation between the strength of the K reversal and the mean amplitude of the intrinsic polarization variation in the sense that those stars which had larger variations tended to show weaker reversals. Their conclusions were construed as tentative, however, due to the small statistics and the heterogeneous nature of the polarization data as regards observers and types of equipment used.

In view of the possible importance of such a correlation the author decided to undertake a detailed investigation of intrinsic polarization, H and K emission and to a lesser extent emission lines

in general. Dr. Dyck has provided much additional polarization data while the author has obtained the spectroscopy. The details of the polarimetric study have been presented elsewhere (Dyck and Jennings 1971a, hereafter DJ, and Dyck, Sandford, and Jennings 1971) and will not be discussed here.

Observations and Reductions

The H and K Lines

The first problem was the choice of a proper sample of stars. Desiring to examine a homogeneous yet representative group, Dyck and Jennings adopted the following selection criteria:

1. The stars are of the semi-regular and irregular type with Miras being specifically excluded. The latter condition arose from the fact that a preliminary investigation of Miras indicated that they did not satisfy the Dyck-Johnson relation.
2. Binaries of period less than 100 days have been excluded since it has been shown (Gratton 1950, Hossack 1954, Bidelman 1964, Abt, Dukes, and Weaver 1969, Jennings and Abt 1970) that these stars exhibit anomalous H and K emission strengths.
3. Carbon stars are excluded due to a lack of spectroscopic data in the ultraviolet. Further, the weak flux of the

stars in the region of λ3900 would have necessitated prohibitive exposure times with a moderate size telescope.

4. Stars earlier than the arbitrarily set limit of K0 are excluded since WB have demonstrated an intrinsic weakness of the calcium reversal among early types. This phenomenon may be understood, quite independently of any polarization considerations, by invoking the following points. First, the continuous flux at λ3900, with which the reversal must compete for detection, increases exponentially with temperature. Secondly, the availability of acoustical energy to excite a chromosphere declines with increasing surface temperature. This results from the fact that the energy generated per square centimeter per second by turbulence depends on the fifth power of the Mach number, (V_{turb}/V_s), (Biermann and Lüst 1960) and while the turbulent velocity remains approximately constant among late type stars (Kippenhahn and Temesváry 1958) the sound velocity increases as one considers earlier spectral types. Finally, among the giants earlier than K0 no theory exists for the formation of grains in or immediately above the photosphere.

5. The luminosity class of all stars lies in the range of III to I on the MK System. Dwarfs are excluded since Zappala (1969) failed to find polarization for dwarfs as late as M4. Theoretical justification for this criterion will be given later (see Chapter 4).
6. Stars on the list of high velocity objects (Roman 1955) or those with motion components satisfying the usual high velocity criteria (Roman 1965) are absented in an attempt to restrict the sample to Population I.

Bidelman's (1954) list of hydrogen emission objects served as an important source of candidate stars since it had been previously demonstrated (Serkowski 1969a, b) and later confirmed (Jennings and Dyck 1971b, and DJ) that stars which have displayed or are displaying hydrogen emission tender an unwonted percentage with intrinsic polarization. The selection process yielded 32 stars satisfying the preceeding criteria. It should be noted that two stars α UMa and RW Cep, while not part of the spectroscopic program, will be included in the data presentation and subsequent discussion: RW Cep on the basis of its literature and α UMa employing a coudé spectrum obtained by Helmut Abt.

All observations were made with the Cassegrain spectrograph on the Kitt Peak National Observatory (KPNO) No. -1 36-inch telescope. Gratings of 1200 mm^{-1} and 831 mm^{-1} were used in the first

and second orders respectively, yielding dispersions of 88, 44, and 66 $\mathring{A}$-mm^{-1}. The various dispersions were used to control exposure times and do not reflect any difference in intensity information content among the spectra. Indeed, Jennings and Dyck (1971a, hereafter JD) have demonstrated the detectability of WB intensity class 2 at all three dispersions.

Exposure progress was monitored with a photoelectric meter used in conjunction with an 85 $\mathring{A}$ wide filter centered on λ3960. This system ensured density uniformity in the H and K region from plate to plate and thereby significantly reduced the possibility of errors due to poorly exposed plates. All spectra were exposed to five times "normal" density on unbaked IIa-O emulsion and were developed in D-76 for an amount of time consistent with the ambient temperature.

No calibration plates were obtained as a part of this program. However, five plates covering the range of densities in question and a coincident period in time, but taken by other observers, were requisitioned. The question of the applicability of alien calibrations has been considered previously (Jennings 1969) with affirmative results. A calibration plate consists of 13 spots of equal area graduated in the normalized intensity they receive from one to 147.3. All calibrations were filtered for the region around λ4000, exposed on unbaked IIa-O emulsion, and developed in D-76.

The first step in the reduction procedure was the tracing of the calibration plates and subject spectra. All tracing was performed on the KPNO Joyce-Loeble microphotometer at a magnification of 200:1 for the spectra and 2:1 for the calibration plates. A wedge range of 2.4 decades was used in all cases.

The calibration plates were traced in the line of the spots with the intention of using an interpolation between the fog on either side of a spot as the measuring datum. Each calibration plate was traced twice; both as a check on internal consistency and to reduce possible accidental errors. A representative calibration tracing with datum and intensity lines drawn in may be seen in Figure 2-1.

The spot heights were measured to an accuracy of 0.1cm with a hand scale and results of this may be seen in Table 2-1. Column one lists the KPNO plate number and a code (i or ii) to identify the tracing as the first or second. The next thirteen columns present the density readings in order from darkest to lightest. Immediately below the data for a given plate the relative energy each spot received, referred to a datum of six minutes exposure through a 7.3 magnitude neutral density filter, is given in its respective column.

A graphical presentation of the data in Table 2-1 may be found in Figure 2-2 where one sees the excellent agreement among the plates. The curve appearing on the graph was drawn empirically and represents the adopted density to intensity transformation relation.

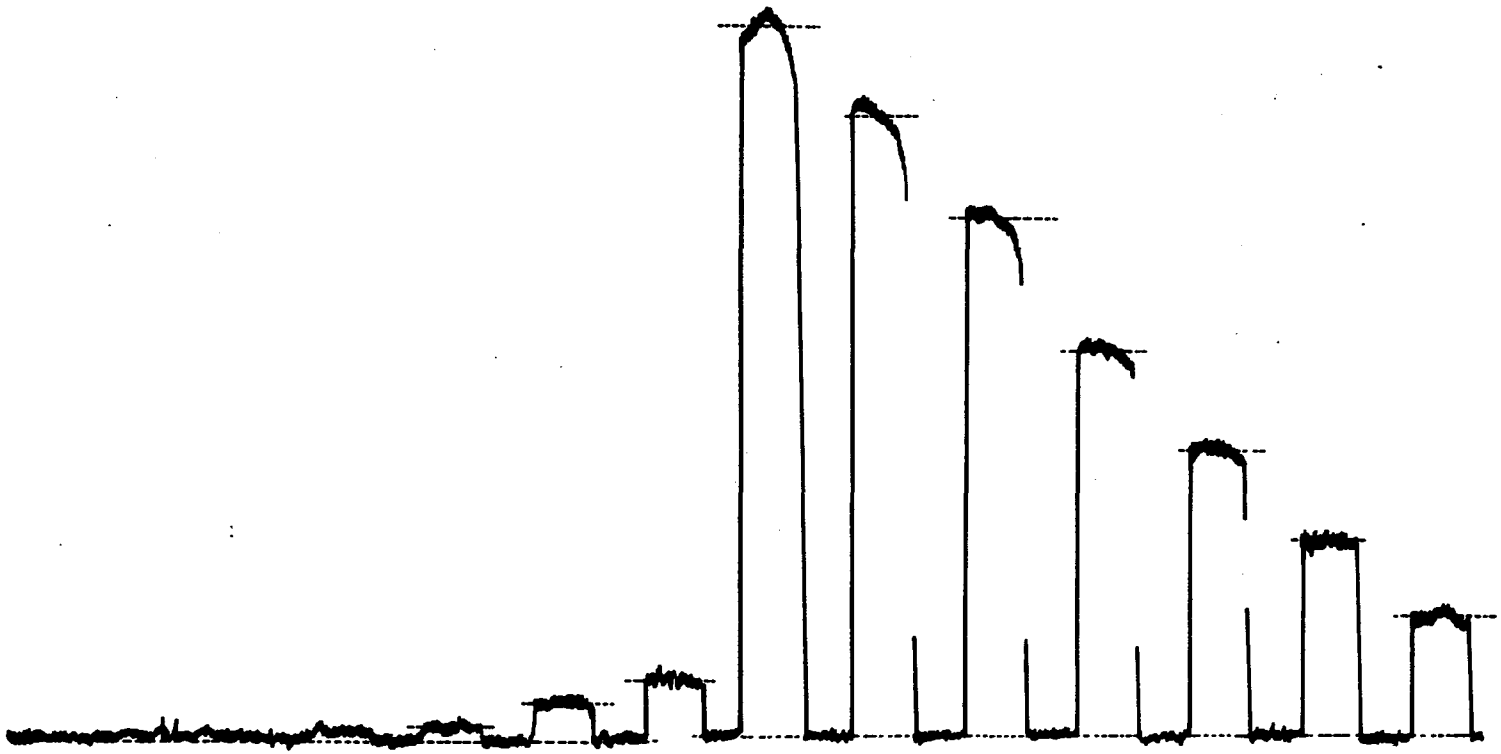

Fig. 2-1. Representative Calibration Tracing.

TABLE 2-1. Calibration Plate Spot Heights and Relative Intensities.

Plate \ spot number		1	2	3	4	5	6	7	8	9	10	11	12	13
C-631-2	i	15.2	13.9	11.8	9.6	7.9	5.8	3.9	2.2	1.3	0.7	0.5	0.2	*
	ii	15.2	13.9	11.8	9.6	7.8	5.7	3.9	2.3	1.3	0.7	0.5	0.2	0.1
Inorm		280	204	142	88	58	39	28	16.4	11.8	6.2	5.5	3.1	1.9
D-1284	i	11.9	10.4	8.5	6.4	4.6	3.0	1.9	.9	0.6	0.2	*	*	*
	ii	11.9	10.4	8.5	6.4	4.6	3.1	2.0	.9	0.6	0.2	0.1	*	*
Inorm		147.3	107.8	74.9	46.7	30.5	20.3	14.9	8.6	6.3	3.6	2.9	-	-
D-1403	i	11.9	10.3	8.6	6.5	4.9	3.5	2.3	1.2	0.7	0.2	0.1	*	*
	ii	11.9	10.2	8.7	6.6	4.9	3.5	2.3	1.2	0.7	0.2	0.1	*	*
Inorm		147.3	107.8	74.9	46.7	30.5	20.3	14.9	8.6	6.3	3.6	2.9	-	-
D-1410-11	i	12.0	10.5	8.7	6.5	4.7	3.4	2.1	1.0	0.6	0.2	0.1	*	*
	ii	12.0	10.7	8.6	6.4	4.8	3.3	2.0	1.0	0.7	0.3	0.1	*	*
Inorm		147.3	107.8	74.9	46.7	30.5	20.3	14.9	8.6	6.3	3.6	2.9	-	-
A-1696	i	+	+	+	+	+	+	18.5	14.1	11.9	9.9	8.5	5.6	3.6
	ii	+	+	+	+	+	+	18.5	14.0	11.9	9.9	8.4	5.6	3.6
Inorm		-	-	-	-	-	-	390	224	164	93	75	43	26

NOTE:

* Spot to faint to measure

\+ Spot density exceeded full scale

Fig. 2-2. Calibration Spot Height versus Relative Intensity.

Plate		Symbol
C 631	i and ii	v
D-1284	i	Δ
	ii	▲
D-1403	i	O
	ii	θ
D-1410-11	i	+
	ii	*
A-1696	i and ii	^

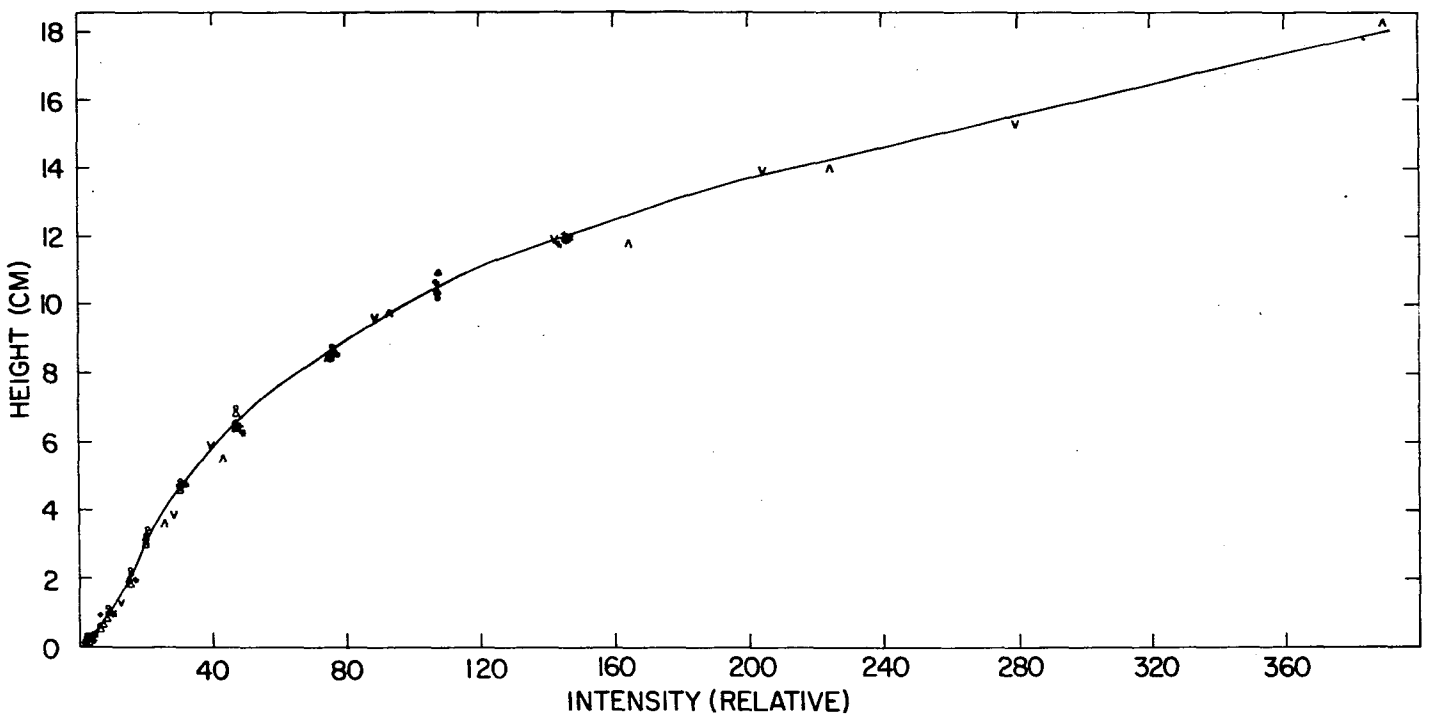

Fig. 2-2. Calibration Spot Height versus Relative Intensity.

The spectra were reduced by first tracing a strip immediately off the spectrum to record the ambient density, which would serve as the measuring datum, and then tracing the spectrum in the subject region. Figures 2-2 through 2-11 exhibit reproductions of the K region of all program stars. The H line was not considered quantitatively for two reasons: the superiority of the K line in oscillator strength ($gf_K = 1.4$ while $gf_H = 0.7$), and the possibility of befoulment by H_ε. Figures 2-3 and 2-4 (group A), will be seen to be high polarization objects while Figures 2-5 through 2-11 (group B), will have small or no polarization.

For the purposes of this program a meaningful measure of emission intensity may be defined as the ratio of the height of the K reversal above the base of the line to the height of the continuum at the position of the reversal maximum. The author feels that a more complex measure of emission strength, e.g., equivalent width, is unwarranted since WB have demonstrated the unique dependence of reversal width on luminosity and that for a given MK class a broad range of peak intensities may be expected. Since the reversal obscures the base of the atmospheric K line an effective base has been arbitrarily defined as the average of the height determined by the intersection of a linear extension of the wings and the average height of the minima bracketing the reversal. In the few cases where the extended wings failed to meet above the ambient density the latter was

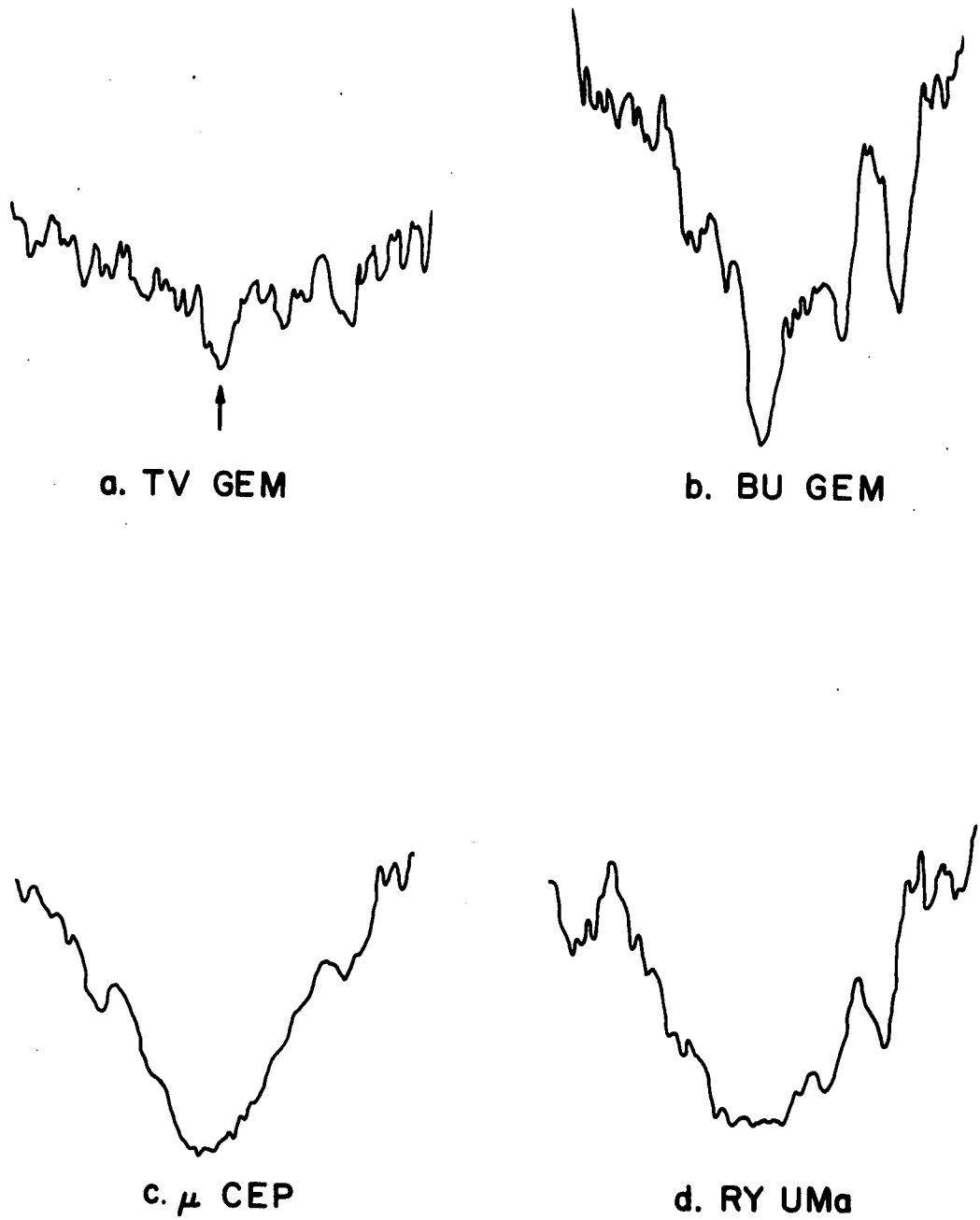

Fig. 2-3. K Line Density Tracing of TV Gem, BU Gem, μ Cep, and RY UMa.

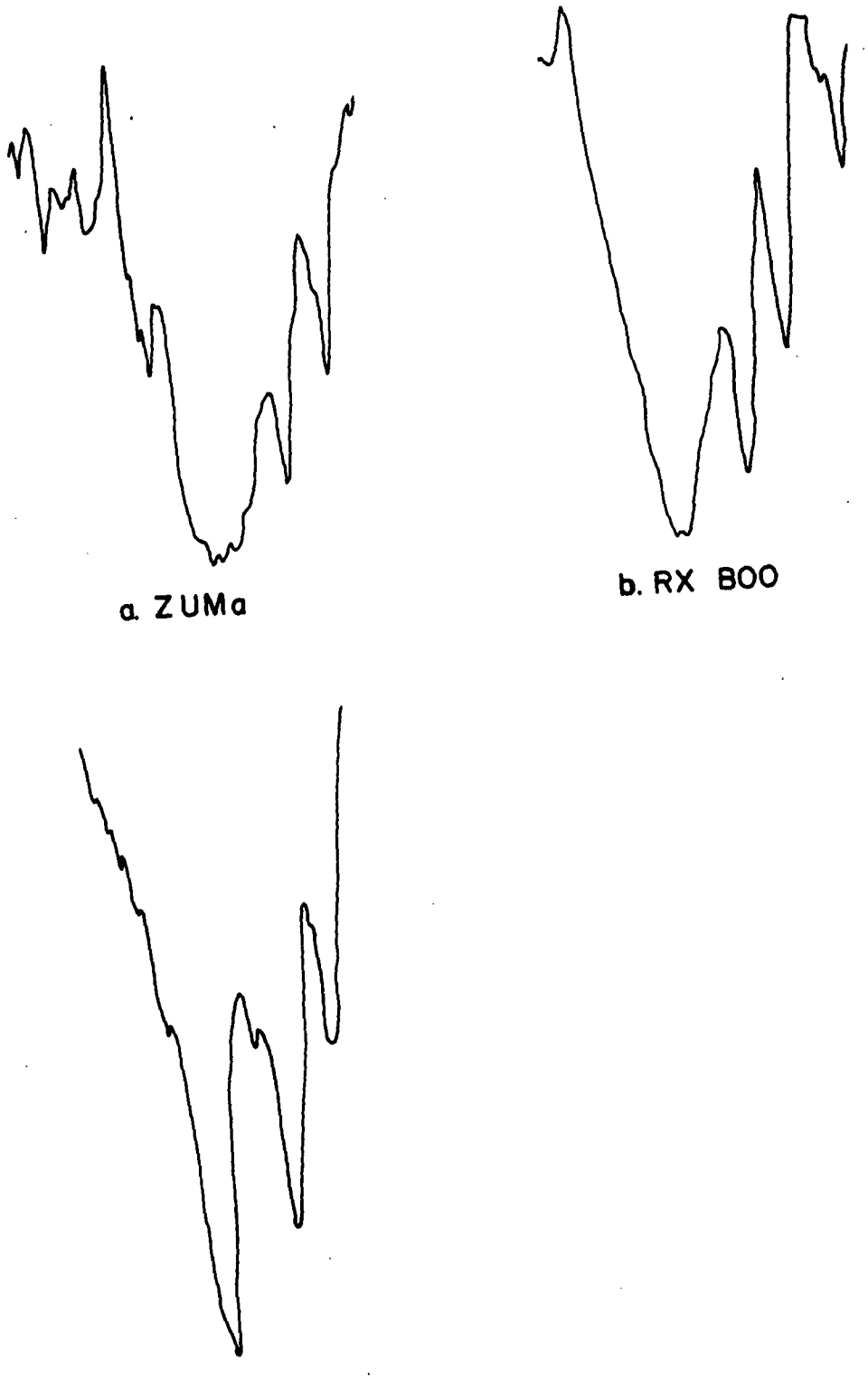

Fig. 2-4. K Line Density Tracing of Z UMa, RX Boo, and τ^4 Ser.

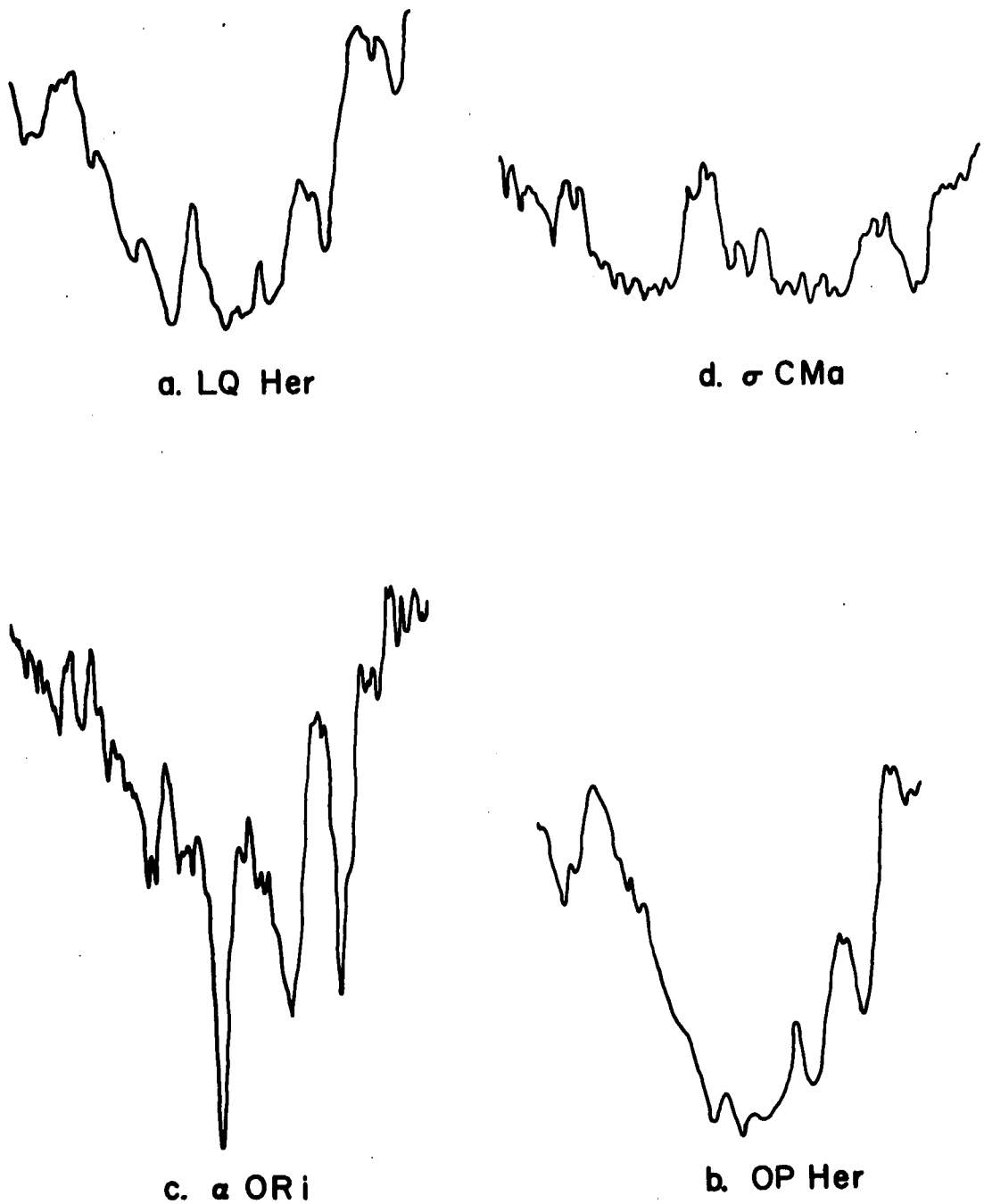

Fig. 2-5. K Line Density Tracing of LQ Her, σ CMa, α Ori, and OP Her.

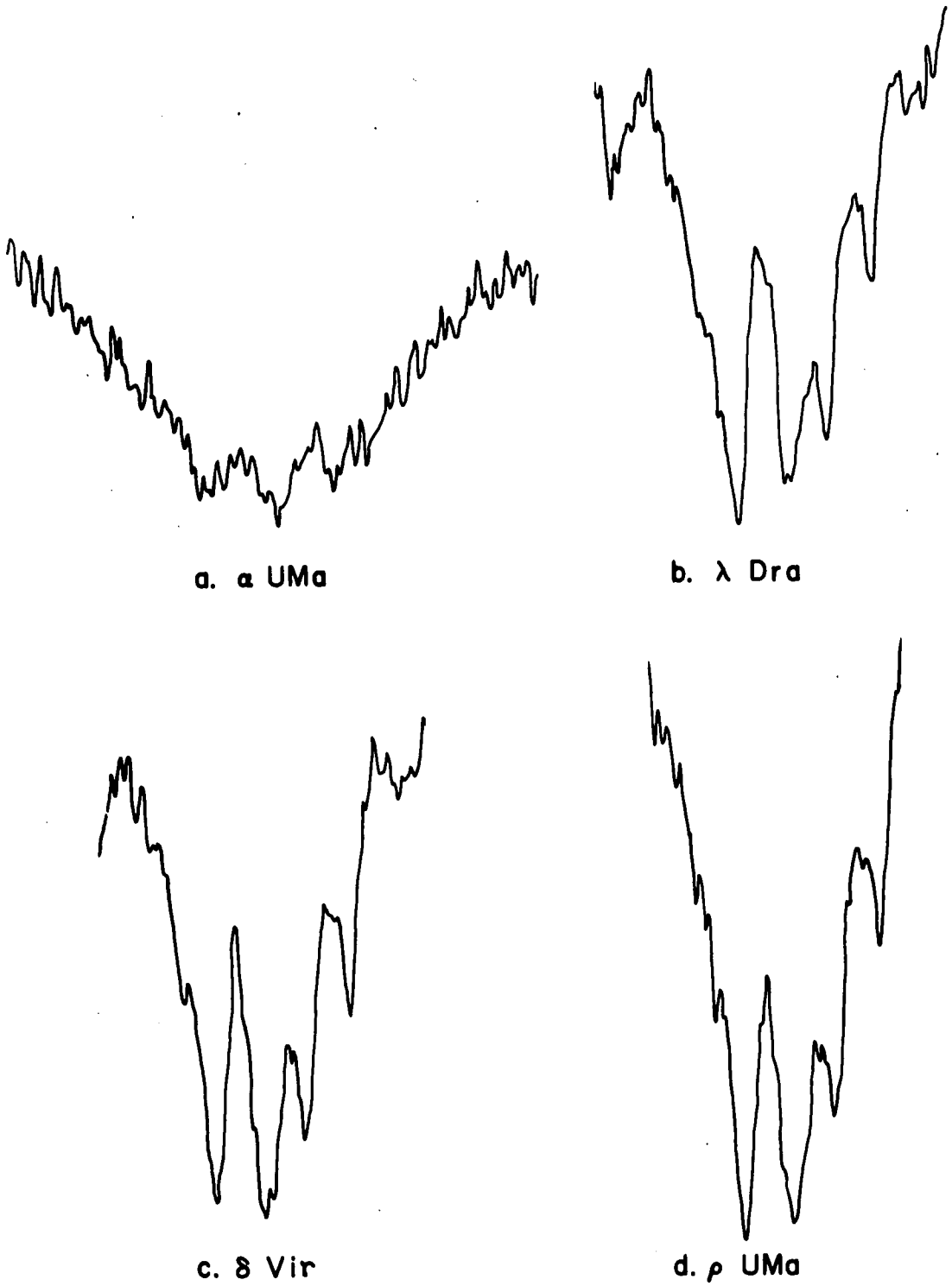

Fig. 2-6. K Line Density Tracing of α UMa, λDra, δ Vir, and ρUMa.

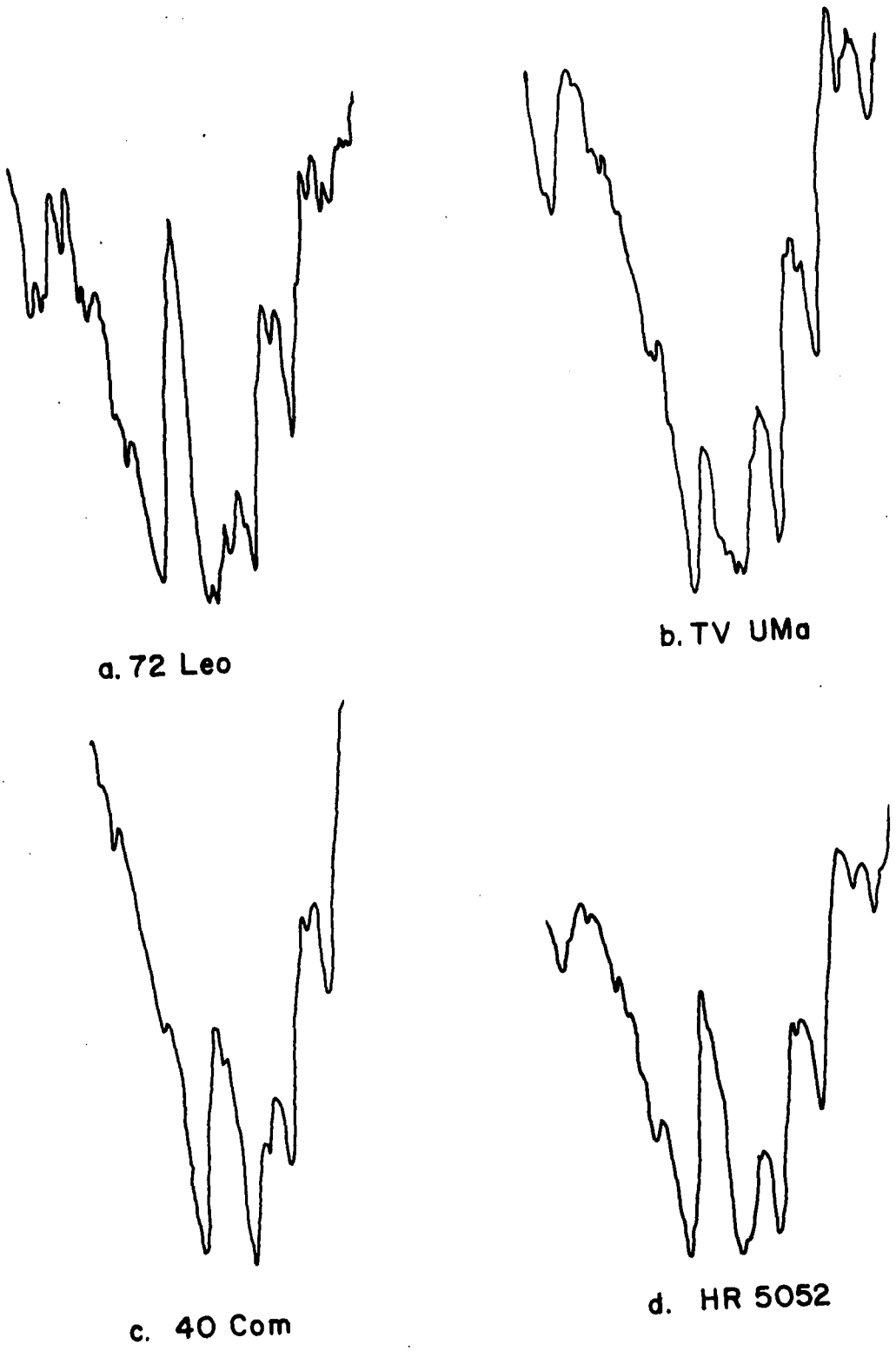

Fig. 2-7. K Line Density Tracing of 72 Leo, TV UMa, 40 Com, and HR 5052.

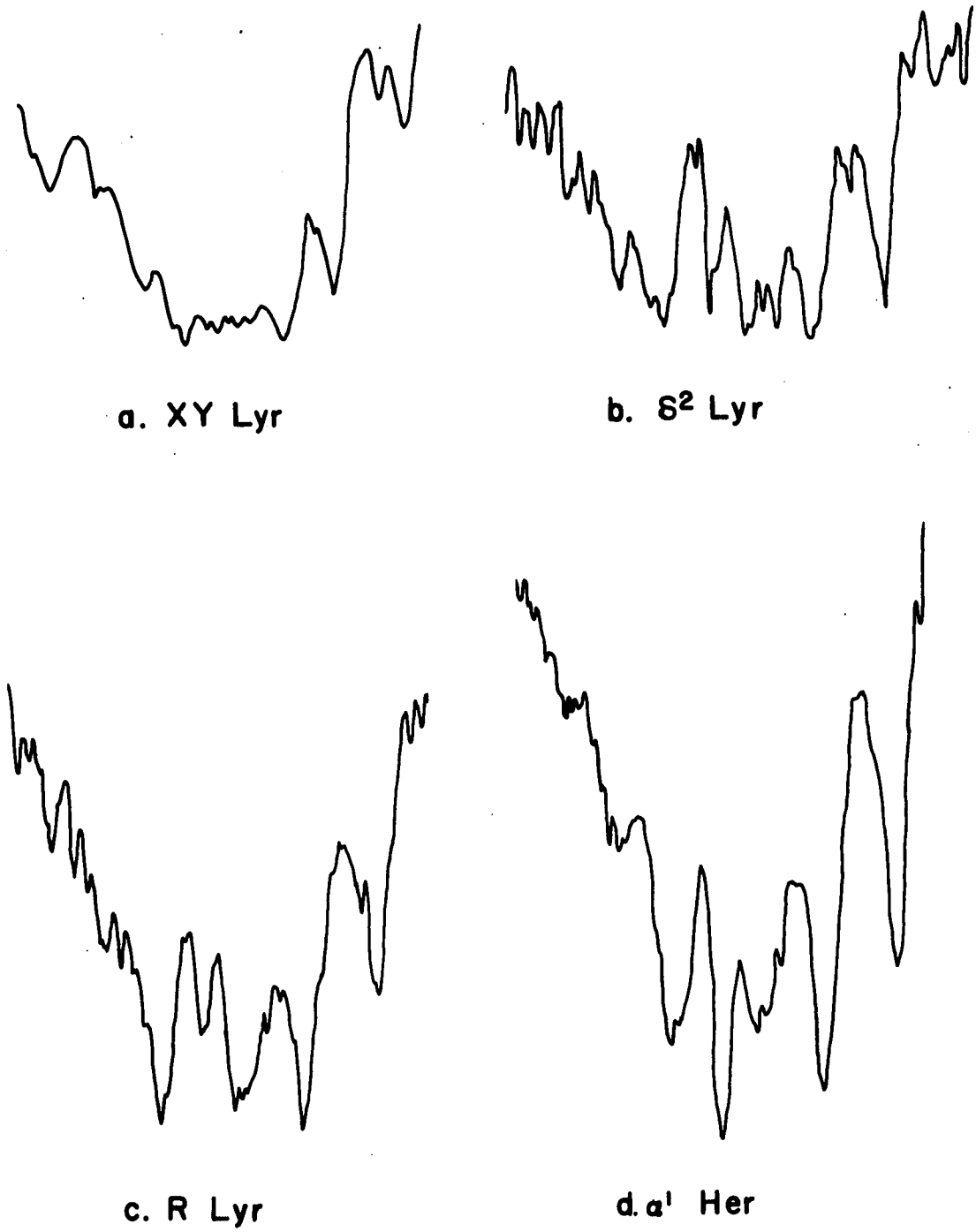

Fig. 2-8. K Line Density Tracing of XY Lyr, δ^2 Lyr, R Lyr, and α^1 Her.

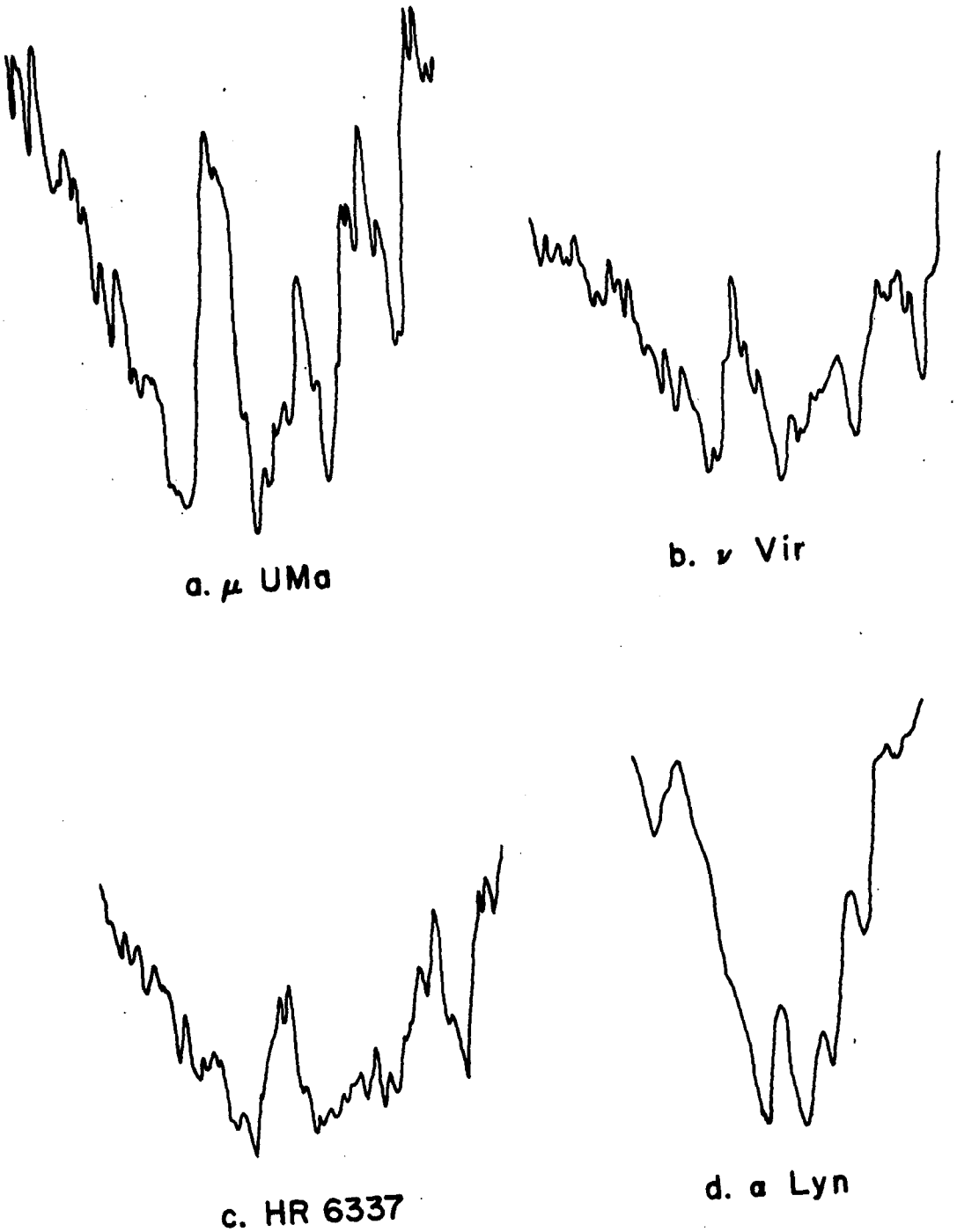

Fig. 2-9. K Line Density Tracing of μ UMa, ν Vir, HR 6337, and α Lyn.

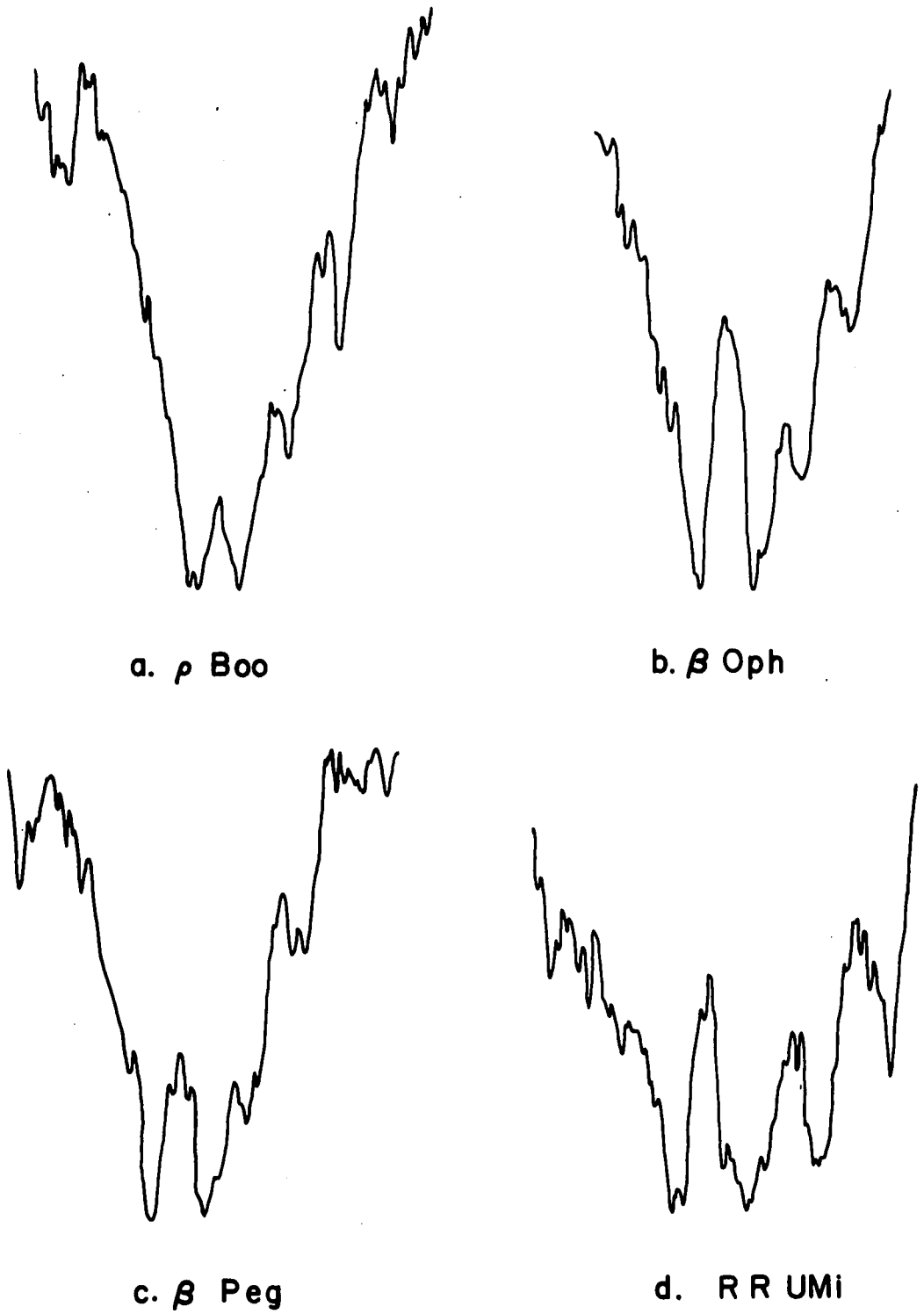

Fig. 2-10. K Line Density Tracing of ρBoo, βOph, β Peg, and RR UMi.

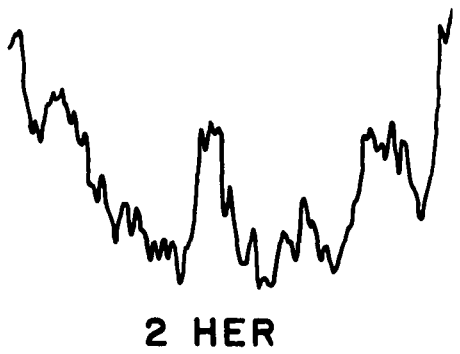

Fig. 2-11. K Line Density Tracing of 2 Her.

adopted as the intersection value. Figure 2-12 presents a schematic reversed K line with the measurements needed to evaluate the intensity ratio indicated.

All quantities were measured by hand to an accuracy of 0.1cm. The results of measuring and the subsequent reductions may be seen in Table 2-2. The first three columns contain the star name, the KPNO plate number and the dispersion in $\overset{*}{A}$-mm^{-1} respectively. Columns 4 through 7 display the quantities defined in Figure 2-12 in density units, while columns 8 through 11 present these quantities upon transformation to intensity units. The height of the defined line base (i.e. (a+b)/2) occupies column twelve, while columns thirteen and fourteen contain the height of the reversal and ratio of the reversal to the continuum. The final column presents the reversal-continuum ratio corrected for the effect of the instrumental profile, assuming the profile to be Gaussian. One performs this correction by noting that the amplitude (B) of a Gaussian which results from the convolution of an initial Gaussian of amplitude (A) and dispersion σ_1, with a perturbing Gaussian of dispersion σ_2 is given by:

$$(1) \qquad B = A\sigma_1/(\sigma_1^2 + \sigma_2^2)^{\frac{1}{2}}$$

this may be rewritten as

$$(2) \qquad B = AW_1/(W_1^2 + W_2^2)^{\frac{1}{2}}$$

where the W's are related to the σ's via $W_i = k\sigma_i$ where k equals a

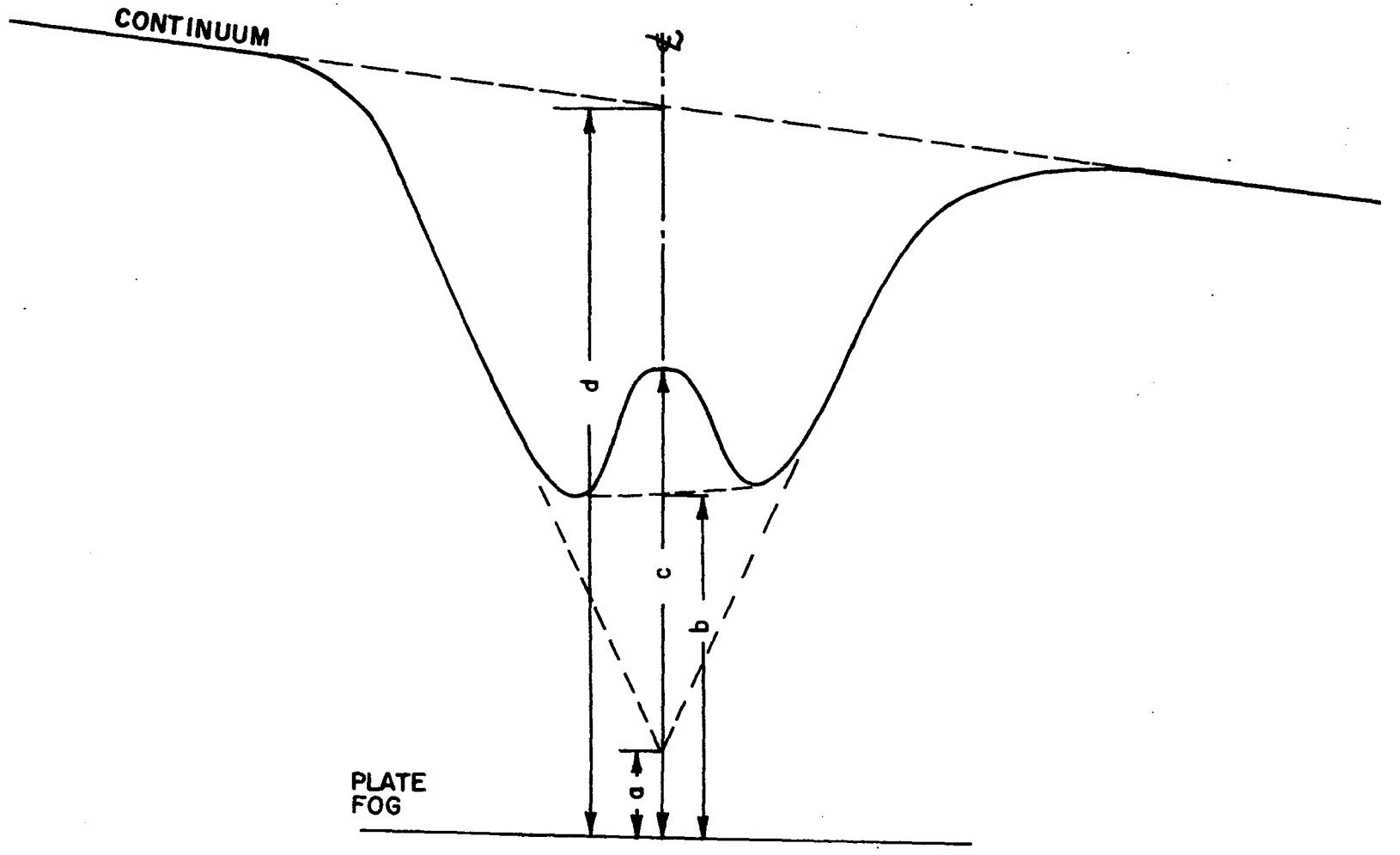

Fig. 2-12. Schematic Reversed K Line.

TABLE 2-2. Data Relating to the Emission Strength of the K Line.

Star	Plate	Disp.	a_D	b_D	c_D	d_D	a_I	b_I	c_I	d_I	$\frac{e_I}{(a+b)_I}$	$\frac{f_I}{c_I e_I}$	g_I f_I/d_I	g_I corrected
LQ Her	A-3799	66	0.0	0.4	2.3	6.1	0	4	12	41	2	13	0.32	0.40
OP Her	A-3799	66	0.0	0.4	0.9	8.0	0	4	8	62	2	6	0.10	0.13
α Ori	A-3593	66	7.4	*	13.2	16.2	55	*	182	308	55	127	0.41	0.46
σ CMa	C-799	36	.4	1.2	2.8	5.0	4	10	18	32	7	11	0.34	0.34
λDra	A-3593	66	3.1	5.7	10.2	15.9	19	38	100	296	28	72	0.24	0.30
δ Vir	A-3593	66	3.0	5.4	10.4	15.7	14	35	104	287	27	77	0.27	0.34
ϱ UMa	A-3735	66	1.3	3.7	8.2	14.8	10	23	65	256	16	49	0.19	0.24
72 Leo	A-3736	66	2.7	4.8	11.2	15.2	17	31	121	280	24	97	0.34	0.43
TV UMa	A-3736	66	1.0	3.0	5.4	14.8	9	19	35	258	14	21	0.08	0.10
40 Com	A-3736	66	2.0	4.0	8.0	15.4	14	25	62	292	20	42	0.15	0.19
HR 5052	A-3736	66	1.1	2.7	7.3	12.2	9	17	54	148	13	41	0.28	0.35
XY Lyr	-	-	-	-	-	-	-	-	-	-	-	-	0.0	0.0
δ^2 Lyr	A-3184	44	4.0	1.4	4.9	6.9	4	15	31	50	7	24	0.48	0.52
R Lyr	A-3184	44	0.0	1.6	5.8	8.8	0	12	39	64	6	33	0.52	0.57
α^1 Her	A-3176	44	1.5	3.2	6.7	11.4	11	20	48	126	15	33	0.26	0.27
μ UMa	A-3183	44	0.9	2.6	8.5	11.0	8	17	69	117	13	56	0.48	0.54
ν Vir	A-3183	44	0.0	0.5	3.9	6.1	0	5	24	41	3	21	0.51	0.57
HR 6337	A-3184	44	0.0	0.7	3.1	6.0	0	7	19	41	3	16	0.39	0.44
α UMa	D-1284	13	0.0	1.0	2.0	9.3	0	9	14	82	5	9	0.12	0.12
α Lyn	A-3590	88	0.5	1.9	3.7	10.6	5	13	23	108	9	14	0.13	0.19
ϱBoo	A-3594	66	1.7	3.6	5.0	14.6	13	22	32	246	23	9	0.04	0.05
δ Oph	A-3594	66	2.5	4.2	8.3	14.0	16	26	66	215	21	45	0.21	0.26
β Peg	A-3267	66	2.8	4.8	7.3	13.4	18	30	54	190	24	30	0.16	0.20
RR UMi	A-3184	44	0.0	0.9	4.4	7.9	0	8	17	61	4	13	0.21	0.23
2 Her	A-3184	44	0.0	0.1	2.2	4.9	0	1	15	31	1	14	0.45	0.48

* Minima not well defined

constant. Rearranging (2) the ratio of the unperturbed to perturbed amplitude is:

$$\frac{A}{B} = (W_1^2 + W_2^2)^{\frac{1}{2}}/W_1$$

Using the values of intrinsic line widths as a function of luminosity class and instrumental line width as a function of dispersion given in JD the corrections, seen in Table 2-3, were derived.

TABLE 2-3. Corrections for the Effect of the Instrumental Profile.

Lum. Class \ Disp.	44	63	88
I	A/B = 1/.95	1/.89	1/.84
III	1/.89	1/.80	1/.69

No correction was applied to the intensity measure of α UMa due to the negligibility of the instrumental effect at a dispersion of 13 $\mathring{A}$-mm^{-1}.

The Hydrogen Lines

To augment the ultraviolet observations additional spectra were obtained in the region of H_α for nine stars (μ Cep, RW Cep, RX Boo, LQ Her, OP Her, XY Lyr, R Lyr, ζ^A Ser, Z UMa). These were acquired with the same equipment and under the same conditions previously delineated with the obvious exception of the emulsion, which was unbaked IIa-E. The data of this program were combined with a

literature search based on information given by Bidelman (1954) to form a body of data representative in both MK class and time. The Balmer emission data is summarized in Table 2-4. For those stars showing or having shown emission the lines observed and the references, with dates, are presented. Exclusion of a star from this table indicates current spectra are devoid of emission and the author was unable to find any reference to emission in the literature.

Other Emission Lines

Since a general observational discussion of circumstellar emission lines was beyond the scope of this program the literature was used as the sole source of information. The contents of Table 2-5 presents those stars which have shown metallic emission and the species observed.

Synopsis of the Observations

Table 2-6 consolidates the observational data of this program and places it in juxtaposition to extant polarization and infrared data. Columns one through three are obvious; the source of the spectral types has been discussed elsewhere (DJ). The fourth and fifth columns contain, respectively, the mean polarization and the mean time variation of polarization derived from DJ, or as indicated. Both quantities are given in percent and have been calculated without regard to color. The O-L color index (Dyck et al. 1971), a measure of infrared excess

TABLE 2-4. The Observed Occurrence of Balmer Emission.

Star	Hα	Hβ	Hγ	Hδ	Hε	Other	Remarks
RX Boo	a_7	*	$e_{8,7}$	e_7	a_7	H_8-H_{11} e_7	The following references do not mention hydrogen emission: 4, 9, 10, 18
							9 notes v. strong ABS. bands
							7 finds weak emission
Z UMa	a_7	*	$e_{6,7,13,16}$	$e_{6,7,13,16}$	a_7	H_8-H_{11} e_7	The following reference does not mention hydrogen emission: 5
							The following references note emission but not specific lines: 14, 15, 18
							13 finds weak emission
							7 finds v. strong emission
RY UMa	*	*	ab_7	ab_7	a_7	H_8-H_{11} a_7	The following reference notes emission but not specific lines: 8
							7 finds weak absorption
							18 finds emission on one plate of six
μ Cep	*	e_{12}	ab_7, e_{12}	$e_{12}, e::_7$	a_7	H_8-H_{11} a_7	The following references do not mention hydrogen emission: 1, 2, 3, 9, 11, 17
							12 notes emission at maximum light and absorption at minimum

NOTE: a ≡ absent, e ≡ emission, ab ≡ absorption, * ≡ information not available

1. Adams, W. S., Joy, A. H., and Humason, M. L. 1926, Ap. J., 64, 225.
2. _____, and Brayton, A. M. 1935, Ap. J., 81, 187.
3. Campbell, W. W. and Moore, J. H. 1928, Lick Obs. Publ., Vol. 16.
4. Cannon, A. J. 1903, Harvard Obs. Ann., 48, 91.
5. Espin, T. E. 1895, Astr. Nach., 137, 369.
6. Fleming, W. D. 1912, Harvard Obs. Ann., 56, 165.
7. Jennings, M. C. and Dyck, H. M. 1971 (to be published).
8. Joy, A. H. 1942, Ap. J., 96, 344.
9. Krüger, F. 1893, Kiel Sternwarte Publ., 8, 1
10. Lee, O. J. and Bartlett, T. J. 1947, Dearborn Obs. Ann., 5, pt. 1B.
11. Maury, A. C. 1897, Harvard Obs. Ann., 28, 1.
12. McLaughlin, D. B. 1946, Ap. J., 103, 35.
13. Merrill, P. W. 1923, Ap. J., 58, 215.
14. _____. 1941, Ap. J., 93, 380.
15. _____. 1941, Ap. J., 94, 171.
16. Pickering, E. C. 1904, Harvard Obs. Circ., No. 76.
17. Rimmer, W. B. 1925, Mem. R.A.S., 64, 1.
18. Townley, S. D., Cannon, A. J., and Campbell, L. 1928, Harvard Obs. Ann., 79, 159.

TABLE 2-5. The Observed Occurrence of Heavy Element Emission.

Star	Species Seen in Emission
RW Cep	(FeI, TiI, NiI, CcI, VI, MgI, AlI, ScI, CaI, ScII*, TiII*, SvII*, BaII*)$_4$
RX Boo	(SiI)$_3$
α Ori	(FeII)$_1$
δ^2 Lyr	(FeII)$_1$
R Lyr	(FeII)$_1$
β Peg	(FeII)$_1$
α^1 Her	(FeI, FeII)$_2$

* Tentatively identified in emission

[1]Bidelman, W. D. and Pyper, D. M. 1963, P. A. S. P., 75, 389.
[2]Herzberg, G. 1948, Ap. J., 107, 94.
[3]Joy, A. H. 1942, Ap. J., 96, 344.
[4]Merrill, P. W., and Wilson, O. C. 1956, Ap. J., 123, 392.

TABLE 2-6.. Synopsis of the Observational Data.

Star	HD	Spectral Type	<P>	<ΔP>	O-L	Ik/I$_{cont}$	Hydrogen emission	Other Emission ionized	Other Emission neutral
RW Cep	212466	K00b	2.75	0.5	-2.91	0.	No	Yes:	Yes
TV Gem	42475	M1:Ia	2.51	0.22	-1.89	0.0	No	No	No
BU Gem	42543	M2:Iab	2.10	0.18	-1.69	0.0	No	No	No
μ Cep	206936	M2 Ia	1.60$_2$	0.52	-1.86	0.0	Yes	No	No
RY UMa	107397	M3:111	1.33	0.38	-1.71	0.0	Yes	No	No
Z UMa	103681	M5 111	1.0	0.45	- .93	0.0	Yes	No	No
RX Boo	126327	M8:	0.64	0.38	-1.32	0.0	Yes	No	Yes
γ^4 Ser	139216	M5 IIb-IIIa	0.51	0.21	-0.83	0.0	No	No	No
LQ Her	145713	M4 111	0.47	0.08	*	0.40	No	No	No
OP Her	163990	M5 IIb-IIIa	0.31	.10	*	0.13	No	No	No
α Ori	39801	M2Iab	0.24	0.08	-1.07	0.46	No	Yes	No
σ CMa	52877	MO Iab	0.20	0.05	-0.19	0.34	No	No	No
α UMa	95689	K0 111	0.12	0.07	-0.08	0.12	No	No	No
ν Dra	100029	MO 111	0.06	0.05	*	0.30	No	No	No
δ Vir	112300	M3 111	0.10	0.07	-0.25	0.34	No	No	No
ϱ UMa	76827	M3 111b	0.04	0.07	*	0.24	No	No	No
72 Leo	97778	M3 111	0.04	0.07	-0.11	0.43	No	No	No
TV UMa	102159	M4 111	0.00	0.07	*	0.10	No	No	No
40 Com	113866	M5 111	0.05	0.04	-0.26	0.19	No	No	No
HR 5052	116581	M3 111	0.07	0.08	*	0.35	No	No	No
XY Lyr	172380	M4-5Ib-II	0.11	0.04	-0.23	0.0	No	No	No
δ^2 Lyr	175588	M4 II	0.04	0.03	- .21	0.52	No	Yes	No
R Lyr	175865	M4-5	0.06	0.05	-0.12	0.57	No	Yes	No
α^1 Her	156014	M5:Ib-II	0.15	0.05	-0.37	0.27	No	Yes	No
μ UMa	89758	MO III	0.07	0.04	-0.16	0.54	No	No	No
ν Vir	102212	M1 111	0.05	0.05	*	0.57	No	No	No
HR 6337	154143	M3$^-$111	0.12	0.06	*	0.44	No	No	No
α Lyn	80493	K5$^+$111	0.02	0.03	*	0.19	No	No	No
ϱ Boo	127665	K3 111	0.02	0.07	*	0.05	No	No	No
δ Oph	146051	MO.5 11	0.02	0.03	*	0.26	No	No	No
β Peg	217906	M2-3 II-III	0.0$_3$	0.0	-0.10	0.20	No	Yes	No
RR UMi	132813	M5 111	0.08	0.05	-0.14	0.23	No	No	No
2 Her	142780	M3 111	0.02	0.04	*	0.48	No	No	No

*Not Available

[1]Merill, P. W. and Wilson, O. C. 1956, Ap. J., 123, 392.

[2]Coyne, G. V. and Kruzewski, A. 1968, A. J., 73, 20.

[3]Dyck, H. M. 1968, A. J., 73, 688.

emission (Ney and Allen 1969, Stein and Gillett 1969, Gerhz, Ney, and Strecker 1970) may be found in column six. It should be noted that for α Boo, a nonexcess star, (O-L) = -.15 while for a 2200 K black body (O-L) = -.6 (Gerhz, Ney, and Strecker 1970). The intensity measure of the K line occupies column seven. The eighth column indicates whether or not Balmer emission has been observed, while the last two columns indicate the observed presence or absence of, respectively, ionized and neutral heavy elements in emission.

Discussion

The H and K Lines

Figure 2-13 exhibits a plot of the mean change in polarization, a primary indicator of intrinsic polarization, and the intensity measure of the K line; fundamentally the same plot used by Dyck and Johnson. One immediately notices the resolution of the points into two groups, which upon inspection are seen to be those previously defined as group A and group B. It is further noted that the spectral and luminosity types are randomly distributed. The evidence of this figure leads one to conclude the existence of a strong anti-correlation between the presence or absence of calcium H and K emission and the absence or presence of time variable polarization.

In Figure 2-14 one sees a plot of mean polarization versus the K line intensity measure. Again the points resolve themselves into

Fig. 2-13. Mean Change in Polarization versus the Intensity Measure of the K Line.

Spectral Class	Symbol
KO-K4	○
K5-K9	□
MO-M4	△
M5-M9	◇

The enclosed number indicates the luminosity of class.

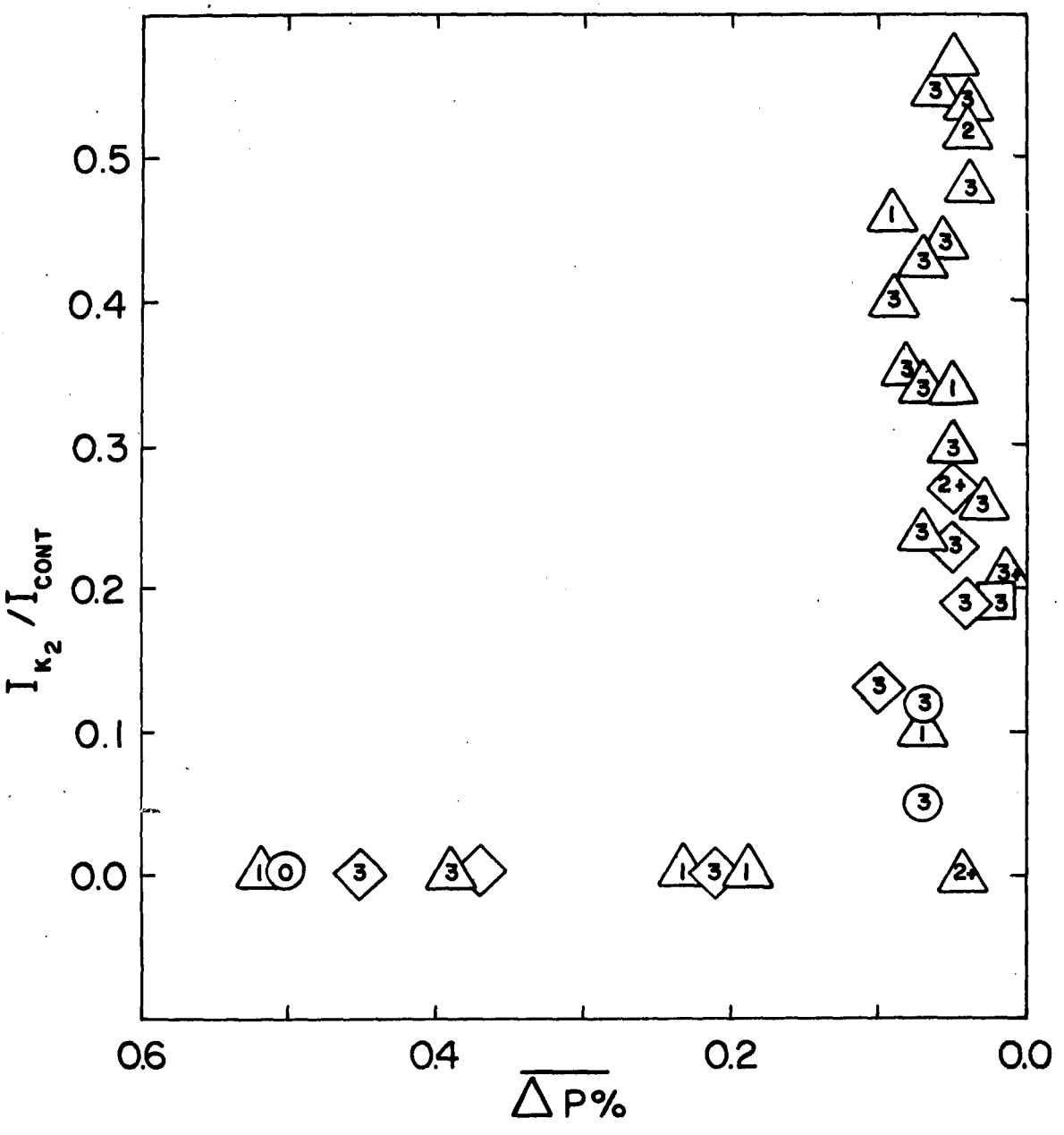

Fig. 2-13. Mean Change in Polarization versus the Intensity Measure of the K Line.

Fig. 2-14. Mean Polarization versus the Intensity Measure of the K Line.

Spectral Class	Symbol
KO-K4	O
K5-K9	□
MO-M4	△
M5-M9	◇

The enclosed number indicates the luminosity class.

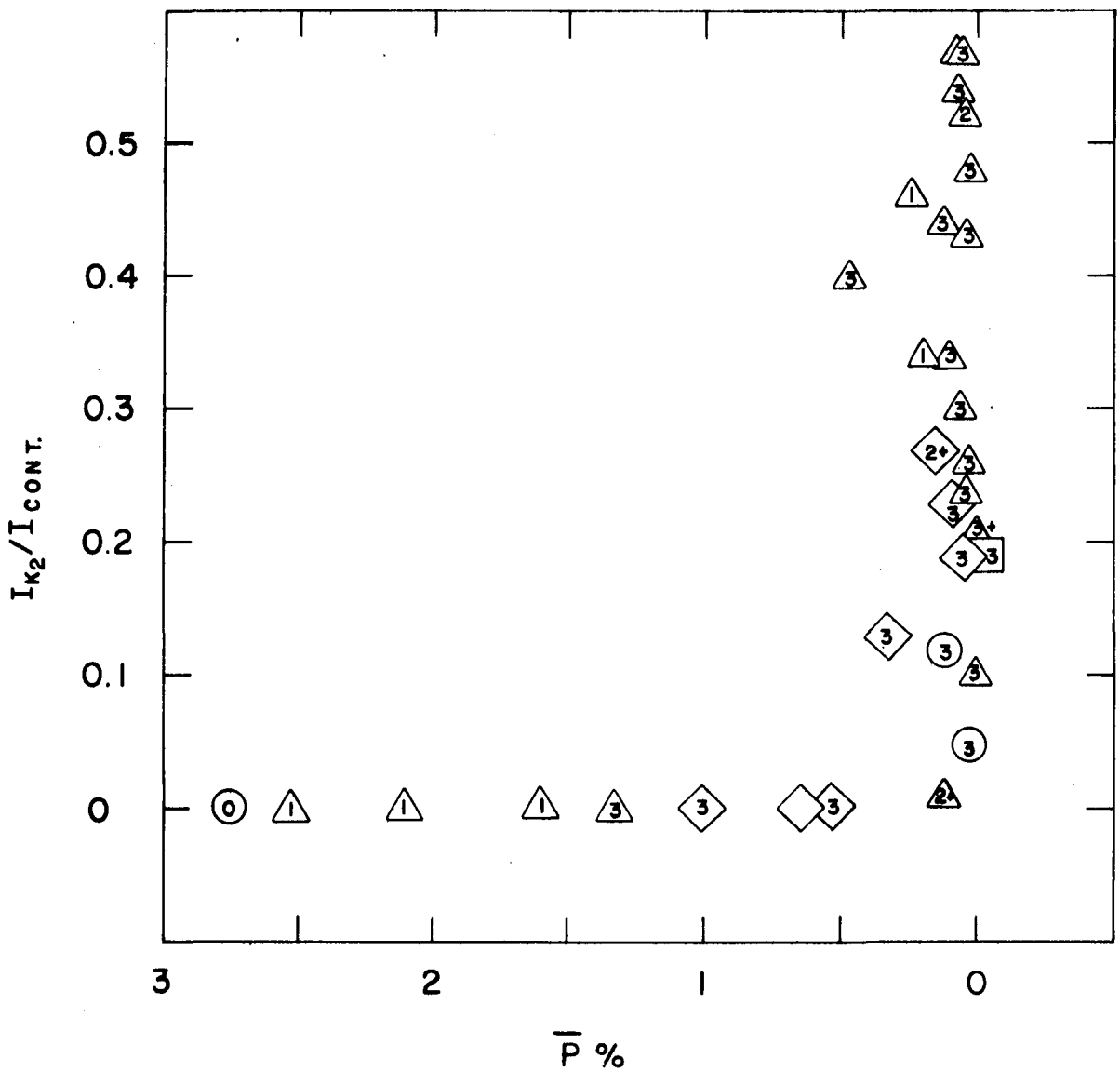

Fig. 2-14. Mean Polarization versus the Intensity Measure of the K Line.

groups A and B and are distributed randomly with respect to MK class. One notes, however, that the points of group B are not as closely clustered to the P = O line as they were to the $\Delta P = O$ line of Figure 2-13. This arises from the fact that the mean polarization of some stars may contain a small, albeit non-negligible, contribution from interstellar polarization while the mean change in polarization is much less likely to be influenced by the interstellar component. Yet regardless of this effect, the figure displays a clear anti-correlation between H and K emission and the mean polarization of those stars satisfying the intrinsic polarization criteria. By virtue of this anti-correlation another anti-correlation may be immediately enunciated: that of H and K emission and infrared excess. This relies on the fact that Dyck et al. (1971) have demonstrated a linear relation between polarization and excess radiation at 11μ.

Although Figure 2-13 supports Dyck and Johnson's suggestion of a relation between emission strength and variations, it indicates a behavior more akin to a step function than a continuous weakening of the emission reversal with a complimentary strengthening of the variation as originally suggested. It is not a sharp step, however. Indeed in both Figure 2-13 and 2-14, three stars, LQ Her, OP Her, and α Ori, appear to bridge the gap between group A and extreme group B. All three show weak polarization, small mean variations, the presence of calcium emission, and in the case of α Ori a weak

infrared excess and Fe II in emission. Although insufficient data prevents a detailed discussion of this bridging phenomenon, it is suggested that these stars are true intermediate cases with physical characteristics somewhere between the limits represented by group A and extreme group B.

The Hydrogen Lines

Among the spectra of this program only two, those of Z UMa and RX Boo, show Balmer emission coeval with polarization. On the broader time base of the literature search, however, one sees that μ Cep and RY UMa, which currently show polarization have histories of hydrogen emission, and that the emission in RX Boo and Z UMa appears to undergo secular variations. In all, fifty-two percent of the stars in group A have been observed to show hydrogen emission at some time while in group B none are known emitters. This supports the previous suggestions of a correspondence between intrinsic polarization and Balmer emission, but conflicts with Serkowski's statement that the appearance of intrinsic polarization necessitates coeval hydrogen emission.

A casual inspection of Table 2-4 reveals that these stars are possessed of truly remarkable Balmer decrements. A similar phenomenon has been observed among the Mira type stars by a number of investigators including Merrill (1945) and Joy (1947). These

authors find the decrement to be severly distorted at the onset of emission but note that as the cycle progresses the decrement tends toward normalcy. Following suggestions by Clerke and Shane (1948) they attribute the emission to an outward propagating shock wave originating deep in the atmosphere. In this model the anomalous decrement arises from the effects of overlying absorption from various sources on a decrement normal at its point of origin. As the shock moves outward the amount of absorbing material above it diminishes and the decrement takes on its characteristic appearance. This type of model is particularly attractive due to the difficulty of explaining such a distinctly anomalous decrement arising in a totally optically thin region.

Although their work applies explicitly only to Miras, it also appears to be a resonable explanation for the irregular star observations, since the details of the anomaly correspond so closely to those seen in Miras. Should this be the case, one must conclude that the calcium emission and Balmer emission arise in different regions and that one would not necessarily expect an agent acting on one to effect the other. Thus the existence of a strong anti-correlation for calcium emission and polarization, while the Balmer emission versus polarization relation is much weaker, simply implies that polarization agents are intimately involved in the state of the chromosphere but do not hold sway in the region of hydrogen emission. As an alternative

to Serkowski's suggestion this author would prefer to avoid defining any specific relation between hydrogen emission and polarization and in its place substitute the view that the emission indicates that the star has placed itself in a state conducive to the production of aerosols.

Heavy Element Emission

The data of Table 2-5 show that none of the high polarization stars definitely show ionized emission and only two, RW Cep and RX Boo, display emission from neutrals. On the other hand, ionized emission, especially Fe II, is fairly common among the unpolarized objects. With the ionization potential of Fe I being 7.87ev, it is obvious that Fe II emission can not be an atmospheric phenomenon, but requires the temperatures associated with chromospheres. Thus the absence of ionized emission, particularly Fe II, among the polarized objects may be construed as further evidence for an alteration of the chromospheric structure by the polarizers.

The lack of Fe II emission for those stars with strong polarization and infrared excesses contradicts a correlation between infrared emission and Fe II and/or [Fe III] emission suggested by Geisel (1970). Her statement that Bidelman and Pyper's (1963) work implies a high incidence of Fe II emission among late type stars fails to recognize that their results contain only one star, α Ori, with an infrared

excess, and the weakness of this excess when viewed in juxtaposition to other known excesses among similar stars. Further, the coexistence of Fe II emission and weak aerosol indications in α Ori may be understood in the context of its designation as an object of intermediate properties.

It should be noted the neutral emission from RW Cep and RX Boo requires a much lower temperature than would the maintenance of a significant number of an ionized species, and even the tentatively identified ionized emissions (Sc II, Sr II, Ba II, Ti II), of RW Cep arise from species of significantly lower ionization potential than Fe I. These observations are therefore consistent with the idea of a perturbed chromosphere.

Conclusions

From the foregoing figures, tables, and discussion a clear relation has emerged: the presence or absence of calcium H and K emission correlates strongly, almost discontinuously, with the absence or presence of intrinsic polarization and infrared excess. Further, one also finds a similar relation for other non-hydrogen emissions, especially of ionized species. Although most stars seem to fit easily into these two gross categories of polarized or unpolarized, a small number, displaying the characteristics of both regimes

occupy the transition region between the two and appear to be elements in a true sequence of physical states between these groups.

Since emission lines of ionized calcium and heavy elements are taken as evidence for the presence of a chromosphere, their disappearance leads one to conclude that either the chromosphere's presence has been veiled or that it has been significantly reduced in intensity or removed entirely. One can visualize a number of ways of achieving these possibilities:

1. The chromosphere has been drastically altered prior to the appearance of the grains.
2. The grains act via a radiative transfer mechanism to quench chromospheric indicators and thus conceal the chromosphere.
3. Thermodynamic perturbations due to the presence of grains cause the chromosphere to dissipate.
4. Secondary effects of the dynamic consequences of grains obviate the possibility of sustaining a chromosphere.

Regarding the first suggestion, at present no theory exists which would account for the disappearance of an active chromosphere without substantial changes in the fundamental structure of the star, e.g., the disappearance of the hydrogen convection zone. In addition any attempt at the formulation of such a theory would be severly hampered by the current paucity of information regarding the detailed structure

of the outer layers of late type stars. For these reasons a discussion of the pre-grain alteration of the chromosphere lies beyond the scope of this work. The idea of grains acting through a purely radiative coupling with the line radiation has been discounted due to the difficulty of visualizing how an obviously optically thin grain field can operate over a broad spectral range to quench resonance and non-resonance lines alike. Having discarded the first two possibilities, a mechanism involving thermodynamic or indirect dynamic effects, or a combination of the two, seems to be the most direct approach. Thus the thermal and dynamic consequences of grains in a stellar atmosphere will be discussed in detail in Chapters 3 and 4 respectively.

The observations of this program support a correspondence between Balmer emission and polarization, but necessitate discarding the suggestion that a coincidence relation exists. The author concludes that polarizers and hydrogen emission are only indirectly related; that relation being a statement as to the general condition of the star, a condition conducive to the production of aerosols, rather than to a physical coupling between grain and Balmer emission processes.

A question, which this program was not designed to explore, but which the data intimates, is that of possible secular or periodic variations of the various observational quantities. For example, RY UMa, and μ Cep which do not show hydrogen emission at the current epoch, have been observed to do so in the past. Further, the Balmer

emission lines of Z UMa have been described as moderate (Merrill 1941) and faint (Joy 1942), while at the current epoch they appear quite strong. Some evidence for a change in H and K emission intensity also exists (Joy and Wilson 1949). Further, emission in α UMa was undetected at 43 $\mathring{A}$-mm^{-1} although listed as intensity class two by WB. The fact that the most comprehensive (WB) as well as other works on H and K emission intensities are of a qualitative nature severly limits any current attempt at a detailed discussion of their variations.

The variability of polarization with time is well documented and indeed observations now exist (Dyck and Jennings 1971b) which trace a periodic variation in the polarization of RY UMa during an observing period of one year. In view of the above evidence a monitoring program of spectroscopy, polarimetry, and visual and infrared photometry of selected objects would seem to be a worthwhile future endeavor.

CHAPTER 3

THE THERMODYNAMIC EFFECT OF GRAINS ON A COLD PLASMA

With the observational evidence being decidedly in favor of altered chromospheres, one may proceed in an attempt to understand the phenomenon within a theoretical framework. With this goal in mind the thermodynamic conditions necessary to explain the observations will be derived and it will be shown that grains may produce these conditions under the proper circumstances.

The Dependence of Emission Strength on the Chromospheric Temperature Structure

Since the observations indicate that the H and K lines are highly sensitive to the presence of grains, a quantitative examination of their quenching by application of the transfer formalism should reveal the required chromospheric structure changes. While an exact treatment of the H and K transfer problem remains beyond our ability for all stars save the sun, a picture of its gross behavior may be gained through a very simplified approach.

Consider a semi-infinite plane parallel slab of gas whose monochromatic opacity k_ν, consists of both a pure absorption

component, κ_ν , and an isotropically and coherently scattering component σ_ν . Further, let the temperature in the slab be given by

$$(3\text{-}1) \quad T = T_o (1 + \psi \tau_\nu)^{-1}$$

where T_o and ψ are constants and τ_ν is the total monochromatic optical depth defined in the usual way and measured from the surface of the slab. It should be noted that the proper choice of T_o and ψ will closely reproduce the structure of the solar chromosphere. T_o may be interpreted as the temperature at the position above which Ca II absorption may be neglected.

The monochromatic equation of transfer in the slab may be written as:

$$(3\text{-}2) \quad \mu \frac{dI_\nu}{d\tau_\nu} = I_\nu - S_\nu$$

where

$$(3\text{-}3) \quad S_\nu \equiv L_\nu B_\nu(T) + (1 - L_\nu) J_\nu$$

$$(3\text{-}4) \quad L_\nu \equiv \kappa_\nu / (\kappa_\nu + \sigma_\nu)$$

Due to the weak temperature dependence of L_ν it will be treated as a constant in the following analysis. Henceforth the ν subscript will be deleted and all quantities are to be taken as monochromatic.

In the Eddington approximation, viz., $K = 1/3\ J$, equation (3-2) becomes:

$$(3\text{-}5) \quad \frac{d^2 J}{d\tau^2} = 3L\,(J - B)$$

Noting that:

$$(3\text{-}6)\quad B(T(\tau)) = \frac{2h\nu^3}{c^2} e^{-\frac{h\nu}{KT_o}} (1 + \psi\tau)$$

and that in the Eddington approximation one has the following boundary condition:

$$(3\text{-}7)\quad J(0) = 2H(0) = \frac{2}{3}\frac{dJ}{d\tau}(0)$$

one may integrate (3-5) to yield:

$$(3\text{-}8)\quad J(\tau) = \frac{\eta e^{-\xi}}{\xi^2\psi^2-\lambda^2}\left(\frac{2\xi\psi}{2\lambda+3} e^{-\lambda\tau} - e^{-\xi\psi\tau}\right)$$

where: $\eta \equiv 6Lh\nu^3/c^2$

$\xi \equiv h\nu/KT_o$

$\lambda \equiv \sqrt{3L}$

Combining (3-3), (3-6), and (3-8) one finds for the source function:

$$(3\text{-}9)\quad S(\tau) = \eta e^{-\xi(1+\psi\tau)}\left[\frac{1}{3} - \frac{(1-L)}{\xi^2\psi^2-\lambda^2}\right] + \frac{e^{-(\xi+\lambda\tau)}}{(\xi^2\psi^2-\lambda^2)}\left(\frac{2\xi\psi+3}{2\lambda+3}\right)(1-L)$$

Using equation (3-9) one may derive the emergent intensity via:

$$(3\text{-}10)\quad I(0,0) = \int_0^\infty S(\tau) e^{-\tau} d\tau$$

which produces:

$$(3\text{-}11)\quad I(0,0) = B(T_o)\left(\frac{L}{\xi\psi+1} + \frac{\lambda^2(1-L)}{\xi^2\psi^2-\lambda^2}\left[\frac{1}{(\lambda+1)}\left(\frac{2\xi\psi+3}{2\lambda+3}\right) - \frac{1}{\xi\psi+1}\right]\right)$$

From the H and K polarization anticorrelation one has that $\frac{H(0,)\text{perturbed}}{H(0,)\text{ambient}} < 1$ and one therefore wishes to ascertain what changes in the parameters T_o and ψ of (3-11) will decrease I(0, 0). By inspection one sees that a reduced terminal temperature, T_o, will result in a smaller I(0, 0) through the lessening of $B(T_o)$ and the increasing of ξ.

It should be noted that while $L\alpha T^{-\frac{1}{2}}$ its tendency to increase I is easily overpowered by the strong functional dependence of $B(T_o)$ and ξ. Forming the partial derivative of I(0, 0) with respect to ψ yields

$$(3\text{-}12)\quad \frac{\partial I(0,0)}{\partial \psi} = B(T_o)\left[-\frac{\xi L}{(\psi\xi+1)^2} + \lambda^2(1-L)\frac{\partial}{\partial \psi}\left[\frac{1}{(\xi^2\psi^2-\lambda^2)}\right.\right.$$

$$\left.\left.\left(\frac{1}{\lambda+1}\right)\left(\frac{2\xi\psi+3}{2\lambda+3} - \frac{1}{\xi\psi+1}\right)\right]\right]$$

The first term on the right side is obviously negative; the second term, however, requires further consideration. Due to the smallness of λ when compared to the other parameters (Athay and Skumanich 1968) the term on the far right side may be rewritten as:

$$(3\text{-}13)\quad \frac{\partial}{\partial \psi}\frac{1}{\xi^2\psi^2}\left(\frac{2\xi\psi+3}{3} - \frac{1}{\xi\psi+1}\right)$$

which upon differentiation becomes:

$$(3\text{-}14)\quad -\frac{2}{\xi^2\psi^3}\left(\frac{2\xi\psi+3}{3} - \frac{1}{\xi\psi+1}\right) + \frac{2}{3\xi\psi^2} + \frac{1}{\xi\psi^2(\xi\psi+1)^2}$$

which may be rearranged as:

$$(3\text{-}15)\quad -\frac{4}{3}\xi\psi - 2 + \frac{2}{\xi\psi+1} + \left(\frac{2}{3} + \frac{1}{(\xi\psi+1)^2}\right)\xi\psi$$

or

$$(3\text{-}16)\quad \frac{-2(\xi^2\psi^2+2\xi\psi)+1}{3(\xi\psi+1)^2} - \frac{2\xi\psi}{\xi\psi+1}$$

which is negative for the values of $\xi\psi$ germane to a chromosphere. Thus one sees that an increase in the value of ψ will diminish I(0, 0). Physically an increase in ψ at constant T_o means a deferment of the

temperature rise to positions of lower optical depth and a reduction of the magnitude of the temperature gradient in regions of higher optical depth. If a decrease in T_o accompanies the increase in ψ one may realize a gradient reduction at all optical depths.

From the foregoing analysis one concludes that the H and K lines may be quenched if one limits the amplitude of the chromospheric temperature rise and/or reduces the size of the gradient through a large portion of the chromosphere. It is also noted that these adjustments would serve to explain the general absence of ionized emissions since equation (3-11) may be made applicable to nonresonance lines by a suitable change in the value of L. With the required alterations known one may proceed to investigate whether the grains may effect these changes and if so what time scale is required.

The Thermodynamic Equations

The thermodynamics of the grain-gas interaction may be considered in two parts: an energy balance relation for the grain field and one for the gas. In deriving these relations the following assumptions will be made.

1. The star radiates as a black body.
2. Gas-grain collisions are inelastic, with a gas particle departing an interaction with a velocity given by

$v_g = \left(\frac{3kT_G}{\mu}\right)^{\frac{1}{2}}$, (Capriotti 1970, Huffman 1970) where T_G = internal grain temperature and μ = mass of a gas particle. (cgs units are used throughout.)

3. The grains are non-metallic crystals of the refractory type.

4. The grains are not sputtered. While soft materials and/or those with highly anisotropic lattice structures have been shown to sputter (Mathews 1969) grains of refractory materials are much more resistent to impact loads. Moreover, Barlow (1971) has indicated that sputtering may be much less important than it is currently held to be.

5. The gas is pure hydrogen.

6. The possible effects of magnetic fields are not important.

One should note that throughout this analysis whenever a choice between physical conditions has presented itself the one producing the worst case (i.e., least cooling) has been selected. This was done in attempts to offset the effects of the idealizing assumptions. Further, if the mechanism works for the worst case it must also work for more efficient situations.

The Grain Energy Equation

Grain is assumed to gain energy via the following processes:

1. Absorption of radiation from the star.
2. Collisions with gas particles of high velocity, i.e.,

$$(3\text{-}17)\quad v_g > \left(\frac{3kT_G}{\mu}\right)^{\frac{1}{2}}$$

Energy losses to the grain occur through the following mechanisms.

1. Radiation by the grain.
2. Collisions with low velocity gas particles, i.e.,

$$(3\text{-}18)\quad v_g < \left(\frac{3kT_G}{\mu}\right)^{\frac{1}{2}}$$

The power absorbed by a grain from the radiation field of the star is given by:

$$(3\text{-}19)\quad \frac{\delta E^+}{\delta t} = \pi a_o \mathcal{R}^2 \int_o^\infty Q_\nu B_\nu (T_*) d\nu$$

where $a_o \equiv \pi a^2$, $a \equiv$ radius of a grain,

Q_ν absorption cross section in units of the geometrical cross section,

$\mathcal{R}$ radial position of the grain in units of the stellar radius,

T_* stellar effective temperature.

The amount radiated away by the grain is:

$$(3\text{-}20)\quad \frac{\delta E^-}{\delta t} = 4\pi a_o \int_o^\infty Q_\nu B_\nu (T_G)\, d\nu$$

The energy transmitted to, or removed from, a grain during a collision with a gas particle may be written as:

$$(3\text{-}21)\quad \frac{\delta E}{\delta t} = 1/2\mu\, v^2 - 3/2kT_G$$

where the sign indicates the sense of the heat flow and v is the initial particle velocity. The following relation expresses the number of collisions per second sustained by a grain with particles of species i traveling at velocity v.

$$(3\text{-}22)\quad N_c = N_i a_o v f_i(v) dv$$

where N_i is number-cm^{-3} of the ith species and f(v) is the maxwellian distribution. Justification for using a maxwellian distribution may be found in Appendix A. The above relation assumes that the grains are uncharged; a worst case situation since, if charged, they would act as bremsstrahlung acceleration centers, enhancing the cooling rate of the gas. Spitzer (1948) finds grains to be charged under conditions found in the interstellar medium; however, the situation under chromospheric conditions has not been examined in detail. Also his results indicate that refractory solids tend to accumulate far less charge than other types of materials.

Combining equations (3-21) and (3-22) allows one to write an expression for the net collisional transfer of energy to a grain per second by species i at velocity v.

$$(3\text{-}23)\quad \frac{\delta E}{\delta t} = N_i a_o v f_i(v)\left(\frac{1}{2}\mu_i v^2 - \frac{3}{2}k\ T_G\right)dv$$

Finally, the total transfer by all species may be written as:

$$(3\text{-}24)\quad \frac{\delta E}{\delta t} = a_o \sum_i N_i \int_o^\infty \left(\frac{1}{2}\mu_i v^2 - \frac{3}{2}kT_G\right) v f_i(v)dv$$

In a steady state the gains must balance losses and one has upon combining (3-19), (3-20), and (3-24):

$$(3\text{-}25)\quad 4a_o\pi\int_o^\infty Q_\nu B_\nu(T_G)d\nu = a_o R^2\pi\int_o^\infty Q_\nu B_\nu(T_*)d\nu + a_o\sum_i N_i\int_o^\infty \left(\frac{1}{2}\mu_i v^2 - \frac{3}{2}kT_G\right)vf_i(v)dv$$

Note that this expression is independent of grain size.

Letting Q_ν be equal to an average, constant Q, substituting explicitly for the maxwell distribution, and recalling that the gas is pure hydrogen, (3-25) may be rewritten as:

$$(3\text{-}26)\quad 4\pi Q\sigma T_G^{\,4} = \pi R^2 Q\sigma T_*^{\,4} + N_e\beta_e\int_o^\infty \left(\frac{1}{2}\mu_e v^2 - \frac{3}{2}kT_G\right)v^3 e^{-\frac{\mu_e v^2}{2kT_e}}dv + N\beta_N\int_o^\infty \left(\frac{1}{2}\mu_N v^2 - \frac{3}{2}kT_G\right)v^3 e^{-\frac{\mu_N v^2}{2kT_e}}dv$$

where N_e = number of electrons-cm^{-3}

N = number of neutrals and protons-cm^{-3}

T_e = gas temperature

σ = Stefan-Boltzman Constant

$\beta_i = 4\,(\mu_i/2\pi kT_e)^{3/2}$; $i = e^-, N$

Performing the integrations and rearranging one has:

$$(3\text{-}27)\quad 4\pi Q\sigma T_G^{\,4} = \pi \mathcal{R}^2 Q\sigma T_*^{\,4} + 2^{1/2} T_e^{\,1/2} k^{3/2} \frac{\left(\frac{N_e}{\mu_e^{\,1/2}} + \frac{N}{\mu_N^{\,1/2}}\right)}{\pi^{1/2}} \left[4T_e - 3T_G\right]$$

Reorganizing yields:

$$(3\text{-}28)\quad T_G^{\,4} = \frac{\mathcal{R}^2 T_*^{\,4}}{4} + \left(\frac{k}{\pi}\right)^{3/2} \frac{2^{1/2}}{\sigma Q} \left(\frac{N_e}{\mu_e^{\,1/2}} + \frac{N}{\mu_N^{\,1/2}}\right) T_e^{\,1/2} \left(T_e - \frac{3}{4} T_G\right)$$

Evaluating the physical constants gives the final expression:

$$(3\text{-}29)\quad T_G^{\,4} = \frac{\mathcal{R}^2 T_*^{\,4}}{4} + \frac{2.39\times10^{-7}}{Q} \left(N_e + N(3.44\times10^{-4})\right) T_e^{\,1/2} \left(T_e - \frac{3}{4} T_G\right)$$

Consider a hypothetical situation in which gas-grain equilibrium is reached with:

$T_e = 10^4$ K

$N_e = 10^{10}$ cm^{-3}

$Q = 10^{-2}$

$T_* = 2.5\times10^3$

$\mathcal{R} = 1$

Note that N may be neglected. Substituting these conditions into (3-29), but neglecting the term $.75T_G$ which will be seen to be valid a posteriori, results in the following expression:

$$(3\text{-}30)\quad T_G^{\,4} \cong 9.75 \times 10^{12} + 2.39 \times 10^{11}$$

From (3-30) one sees that the gas collision contribution, the far right term, is virtually negligible even under this rather extreme situation. Gas conditions commensurate with a corona have not been considered in detail since it is doubtful whether a solar type corona can exist in the reduced gravity of giants and supergiants (Biermann and Lüst 1960) or whether such a hot region can be made consistent with observations (Weymann 1960, 1962b). One should note, however, that gas effects remain negligible for coronal conditions ($N_e = 10^7$ cm^{-3}, $T_e = 10^6$K) derived by Oster (1971) for α Sco. From this one concludes that under giant and supergiant chromospheric conditions the strong radiative ability of a grain (T_G^4) may successfully offset the comparatively weak ($T_e^{3/2}$) contribution to its temperature made by the gas. One may to a high degree of approximation set the grain temperature equal to the local radiation temperature, i.e.,

$$(3\text{-}31)\quad T_G = \mathcal{R}^{1/2} T_* / \sqrt{2}$$

where $\mathcal{R}$ is always approximately unity for regions of interest. Equation (3-31) will be adopted as the grain temperature throughout the remainder of this analysis.

The Gas Equations

Consider a gas which gains energy from:

1. Dissipation of shock of other mechanical forms of energy (Athay and Thomas 1957).

2. Collision of its low velocity members with grains.

Radiative ionization has been deleted since a chromosphere obviously can not be generated by radiation from a cool star.

The gas loses energy via the following processes:

1. Recombination

2. Collision of high velocity members with grains.

Bremsstrahlung losses are assumed to be unimportant in the regime of grain cooling, which will be verified a posteriori. However, the assumption that all non-grain cooling occurs via recombination undoubtedly stands as the most uncertain in view of the fact that Osterbrock (1961) has demonstrated the importance of negative hydrogen emission in cooling the lower solar chromosphere and that cooling by heavy elements has been neglected. Yet, a more detailed treatment is precluded, due to the complexity of the non-LTE problem (Thomas 1948, 1949, Giovanelli 1948, 1949, 1967, Matsushima 1952, Athay and Thomas 1956) and the almost total lack of reliable data concerning the structure of late star chromospheres (Biermann and Lüst 1960, Underhill 1971).

The total kinetic energy in a cubic centimeter of a cold plasma is given by:

$$(3\text{-}32)\quad E_{tot} = \frac{3}{2} k (N_e + N) T_e$$

Differentiating with respect to time (t) yields:

$$(3\text{-}33)\quad \frac{dE}{dt} = \frac{3}{2}k\left[(N_e+N)\frac{dT_e}{dt} + T_e\frac{dN_e}{dt}\right]$$

where $\frac{dN}{dt} \equiv O$ since in a star the tendency of the cooling gas to collapse will be in part offset by the reduced effective gravity caused by the grain outflow.

Consider the required expression for $\frac{dN_e}{dt}$. Electrons are lost to the gas by recombination, which may be expressed as:

$$(3\text{-}34)\quad \frac{\delta N_e^-}{\delta t} = -N_e^2 \sum_{n=2}^{\infty} \langle \sigma_{Rn}, v\rangle$$

where σ_{Rn} is the recombination cross section to the Nth level and:

$$(3\text{-}35)\quad \langle \xi(v), v\rangle \equiv \int_o^{\infty} \xi(v) v f(v) dv$$

The summation from $2 \rightarrow \infty$ rather than $1 \rightarrow \infty$ indicates that the gas is optically thick to Lyman radiation thus making it subject to the "on the spot" approximation. The integral and summation may be evaluated (Williams 1970) and (3-35) rewritten as:

$$(3\text{-}36)\quad \frac{\delta N_e^-}{\delta t} = -\frac{N_e^2 \Psi}{T_e^{1/2}}$$

$$\text{where } \Psi \equiv \frac{16\pi a_1}{c^2}\left(\frac{h^{-1/3}}{2\pi\mu e}\right)^{3/2} (h\nu_1)^2$$

a_1 = ionization cross section of the first level

ν_1 = frequency associated with one Rydberg

The gas gains electrons through collisional ionization and this rate may be written as:

$$(3\text{-}37)\quad \frac{\delta N_e^+}{\delta t} = k_o N_e (N - N_e)$$

where k_o is defined to be constant thus neglecting the temperature dependence of the ionization rate. At temperatures below ambient this results in an energy input above that expected from a pure hydrogen gas (see 3-44) and hence makes a crude allowance for this assumption. Combining equations (3-36) and (3-37) one may write the expression for the time derivative of the electron number density.

$$(3\text{-}38)\quad \frac{dN_e}{dt} = k_o N_e (N - N_e) - \frac{N_e^2 \Psi}{T_e^{1/2}}$$

The constant k_o may be evaluated by noting that in the ambient plasma a steady state exists and therefore $\frac{dN_e}{dt} = O$. If the ambient electron number density and temperature are N_o and T_o respectively, equation (3-38) may be written as:

$$(3\text{-}39)\quad k_o N_o (N - N_o) = \frac{N_o^2 \Psi}{T_o^{1/2}}$$

whereupon:

$$(3\text{-}40)\quad k_o = N_o \Psi / T_o^{1/2} (N - N_o)$$

Equation (3-38) may then be written in a generally applicable form:

$$(3\text{-}41)\quad \frac{dN_e}{dt} = \frac{N_o \Psi N_e (N - N_e)}{T_o^{1/2} (N - N_o)} - \frac{N_e^2 \Psi}{T_e^{1/2}}$$

To complete the derivation one needs to examine the form of $\frac{dE}{dt}$. The loss of power by recombination is given by:

$$(3\text{-}42)\quad \frac{\delta E^-}{\delta t} = -\sum_{n=2}^{\infty} N_e^2 \langle \sigma_{Rn}, 1/2\ \mu_e v^2, v \rangle$$

Again following Williams (1970) one has:

$$(3\text{-}43)\quad \frac{\delta E^-}{\delta t} = -N_e^2 \Psi k T_e^{1/2}$$

The loss rate due to the grains is given by the negative of (3-24), i.e.:

$$\frac{\delta E^-}{\delta t} = -a_o \sum_i N_i \langle (\tfrac{1}{2}\mu_i v^2 - \tfrac{3}{2} k T_G), v \rangle,\ i = e^-, N$$

The gain rate due to collisional ionization may be written in the following form:

$$(3\text{-}44)\quad \frac{\delta E^+}{\delta t} = \frac{\varepsilon N_o \Psi N_e (N - N_e)}{T_o^{1/2} (N - N_o)}$$

where ε is the average energy supplied per collision and will be assumed to always maintain its ambient value. The remaining terms describe the ionization rate (see 3-41). Summing all losses and gains yields:

$$(3\text{-}45)\quad \frac{dE}{dt} = \frac{\varepsilon N_o \Psi N_e (N - N_e)}{T_o^{1/2} (N - N_o)} - N_e^2 \Psi k T_e^{1/2} -$$

$$a_o \sum N_i \langle (\tfrac{1}{2}\mu_i v^2 - \tfrac{3}{2} k T_G), v \rangle,\ i = e^-, N$$

ε may be evaluated by again invoking a steady-state in the absence of grains, producing the following relation:

$$(3\text{-}46)\quad \frac{\varepsilon N_o \Psi N_e (N - N_o)}{T_o^{1/2} (N - N_o)} - N_o^2 \Psi k T_o^{1/2} = O$$

or:

$$(3\text{-}47)\quad \mathcal{E} = kT_o$$

Employing (3-47) and expanding the grain loss term allows one to write the final expression for $\frac{dE}{dt}$.

$$(3\text{-}48)\quad \frac{dE}{dt} = \left(\frac{kT_o^{1/2} N_o \Psi}{(N-N_o)}\right) N_e (N-N_e) - N_e^2 \Psi k T_e^{1/2} - 4 N_G k^{3/2} \frac{2^{1/2}}{\pi^{1/2}} \left(\frac{N_e}{\mu_e^{1/2}} + \frac{N}{\mu_N^{1/2}}\right) T_e^{1/2} \left(T_e - \frac{3}{4} T_G\right)$$

where N_G = grains-cm^{-3}. Combining (3-33), (3-41), and (3-48) produces an expression for the time rate of change of the gas temperature.

$$(3\text{-}49)\quad \frac{dT_e}{dt} = \frac{1}{(N+N_e)} \left[\frac{N_o \Psi N_e (N-N_e)}{(N-N_o)} \left(\frac{2}{3} T_o^{1/2} - \frac{T_e}{T_o^{1/2}}\right) + \frac{N_e^2 \Psi T_e^{1/2}}{3} - \frac{2^{7/2}}{3} a_o \left(\frac{k}{\pi}\right)^{1/2} N_G \left(\frac{N_e}{\mu_e^{1/2}} + \frac{N}{\mu_N^{1/2}}\right) T_e^{1/2} \left(T_e - \frac{3}{4} T_G\right) \right]$$

In summary, the time dependent thermodynamic state of the gas may be described by the simultaneous solution of two nonlinear, coupled, first order differential equations, viz.,

$$(3\text{-}50a)\quad \frac{dN_e}{dt} = \frac{N_o \Psi N_e (N-N_e)}{T_o^{1/2} (N-N_o)} - \frac{N_e^2 \Psi}{T_e^{1/2}}$$

$$(3\text{-}50b)\quad \frac{dT_e}{dt} = (N+N_e)^{-1} \left[\frac{N_o \Psi N_e (N-N_e)}{N-N_o} \left(\frac{2}{3} T_o^{1/2} - \frac{T_e}{T_o^{1/2}}\right) + \right.$$

$$\frac{N_e^2 \Psi T_e^{1/2}}{3} - \frac{2}{3}^{7/2}\left(\frac{k}{\pi}\right)^{1/2} a_o N_G \left(\frac{N_e}{\mu_e^{1/2}} + \frac{N}{\mu_N^{1/2}}\right)$$

$$T_e^{1/2}(T_e - \frac{3}{4}T_G)\Big]$$

Equation (3-50b) has some interesting properties. For fixed T_o and T_G, the final gas temperature depends only on the ratio of the number of neutrals plus ions to the number of grains, not on their absolute values. This result is intuitively obvious, since all gain and loss processes have the same functional dependence on number density. This property is particularly fortunate, since it relieves the model results of any connection to the stellar chromosphere's absolute density structure, the uncertainty of which has already been noted. An examination of the grain cooling term reveals that in cases of strong grain effects one may realize a final gas temperature lower than the grain temperature with the lower limit being $.75T_G$. This results from the assumption that a colliding particle departs with a velocity corresponding to the grain temperature and indicates that this assumption is not strictly true since materials in contact and in equilibrium but with differing temperatures are not observed in nature. A detailed consideration of the disposition of the energy of a colliding particle and the true form of the energy distribution of particles departing a collision should yield a gas equilibrium temperature equal to the grain temperature. However, in view of the complexity of an exact

treatment and the smallness of the discrepancy resulting from the use of the simplified assumption the latter will be retained.

Solution of the Equations

Since equations (3-50a), (3-50b) are not analytically tractable, they have been solved via a simple numerical integration scheme which proceeds as follows. Upon specifying the basic initial conditions (T_o, T_G, N, (N_G a_o)) one may calculate the initial electron number density (see Appendix B), which when combined with the other quantities permits an evaluation of the electron number and temperature derivatives. With these quantities available one may select a time step which satisfies an imposed requirement that the change in the logarithm of both N_e and T_e be less than some specified value, ε_o. In praxis a value of ε_o equal to 10^{-2} has been found to be a good compromise between accuracy and the expenditure of computer time. Values less than 10^{-2} result in miniscule, if any, changes in the final results. The possibility of grossly erroneous solutions due to the inadvertant selection of too large an ε_o are precluded by the fact that in this case numerical instabilities arise which are severe enough to prevent convergence. Having the proper time step one derives new values of t, N_e, and T_e via:

$$t_{i+1} = t_i + \Delta t_i \qquad (3\text{-}51a)$$

$$(3\text{-}51b)\quad f(t_{i+1}) = f(t_i) + \frac{df(t_i)}{dt}\,\Delta t_i \;;\quad f \equiv N_e, T_e$$

Iteration of the above procedure continues until both N_e and T_e converge. An integration was usually terminated when, for a reasonable time step (e.g., 10^3 sec.), the change between successive temperature steps fell below 10^{-2}K. This decision was based on the empirical result that once this stage was reached the amplitude of the derivatives decayed rapidly.

Discussion of the Numerical Results

Integrations were performed for a range of initial conditions which should encompass those of any reasonable chromosphere. Gas temperature varied from 10^4K to 10^5K, while the grain temperature was taken to be 1500K. As it turns out the grain temperature is relatively unimportant except in determining the lowest allowable final gas temperature. The ratio N_G/N spanned the arbitrarily set logarithmic values -13.4 to -7.4 which for particles of radius .1μ and internal density 2.6 gm-cm^{-3} corresponds to mass ratios of 2.5×10^{-4} to 250. The grain characteristics correspond to those commonly suggested for interstellar and circumstellar grains.

Figure 3-1 depicts a plot of gas temperature versus time measured from the onset of cooling. Here one sees that the cooling progresses smoothly with a quasi-exponential dependence on time. Thus while equilibrium was not reached until 9.8×10^4 seconds had

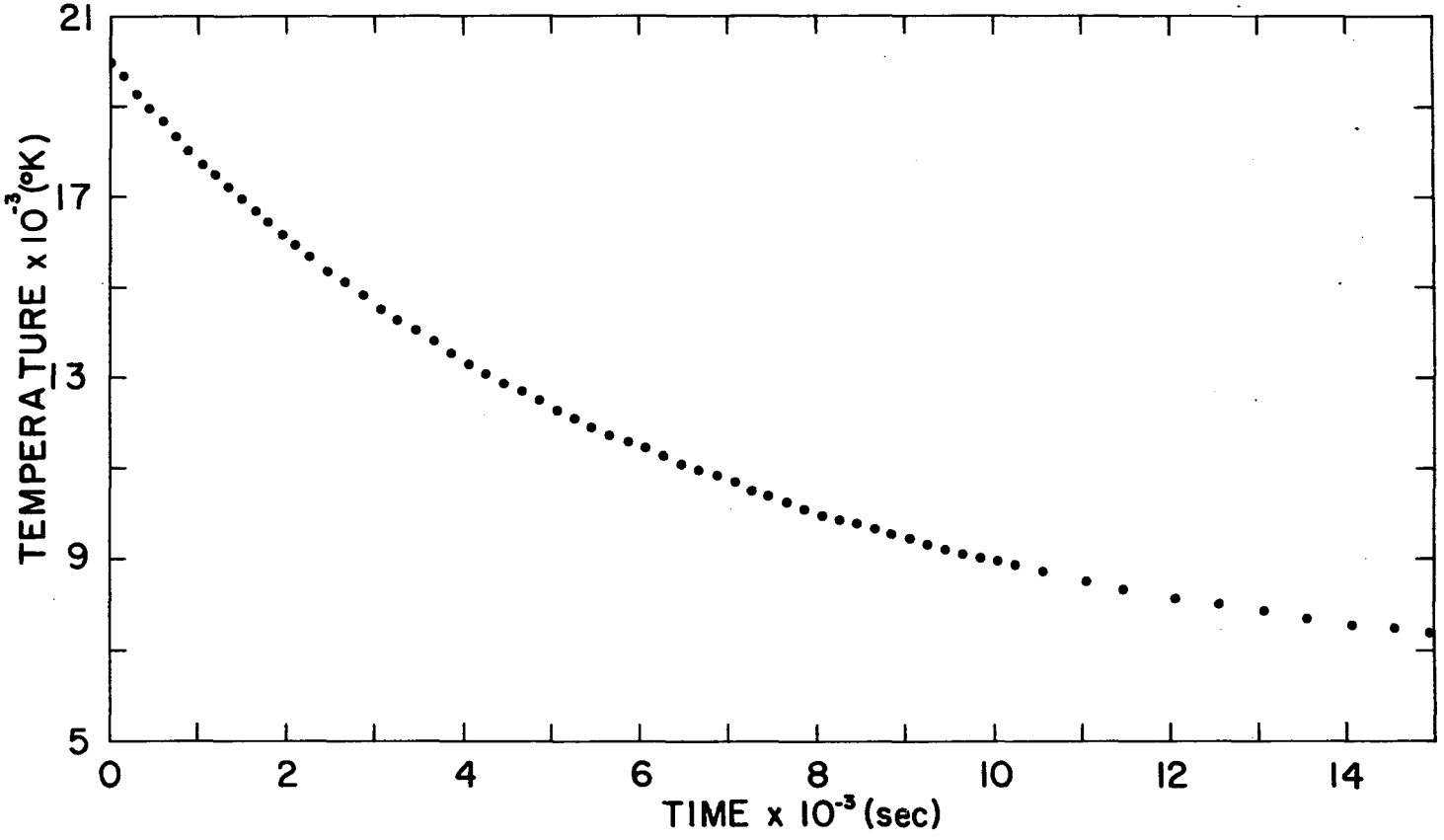

Fig. 3-1. Gas Temperature versus Time from the Onset of Cooling.

elapsed the bulk of the cooling took place within the first 10^4 seconds. Since all integrations produced cooling curves of this same basic form they will not be presented or discussed individually.

A plot of the final gas temperature versus N_G/N for initial gas temperatures of 20000 K and 40000 K may be found in Figure 3-2. From this figure one may ascertain the active domain of grain cooling. For logarithmic number ratios less than -12.4 the grains have only a small effect and indeed for $\log (N_G/N) < -13.4$ grains may be entirely neglected. In the range -12.4 to -7.4 the grains grow in importance with the final temperature being proportional to approximately the inverse .4 power of the number ratio over the logarithmically linear section. As larger number ratios are approached one notes that the curves tend to converge and that the gas temperature falls below the grain temperature in the vicinity of -8.4. For number ratios less than -7.4 the grains cool so effectively that independent of the initial temperature the final temperature attains its lower theoretical limit of .75 T_G predicted by equation (3-50b). One should note, however, that as one considers number ratios substantially larger than -7.4 the maxwellian distribution assumption begins to fail due to the decreased number of electron-electron collisions, and hence energy redistribution opportunities, between the occurrence of electron-grain collisions. This case will not be explored here since it certainly lies outside the range of plausible chromospheric states. Figure 3-2

Fig. 3-2. Logarithm of the Terminal Gas Temperature versus the Logarithm of the Grain to Gas Number Ratio.

Ambient Temperature	Symbol
40000 K	O
20000 K	Δ

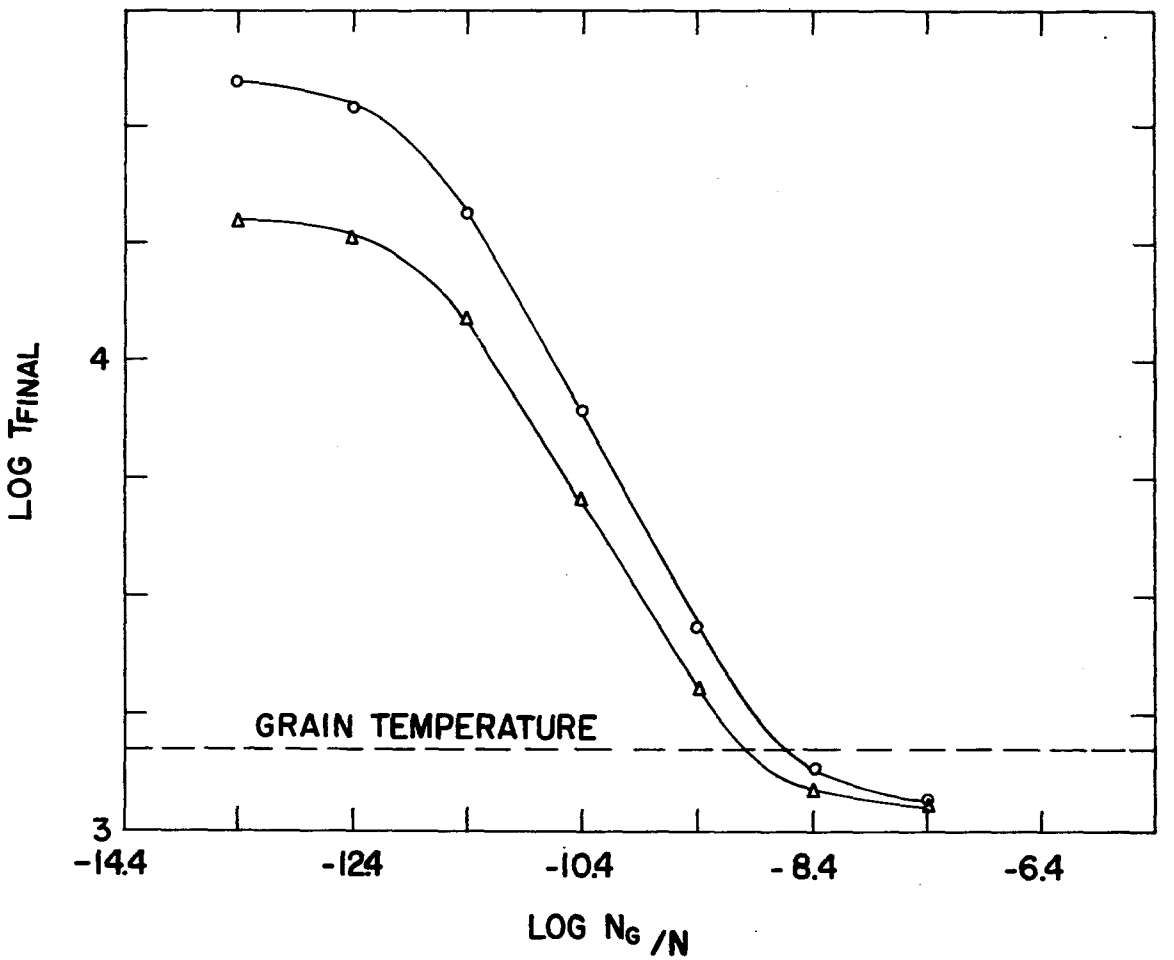

Fig. 3-2. Logarithm of the Terminal Gas Temperature versus the Logarithm of the Grain to Gas Number Ratio.

demonstrates that for sufficiently large number ratios the temperature of a chromosphere may be significantly reduced, thus staisfying one of the conditions for quenching chromospheric indicators.

The validity of the assumption neglecting bremsstrahlung will now be verified. Using the expression for bremsstrahlung losses given by Menzel (1937) and the grain loss rate term of (3-50b) transformed to units of ergs-sec^{-1}, the ratio of the loss rate due to bremsstrahlung to that arising from grain effects may be written:

$$(3\text{-}53)\quad \frac{L_B}{L_G} = \frac{3.4\times10^{-9}}{T_e}\,\frac{N_e}{N_G}$$

Assuming the ratio to be significant for values exceeding one-half and letting $T_e = 10^4$ K, one has:

$$\frac{N_e}{N_G}(3.4\times10^{-13}) = .5$$

but $N_e \simeq .5N$, therefore:

$$\frac{N_G}{N} \leq 3.4\times10^{-13} \quad \text{or} \quad \log\left(\frac{N_G}{N}\right) \leq -12.47$$

before bremsstrahlung losses compete with grain losses. However, Figure 3-2 indicates the ineffectiveness of grain cooling for such small number ratios and therefore the assumed unimportance of bremsstrahlung in this model is validated.

Figure 3-3 augments the previous figure by exhibiting the range of final temperatures corresponding to a domain of initial temperatures

Fig. 3-3. Logarithm of the Terminal Gas Temperature versus the Logarithm of the Initial Gas Temperature at Various Grain to Gas Number Ratios.

Log N_G/N	Symbol
- 7.4	□
- 8.4	θ
- 9.4	△
-10.4	O
-11.4	◇
-12.4	●

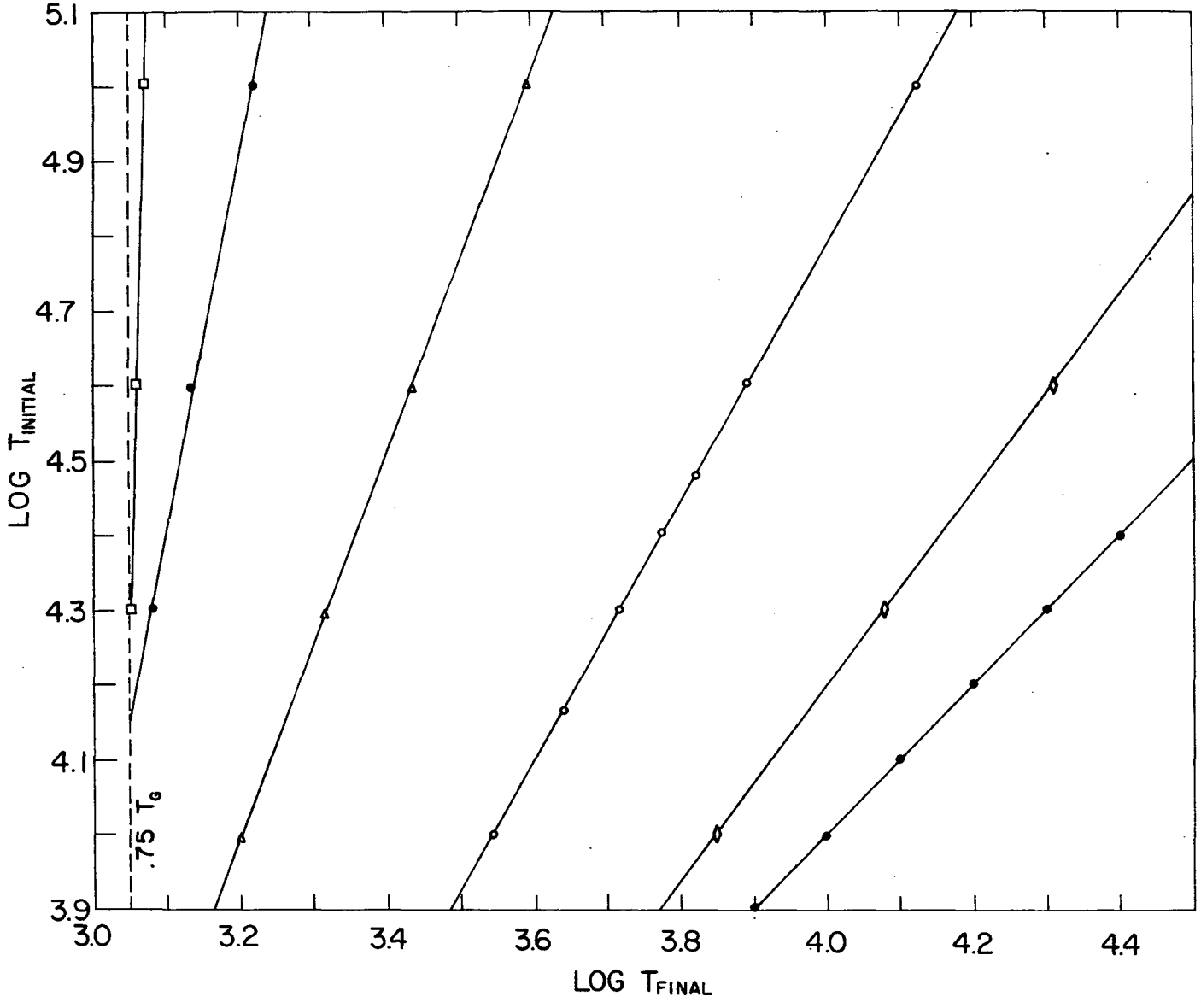

Fig. 3-3. Logarithm of the Terminal Gas Temperature versus the Logarithm.

from 10^4 K to 10^5 K for fixed values of $\log(N_G/N)$. The convergence effect previously noted is clearly seen; as the number ratio increases the final temperature becomes less dependent on the initial temperature. This effect arises from the ability of the high velocity particles to give up a majority of the gas' energy if a sufficient number of grains are present to accept it. A hot gas loses more energy than a cooler gas and thus tends to the same final temperature as the cool gas and may reach it in the limit of high number ratios. Because of this effect, any differences in temperature within the gas, and hence any temperature gradients, would be diminished by the presence of grains, thus satisfying the other condition for chromospheric quenching.

The relation between $\log (N_G)$ and the time required for the gas temperature to reach its minimum value, hereafter referred to as the cooling time (t_{cool}), may be found in Figure 3-4. As the number density of grains increases the cooling time decreases with the approximate functional dependence being:

$$(3\text{-}54) \quad t_{cool} \propto N_G^{-.75}$$

The values of the plotted relation may be understood by noting that they are approximately equal to the time needed for an average particle of the initial epoch to sustain a grain collision and yield up its energy. The collisional time may be written as:

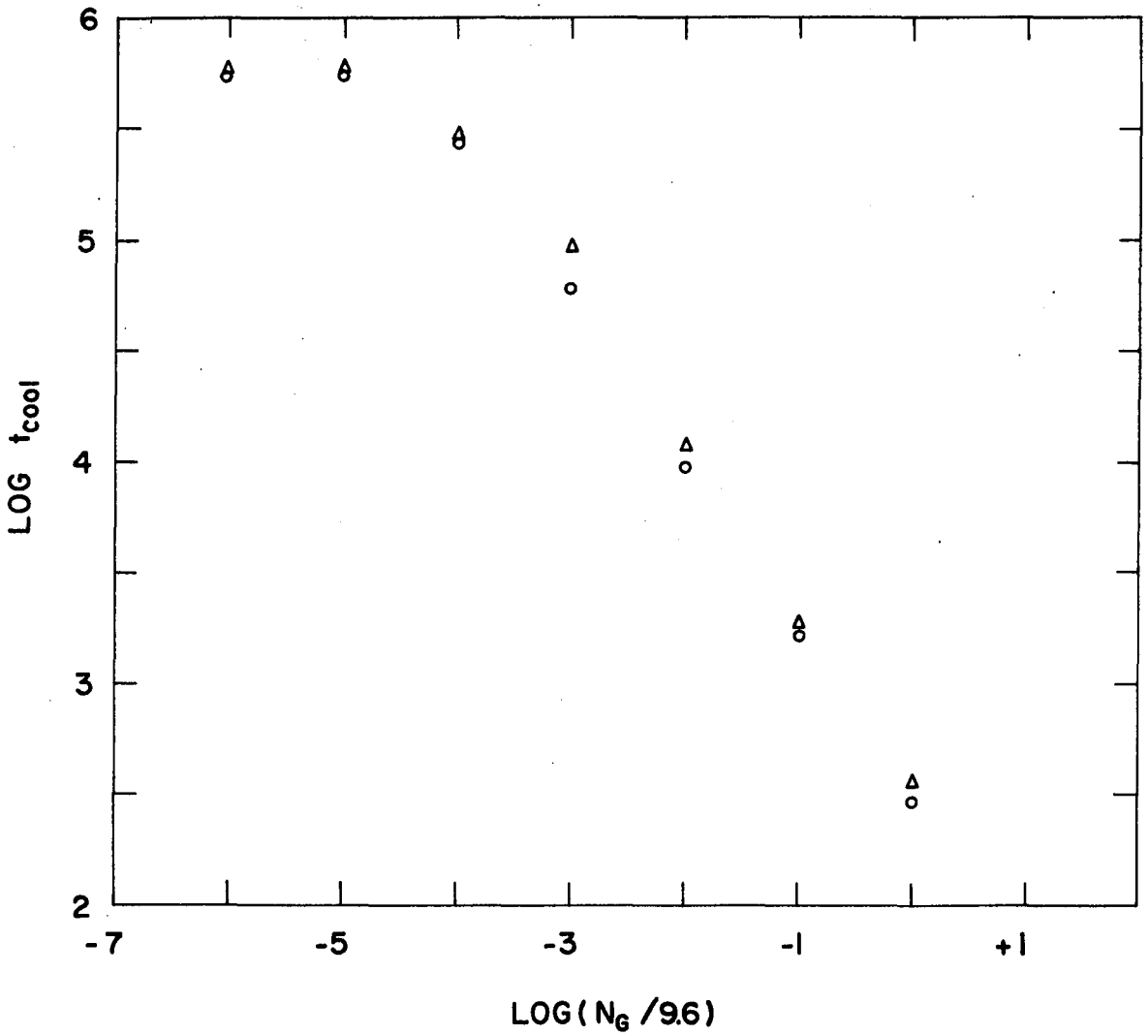

Fig. 3-4. Logarithm of the Cooling Time versus the Logarithm of the Grain Number Density.

Initial Temperature	Symbol
40000 K	O
20000 K	Δ

$$(3\text{-}55)\quad t_{coll} = \left(a_o N_G \left(\frac{3\,k\,T_o}{<\mu>}\right)^{1/2}\right)^{-1}$$

Some deviation from the collisional time arises for large number ratios but is due to the fact that initial epoch conditions are not maintained throughout the integration, and does not represent any inconsistency with the collisional interpretation. The fact that the exponent of N_G in the empirically determined cooling time relation (3-54) lies numerically close to -1.0, supports this argument. It should be noted that the cooling times, especially those associated with large temperature changes are far less than any time scale over which late type stars are observed to vary. Thus a star may be considered to be in a state of quasi-static equilibrium with any grain material it may possess.

While it has been demonstrated that under certain conditions grains may act to produce the changes necessary to the quenching of a chromosphere, the question of whether these conditions are realized in late star chromospheres will be deferred to the next chapter. By doing this the author will be able to invoke dynamical considerations to determine the expected values of the critical ratio N_G/N for various types of stars.

Conclusions

The foregoing analytical and numerical analysis allows one to state the following conclusions regarding the quenching of

chromospheres and the thermodynamic consequences of refractory grains in a cold plasma.

The visibility of chromospheric indicators may be obfuscated or entirely removed by a reduction of the maximum chromospheric temperature, a weakening of the temperature gradient, or a combination of the two. This result applies to resonance and non-resonance lines alike.

The temperature of a grain in close proximity to a late type star depends entirely upon the indigenous radiation field and the heating effects of a gas with chromospheric characteristics may be entirely neglected. A cursory investigation indicates that the same situation also exists in the more severe environment associated with a corona.

The introduction of solid refractory particles into a cold, pure hydrogen plasma may have profound consequences on its temperature provided the number ratio of grains to gas is sufficiently large. For $\log(N_G/N)<-13.4$ the grains are ineffective and the gas retains its ambient state. Over the range $-13.4<\log(N_G/N)<-7.4$ grain effects grow in importance with the final temperature being proportional to the inverse .4 power of N_G/N, while for $-7.4<\log(N_G/N)$ the grains dominate all other processes and the gas achieves a unique final temperature practically independent of its initial temperature. For moderately high grain densities this temperature

approximately equals T_G with the particle velocity distribution being maxwellian, but in the limit of very large number ratios energy redistribution by the gas ceases to occur and while the final temperature still equals T_G the gas velocity distribution becomes a delta function with an argument of $\left(\frac{3kT_G}{\mu}\right)^{1/2}$. If the required number ratios can be achieved in stellar chromospheres the above effects are sufficient to produce both a lessening of the maximum temperature, and a weakening of the temperature gradient, and thus may be able to account for the disappearance of chromospheric indicators in the presence of grains.

Cooling has been found to take place with an approximately exponential dependence on time. The time required to attain equilibrium decreases as the absolute number density of grains increases. The cooling time is, by order of magnitude, the time required for the average particle to collide with a grain and transfer its energy. In all cases of interest this quantity assumes a value less than 1.5×10^6 sec. and is thus smaller than the time scale of observed variations. This infers the existence of a quasi-static thermodynamic state between a star and its grains.

CHAPTER 4

GRAIN DYNAMICS AND STELLAR MASS LOSS

Since the work of Adams and McCormack (1935) it has been known that some red giants and supergiants show a doubling of their lowest term spectral lines, with one component being that normally formed in the photosphere and the other being anomalous and displaced blueward. Following an investigation of the binary α^1 Her, Deutsch (1956) was able to show that the violet-displaced cores are visible at large distances from the star and are to be associated with a secular instability causing the star to lose mass at a minimum rate of 3×10^{-8} $M_\odot$/yr. Subsequent work by Deutsch (1960), and Weymann (1962a) and a compilation of data by Gehrz and Woolf (1971) indicate that the mass loss phenomenon occurs frequently among late stars and that loss rates as large as 10^{-5} $M_\odot$/yr. may be realized.

Numerous attempts have been made to understand the physics of the loss mechanism. Rubbra and Cowling (1959) examined ejection by shock waves, evaporation, radiation pressure, and electromagnetic effects, concluding that none were likely explanations. An exhaustive study of solar wind type flows (Parker 1958, 1960a, b) has been made by Weymann (1960, 1962b) and Weymann and Chapman (1965) who

found that inconsistencies between theoretical predictions and observations make such flows implausible.

Upon the discovery of infrared excesses associated with α Ori (Low 1965) and other stars (Gillett, Low, and Stein 1968, and Woolf and Ney 1969) and the realization that such excesses could arise from grain material at large distances from the star, a number of investigators (Dyck 1970, Jennings 1970, Weymann 1971) privately suggested that mass loss may be induced by grains, while Woolf (1971) and Gehrz and Woolf (1971) independently came to the same conclusion. However, Gehrz, Weymann, and Woolf envisioned creation of grains in a region well removed from the surface of the star, while Dyck and Jennings, citing inorganic grain formation calculations by Fix (1970, 1971), argued for grain production in the stellar atmosphere with subsequent ejection by radiation pressure to large distances.

The design of the following discussion will be to demonstrate the feasibility of grain caused mass loss when grains are produced at or below the surface of a star. The details of the flow will then be used to predict observables and to comment on the possible effect of mass loss on chromospheric structure. This analysis will be carried out within the framework of the following assumptions.

1. The model consists of two components, grains and gas, coexisting in a steady state flow.

2. The flow may be described hydrodynamically and is characterized by an isotropic gas pressure at all points. This is tantamount to stating that the gas mean free path always remains much smaller than the characteristic scale for flow changes. Parker (1960a) and Weymann (1960) have found this to be true in the flows they considered.
3. Both the gas and grain flows are assumed to be spherically symmetric, and rotation effects are neglected. Indeed, one finds no detectable rotation in non-binary M and K giants (Huang and Struve 1960) and one expects rotation to be far less than the detection limit on the basis of evolutionary arguments.
4. The grains remain constant in size. Fix (1971) has shown that grains fully deplete the concentrations of their constituents while in the region of formation and thus accretion at later stages seems unlikely. The results of Chapter 3 demonstrate that grains do not get hot enough to evaporate.
5. Any contribution to the outward force by radiation pressure acting on the gas, particularly molecules, is neglected. Since this would aid rather than hinder the grains, its exclusion may be viewed as a worst case situation.

6. The loss of energy to the gas by thermal radiation and recombination is neglected. Weymann (1960) has shown that such losses serve to accelerate the flow in the subsonic regime and thus one has another worst case assumption. The gas temperature will be assumed to be isothermal at the base of the flow, change to an adiabatic law at some specified distance, and finally become isothermal again when its value falls to 125 K.
7. The star radiates as a black body.
8. Magnetohydrodynamic effects are assumed to be negligible.

The Equations

Continuity and Momentum

Generally applicable equations of continuity and momentum for a perfect fluid may be written (c.f., Sabersky and Acosta 1964) as:

$$(4\text{-}1a)\quad \frac{\partial \rho}{\partial t} + \nabla \cdot (\rho \bar{v}) = 0$$

$$(4\text{-}1b)\quad \frac{\partial \bar{v}}{\partial t} + (\bar{v} \cdot \nabla)\bar{v} = -\frac{1}{\rho}\nabla P + \sum_{j=1}^{n} \bar{f}_j$$

where ρ is the mass density and the f_i's are body forces per unit mass. Imposing the restrictions that the flow be radial, spherically symmetric, and in a steady state, equations (4-1a, b) become:

$$(4\text{-}2) \quad 4\pi\rho_i v_i R^2 = \lambda_i \qquad i = gr,\ g$$

$$(4\text{-}3) \quad v_i \frac{dv_i}{dR} = -\frac{1}{\rho_i}\frac{dP}{dR} + \sum_{j=1}^{n} f_j$$

These equations apply to each flow component individually. V_{gr} and V_g are, respectively, the grain and gas velocities in the reference frame of the star, while λ_{gr} and λ_g are the mass loss rates.

Consider the explicit form of the specific body forces. Gravity acts on the gas and grains alike and its acceleration may be written as:

$$(4\text{-}4) \quad f_{GRAV_{g,gr}} = -GM_*/R^2$$

where M_* is the star's mass. The force on the gas due to momentum transfer in gas-grain collisions may be derived in the following way. The volume of gas swept out by a grain in $cm^3\text{-}sec^{-1}$ is:

$$(4\text{-}5) \quad a_o V_R$$

where V_R is the velocity of the grains relative to the gas, $(V_{gr} - V_g)$, and will be positive by virtue of the assumptions of the model. The number of gas-collisions per second per grain may be written as:

$$(4\text{-}6) \quad (\rho_g/\mu_g)\, a_o V_R$$

The average momentum transferred to the gas per gas-grain collision may be expressed as:

$$(4\text{-}7) \quad \mu_g V_R$$

assuming that the average gas particle's post collision velocity equals the grain velocity. Combining equations (4-6) and (4-7) one may write the momentum transfer rate by grains to the gas in a volume dV:

$$(4\text{-}8)\quad \left(\frac{dP}{dt}\right)_{gr} = a_o V_R^{\,2} \rho_g N_{gr} dV$$

or in acceleration units

$$(4\text{-}9)\quad f_{(g\text{-}gr)g} = \frac{a_o V_R^{\,2} \rho_{gr}}{\mu_{gr}}$$

The retarding force of the gas upon the grains may be written as the negative of equation (4-8), viz.:

$$(4\text{-}10)\quad \left(\frac{dP}{dt}\right)_{gr} = - a_o V_R^{\,2} \rho_g N_{gr} dV$$

which upon conversion to acceleration units becomes:

$$(4\text{-}11)\quad f_{(g\text{-}gr)_{gr}} = - \frac{a_o V_R^{\,2} \rho_{gr}}{\mu_{gr}}$$

The acceleration of a grain due to stellar radiation may be derived from the following considerations. Let L_* represent the luminosity of the star, $\langle h\nu \rangle$ the energy of the average photon and assume that the radiation pressure efficiency factor, Q_{PR} (van de Hulst 1957), is a constant with the value of $Q_{\nu_{PR}}$ at the stellar radiation maximum. Then the number of photons intercepted per second by a grain of cross section a_o at a distance R from the star will be given by:

$$(4\text{-}12)\quad \frac{L_* Q_{PR} a_o}{\langle h\nu \rangle 4\pi R^2}$$

The average momentum transferred to a grain per photon collision may be expressed as:

$$(4\text{-}13)\quad \frac{\langle h\nu \rangle}{c}$$

From Mie theory one finds,

$$(4\text{-}14)\quad Q_{PR} = Q_{EXT} - Q_{SCA} \langle \cos\theta \rangle,$$

where θ is the scattering angle. Since $\langle \cos\theta \rangle$ indicates the average direction of momentum transport by a recoiling photon, Q_{PR} is a measure of the net outward momentum transferred to a grain per photon collision. The Q values were supplied to the author by Shawl (1971) and are the result of calculations based on the Mie theory. Equations (4-12) and (4-13) may be combined to yield the force on a grain due to radiation.

$$(4\text{-}15)\quad \left(\frac{dP}{dt}\right)_{gr} = \frac{L_* Q a_o}{4\pi R^2 c}$$

or in acceleration units:

$$f_{RAD_{gr}} = \frac{L_* Q a_o}{4\pi R^2 c \mu_{gr}}$$

In summary the total body forces acting on the gas and the grains are, respectively:

$$(4\text{-}16a)\quad \Sigma f_{gas} = -\frac{GM_*}{R^2} + \frac{a_o V_R^2 \rho_{gr}}{\mu}$$

$$(4\text{-}16b)\ \Sigma f_{grains} = \frac{L_* Q a_o}{4\pi R^2 c\, \mu_{gr}} - \frac{GM}{R^2} - \frac{a_o V_R^2 \rho_{gr}}{\mu_{gr}}$$

To complete the transformation of the general equations to ones applicable to the problem at hand one must examine the form of the pressure gradient term. Assuming a perfect gas one has:

$$(4\text{-}17)\quad P = \frac{\rho_g kT}{\mu_g}$$

It is noted that if one defines T in the following way, i.e.,

$$(4\text{-}18)\quad T = T_e + \left(\frac{\mu_g V_T^2}{3k}\right) \equiv T_e + T_T$$

where $T_e \equiv$ gas kinetic temperature

$V_T \equiv$ gas turbulent velocity

$T_T \equiv$ fictitious turbulent temperature

then (4-17) may account for the pressure due to fully developed isotropic turbulence, as well as gas kinetic motion. It does not allow for anisotropic turbulence, however, and such turbulence will not be considered in this model. The assumption will be made that the turbulent temperature obeys the same adiabatic law as the kinetic temperature. Differentiating (4-17) with respect to radial position yields:

$$(4\text{-}19)\quad \frac{dP}{dR} = \frac{k}{\mu_g}\left(T\frac{d\rho_g}{dR} + \rho_g \frac{dT}{dR} - \frac{\rho_g T}{\mu_g}\frac{d\mu_g}{dR}\right)$$

Dividing by $\frac{-1}{\rho_g}$ and rearranging produces:

$$(4\text{-}20)\quad -\frac{1}{\rho_g}\frac{dP}{dR} = -\frac{k}{\mu_g}\left(T\frac{d\ln\rho_g}{dR} + \left(1-\frac{T}{\mu_g}\frac{d\mu_g}{dT}\right)\frac{dT}{dR}\right)$$

Employing equations (4-16a, b) and (4-20) equations (4-2) and (4-3) may be written separately for the gas and grains in the following form:

GAS

$$(4\text{-}21a)\quad 4\pi\rho_g V_g R^2 = \lambda_g$$

$$(4\text{-}21b)\quad V_g\frac{dV_g}{dR} = -\frac{k}{\mu_g}\left(T\frac{d\ln\rho_g}{dR} + \left(1-\frac{T}{\mu_g}\frac{d\mu_g}{dT}\right)\frac{dT}{dR}\right) - \frac{GM}{R^2} + \frac{a_o V_R^2 \rho}{\mu_{gr}}$$

GRAINS

$$(4\text{-}22a)\quad 4\pi\rho_{gr} V_{gr} R^2 = \lambda_{gr}$$

$$(4\text{-}22b)\quad V_{gr}\frac{dV_{gr}}{dR} = \left(\frac{L_* Q a_o}{4\pi c\,\mu_{gr}} - GM\right)\frac{1}{R^2} - \frac{a_o V_R^2 \rho_{gr}}{\mu_{gr}}$$

Substituting the continuity restrictions for the densities in the equations of motion and rearranging, one may write two coupled, nonlinear, first order differential equations completely describing the flow, viz.,

$$(4\text{-}23a)\quad \frac{dV_g}{dR} = \frac{V_g}{\left(V_g^2 - \frac{kT}{\mu_g}\right)}\left[\frac{2kT}{\mu_{gr}} - \frac{k}{\mu_g}\left(1-\frac{T}{\mu_g}\frac{d\mu_g}{dT}\right)\frac{dT}{dR} - \frac{GM}{R^2} + \frac{a_o V_R^2 \lambda_g}{4\pi R^2 V_g\,\mu_g}\right]$$

$$(4\text{-}23b)\ \frac{dV_{gr}}{dR} = \frac{1}{V_{gr}R^2}\left(\frac{L_* Q a_o}{4\pi c \mu_{gr}} - GM - \frac{a_o V_R^2 \lambda_g}{4\pi \mu_{gr} V_g}\right)$$

In the adiabatic flow region T and dT/dR are given by the following relations:

$$(4\text{-}24a)\ T = \left(\frac{T_o}{\rho_{g_o}^{2/3} \mu_{g_o}}\right) \rho_g^{2/3} \mu_g$$

$$(4\text{-}24b)\ \frac{dT}{dR} = \left(\frac{T_o}{\rho_{g_o}^{2/3} \mu_{g_o}}\right)\left(\rho_g^{2/3} \frac{d\mu_g}{dR} + 2/3\ \frac{\mu_g}{\rho_g^{1/3}} \frac{d\rho_g}{dR}\right)$$

where $T_o, \rho_{g_o}, \mu_{g_o}$ describe the gas at the point of transition from the isothermal region to the adiabatic one.

Properties of the Equations of Motion

While equations (4-23a, b) can not be solved in closed form they may be manipulated to demonstrate a number of properties of grain driven mass loss. From (4-23b) one sees that for the grains to be driven outward the following condition must be satisfied.

$$(4\text{-}25)\ \frac{L_* Q a_o}{4\pi c \mu_{gr}} - GM > 0$$

The stellar properties needed to evaluate (4-25) are taken from Allen (1963) and Schmidt-Kaler (1965) and are presented in Table 4-1, the first six columns of which are obvious. The seventh column contains the logarithm of equation (4-25) under the assumption that the grains

TABLE 4-1. Physical Stellar Characteristics.

Spectral Type	Log (L/L⊙)	Log (M/M⊙)	Log (R/R⊙)	Log g	Log T_{eff}	$\text{Log}\left(\frac{LQa_o}{4\pi c\mu_g} - GM\right)$
			SUPERGIANTS			
KO	4.00	1.18	2.31	.94	3.62	28.758
K5	4.31	1.19	2.62	.42	3.53	29.065
MO	4.5	1.22	2.70	.25	3.45	29.268
			GIANTS			
KO	2.00	.57	1.21	3.08	3.62	25.973
K5	2.31	.68	1.38	2.32	3.54	26.756
MO	2.20	.70	1.62	1.89	3.48	26.420
M5	3.20	.90	2.20	.94	3.40	27.914

have a radius of .07μ and an internal density of 2.59 gm/cm^3. From this column one sees that grains are lost to giants and supergiants alike. Caution must be exercised with the giants, however, since any appreciable, unfavorable change in grain characteristics, e.g., a smaller Q_{PR}, could result in the grains sinking and the preclusion of mass loss.

Consider the state of affairs on the main sequence. Using a relation given by Harris, Strand, and Worley (1963) the mass-luminosity relation for dwarfs may be written as:

$$(4\text{-}26)\quad L = 4.85 \times 10^{-59} M^{2.76}$$

Substituting (4-26) for L in (4-25) yields:

$$(4\text{-}27)\quad M\left(\frac{4.85 \times 10^{-59} M^{1.76} Qa_o}{4\pi c \mu_{gr}} - G\right) > 0$$

$$(4\text{-}28)\quad M > \left(\frac{4\pi c \mu_{gr} G}{4.85 \times 10^{-59} Qa_o}\right)^{.568}$$

Upon substitution of the grain parameters one obtains:

$$(4\text{-}29)\quad M > 1.36 \times 10^{34}\ \text{gm} = 6.85\ M_\odot$$

Thus one would not expect grains, if they existed, to be ejected from dwarfs later than approximately B6, which is consistent with Zappala's (1969) negative results for polarization observations of dwarfs and justifies the fifth star selection criterion of Chapter 2.

Equation (4-23b) also furnishes information on the required value of the gas-grain relative velocity, upon consideration of the consequences of an imbalance of the forces acting on a grain. Assume that the grain retarding force suddenly vanishes, allowing one to write:

$$(4\text{-}30)\quad V_{gr}\frac{dV_{gr}}{dR} = [L\text{-}GM]\frac{1}{R^2}$$

where $L \equiv \frac{L_* Q a_o}{4\pi c \mu_{gr}}$. Integrating over a path from R_1 to R_2 and letting the velocity at R_2 be expressed as υV_1, where V_1 is the velocity at R_1 and υ is a constant, one has:

$$(4\text{-}31)\quad \frac{V_1^2}{2}(\upsilon^2-1) = \frac{L\text{-}GM}{R_1 R_2}(R_2-R_1)$$

If one defines υ to be a significant change in velocity then (R_1-R_2) may be considered to be the correction distance, or that distance which the grains require to reestablish a quasi-balance of forces. Letting $\delta \equiv (R_2-R_1)$ and assuming $\delta << R$, which will be verified a posteriori (4-31) becomes:

$$(4\text{-}32)\quad \frac{V_1^2}{2}(\upsilon^2-1) = \frac{L\text{-}GM}{R_1^2}\delta$$

or upon reorganizing:

$$(4\text{-}33)\quad \delta = \frac{V_1^2(\upsilon^2-1)}{2(L\text{-}GM)}$$

Using physical parameters for an MO I star from Table 4-1 and letting $V_1 = 10^4$ cm-sec^{-1} and $\nu = 2$ one has:

$$(4\text{-}34)\quad \delta = 9.7 \times 10^4 \text{ cm}$$

Thus a state of unbalanced forces on a grain results in a return to a quasi-balanced state in a correction distance much less than any characteristic scale of the flow. Note also that $\delta << R_1$. The above circumstance may be employed by demanding that the grain flow proceed at the maximum allowed relative velocity, thus allowing one to rewrite (4-23b) as:

$$(4\text{-}35)\quad (\text{L-GM}) - \frac{a_o V_R^2 \lambda_g}{4\pi\mu_{gr} V_g} = 0$$

It should be noted that this assumption remains valid at all points in the flow since with the grains serving as the sole propulsive agent no mechanism exists for accelerating the gas and decoupling it from the grains.

Equation (4-35) may be solved to yield and a useful expression relating the grain velocity to the gas velocity at any point in the flow. Recalling that $V_R \equiv (V_{gr} - V_g)$ one may write:

$$(4\text{-}36)\quad V_{gr}^2 - 2V_{gr}V_g + V_g^2 - V_g c_1 = 0$$

where $c_1 \equiv \dfrac{4\pi(\text{L-GM})\mu_{gr}}{a_o \lambda_g}$, a constant of the flow. Solving (4-36) for V_{gr} results in the following relation:

$$(4\text{-}37)\quad V_{gr} = V_g\left(1+\sqrt{\frac{c_1}{V_g}}\right)$$

Parker (1958, 1960a, b) has demonstrated the importance of the transsonic point in hydrodynamic flows and the fact that a unique solution exists which will yield a finite velocity derivative at the sonic point and acceptable outer boundary conditions. Single component subsonic flows are prohibited since they result in terminal pressures which are unbalanced by any known interstellar pressure, while solutions which become supersonic too quickly are unacceptable since they are double valued. The sonic point condition for the flow under consideration may be obtained in the following way. Within the assumptions of the model the gas temperature may always be written in the form:

$$(4\text{-}38)\quad T = \phi \mu_g \rho_g^{\,n}$$

where ϕ is a constant and n = 0 in isothermal regions and 2/3 in the adiabatic zone. Differentiating (4-38) with respect to R yields:

$$(4\text{-}39)\quad \frac{dT}{dR} = \phi\left[\rho_g^{\,n}\frac{d\mu_g}{dR} + n\mu_g\rho_g^{\,n-1}\frac{d\rho_g}{dR}\right]$$

or upon rearranging

$$(4\text{-}40)\quad \frac{dT}{dR}\left(1-\phi\rho_g^{\,n}\frac{d\mu_g}{dT}\right) = n\mu_g\rho_g^{\,n-1}\frac{d\rho_g}{dR}$$

Using the continuity relation and (4-38), equation (4-40) becomes:

$$(4\text{-}41)\quad \frac{dT}{dR} = -nT\left(\frac{2}{R}+\frac{1}{V_g}\frac{dV_g}{dR}\right)\frac{1}{\zeta}$$

where $\zeta \equiv 1 - \frac{T}{\mu_g}\frac{d\mu_g}{dT}$. Substituting equation (4-41) into (4-23a) results in the following expression:

$$(4\text{-}42)\quad \frac{dV_g}{dR}\left(\frac{V_g^2 - \frac{kT}{\mu_g}}{V_g}\right) = \frac{2kT}{\mu_g R} + \frac{k}{\mu_g}\left[\frac{nT\left(\frac{2}{R} + \frac{1}{V_g}\frac{dV_g}{dR}\right)}{\zeta}\right]\zeta - \frac{GM}{R^2} + \frac{a_o V_R^2 \lambda_{gr}}{4\pi R^2 V_{gr}\mu_{gr}}$$

whereupon one may write:

$$(4\text{-}43)\quad \frac{dV_g}{dR}\left(\frac{V_g^2 - S^2}{V_g}\right) = (n+1)\frac{2kT}{\mu_g R} - \frac{GM}{R^2} + \frac{a_o V_R^2 \lambda_{gr}}{4\pi R^2 V_{gr}\mu_{gr}}$$

where S equals $\sqrt{(n+1)kT/\mu_g}$ and is proportional to the local sound speed. From this one sees that the portion of the left hand term in parenthesis vanishes when the gas velocity equals S and that the velocity derivative remains finite if and only if the right hand side vanishes simultaneously. Thus the sonic point condition which the flow must satisfy may be written as:

$$(4\text{-}44)\quad (n+1)\frac{2kT}{\mu_g R} - \frac{GM}{R^2} + \frac{a_o V_R^2 \lambda_{gr}}{4\pi R^2 V_{gr}\mu_{gr}} = 0$$

Information regarding the ratio of gas mass loss to grain mass loss required to satisfy the sonic condition may be extracted from equation (4-44) in the following manner. Neglecting the term $(n+1)\frac{2kT}{\mu_g R}$, which for temperatures as large as 10000K has a value

much smaller than the other terms, (4-44) may be rewritten as:

$$(4\text{-}45)\quad \frac{GM}{R^2} = \frac{a_o V_R^2 \rho_{gr}}{\mu_{gr}}$$

But from (4-35) one has:

$$(4\text{-}46)\quad \frac{a_o V_R^2 \rho_{gr}}{\mu_{gr}} = \frac{\rho_{gr}}{\rho_g}\left(\frac{L\text{-}GM}{R^2}\right)$$

therefore (4-45) may be expressed as:

$$(4\text{-}47)\quad \frac{\rho_{gr}}{\rho_g}(L\text{-}GM) = GM$$

But $\rho_{gr}/\rho_g = \frac{\lambda_{gr}}{\lambda_g}\frac{V_g}{V_{gr}}$ where V_g and V_{gr} are evaluated at the sonic point. This allows one to write:

$$(4\text{-}48)\quad \frac{\lambda_g}{\lambda_{gr}} = \left(\frac{L\text{-}GM}{GM}\right)\frac{V_g}{V_{gr}}$$

which takes the following form upon employing equation (4-37):

$$(4\text{-}49)\quad \frac{\lambda_g}{\lambda_{gr}} = \left(\frac{L\text{-}GM}{GM}\right)\left(\frac{V_g^{\frac{1}{2}}}{V_g^{\frac{1}{2}} + c_1^{\frac{1}{2}}}\right)$$

Since the λ's are constant the ratio obtained from equation (4-49) may be applied at any point in the flow. It is noted that the term $V_g^{\frac{1}{2}}(V_g^{\frac{1}{2}} + c_1^{\frac{1}{2}})$ assumes a value close to unity for all flows of interest, and that the ratio depends mainly on physical stellar parameters.

Numerical Solution of the Equations of Motion

To summarize the foregoing analysis, one may write the following system of equations

$$(4\text{-}50a)\quad \frac{dV_g}{dR}\left(\frac{V_g^2 - (n+1)\frac{kT}{\mu_g}}{V_g}\right) = (n+1)\frac{2kT}{\mu_g R} - \frac{GM}{R^2} + \frac{a_o c_1 \lambda_{gr}}{4\pi \mu_{gr} R^2 \left(1+\left(\frac{c_1}{V_g}\right)^{\frac{1}{2}}\right)}$$

$$(4\text{-}50b)\quad V_{gr} = V_g\left(1+\left(\frac{c_1}{V_g}\right)^{\frac{1}{2}}\right)$$

$$(4\text{-}50c)\quad \lambda_i = 4\pi R^2 \rho_i V_i \qquad i = g, gr$$

$$(4\text{-}50d)\quad V_R = \left[\frac{\mu_{gr}(L-GM)}{a_o \rho_g}\right]^{\frac{1}{2}}$$

$$(4\text{-}50e)\quad \frac{\lambda_g}{\lambda_{gr}} = \frac{V_g \rho_g}{V_{gr}\rho_{gr}} = \left(\frac{L-GM}{GM}\right)\left(\frac{V_g^{\frac{1}{2}}}{V_g^{\frac{1}{2}} + c_1^{\frac{1}{2}}}\right) \Bigg| \text{ sonic point}$$

These equations may be treated as an initial value problem with the following quantities being needed to begin the integration.

1. Stellar parameters:

Stellar luminosities, masses, and radii are taken from Table 4-1. The gas density at the top of the atmospheric convection zone, where the flow calculations begin, takes the value derived by Carbon (1969, 1970). The initial gas temperature and the distance to which the flow remains isothermal remain as variables to be specified.

2. Grain parameters

The internal grain density and index of refraction are fixed for all models with values of 2.59 gm-cm^{-3} and 1.65 + 10^{-5}i respectively, which are average for silicates. The grain radius and its accompanying Q_{PR}, and the initial external grain density are left as free parameters to be specified.

Having the fixed and variable initial quantities one may proceed with a solution. The first step involves the determination of the initial gas and grain velocities which may be done in the following way. Since the densities are known, equations (4-50d, e) may be used, respectively, to ascertain the gas-grain velocity difference and ratio; quantities which are then combined to yield the individual velocities. It should be noted that the term $V_g^{\frac{1}{2}}/\left(V_g^{\frac{1}{2}} + c_1^{\frac{1}{2}}\right)$ in (4-50e) is assumed to be equal to one at this point. Next calculations of the gas temperature and the mean molecular weight are performed. One now has sufficient information to evaluate the gas velocity derivative. This in turn determines the magnitude of the radial increment through the imposed condition that the change in the logarithm of the velocity not exceeded some value ε_1. Setting ε_1 equal to 5 x 10^{-3} has been found to produce satisfactory results; values appreciably greater than this precipitate numerical instabilities while smaller ones produce no change in the final results. Having the required radial step, flow parameters at the new location may be computed via:

$$(4\text{-}51a)\quad R_{j+1} = R_j + \Delta R_j$$

$$(4\text{-}51b)\quad V_{g_{j+1}} = V_{g_j} + \left(\frac{dV_g}{dR}\right)_j \Delta R_j$$

$$(4\text{-}51c)\quad V_{gr_{j+1}} = V_{g_{j+1}}\left(1 + \sqrt{\frac{c_1}{V_{g_{j+1}}}}\right)$$

$$(4\text{-}51d)\quad \rho_{i_{j+1}} = \lambda_i / 4\pi R^2 V_{i_{j+1}} \qquad i = g, gr$$

During each integration step the gas velocity is tested to see whether it exceeds the value of S. If it remains smaller than S one repeats the above process, sans the determination of the initial velocities. When it exceeds S however, the flow parameters are examined to see if they satisfy the sonic condition (equation (4-44)) within the allowed upper limit set by the term neglected in deriving (4-50d), i.e., $(n+1)2kT/\mu_g R$. In general, the sonic condition will not be satisfied due to the deletion of the term $V_g^{\frac{1}{2}}/\left(V_g^{\frac{1}{2}} + c_1^{\frac{1}{2}}\right)$ in calculating the initial gas and grain velocities. However, one does expect the solution to be close to the required one and thus the gas velocity at the sonic point may be used to evaluate this term which then may be employed to obtain new values of the initial velocities. Iteration of this procedure continues until the flow satisfies the sonic condition. In praxis it has been found that two to three iterations will produce an acceptable solution with sonic point values substantially less than the

allowed upper limit. Erroneous solutions due to the use of incorrect starting velocities are discounted by the great sensitivity of the sonic point to deviations from the allowed solution. For initial velocities which are too small the flow remains subsonic at all distances while flows in which the velocities are too large either fail to fall below the upper limit of the sonic condition or suffer fatal numerical instabilities.

Once a solution passes through the sonic point integration continues to a distance of 10^8 stellar radii whereupon the calculation terminates. This distance exceeds that which a fast flow could attain in the time required to deplete a major fraction of the star's mass and hence to violate the steady state assumption. Also at this point the flow would be dominated by the interstellar medium.

Finally, each flow must satisfy an outer boundary condition which demands that the gas pressure assume an acceptably low value at large distances (Parker 1960a). This stricture may be met by the gas exceeding the escape velocity, for it will then arrive at infinity with finite velocity, zero density, and hence zero pressure. All solutions acceptable at the sonic point have been found to exceed the escape velocity.

Auxiliary Equations: Line Profiles and Infrared Excesses

Using the flow data from the equation of motion solution one may obtain information regarding the expected appearance of an optically thin circumstellar line profile and the amount of infrared radiation arising from the grain field. Consider a radiation field of initial intensity I_o passing through an optically thin absorbing medium which does not emit significant amounts of radiation in the frequency range of interest and which moves radially with respect to the observer. In this case the change in intensity sustained by the radiation as it traverses the medium will be given by:

$$(4\text{-}52)\quad \Delta I(\nu_i) = I_o(\nu_i)\,\Delta\tau_i$$

where i indicates that a particular frequency is being considered. But $\Delta\tau_i$ may be expressed as:

$$(4\text{-}53)\quad \Delta\tau_i = N_{g_i}\,\alpha\,\Delta R_i$$

where N_g is the number density of gas particles moving such that their absorption maximum occurs at ν_i, ΔR_i is the distance over which such particles exist, and α is the radiation cross section per particle. Here it will be assumed the α has a negligible intrinsic width and hence material with an absorption maximum at one frequency will not contribute to absorption at other frequencies. Using the chain rule (4-53) may be rewritten as:

$$(4\text{-}54)\quad \Delta\tau_i = N_{g_i}\,\alpha\left(\frac{\Delta R}{\Delta V}\right)_i \Delta V_i$$

However from the integration one has the imposed restriction that $\frac{\Delta V_i}{V_i} = \mathcal{E}_1$ allowing one to write:

$$(4\text{-}55)\quad \Delta\tau_i = N_{g_i}\,\alpha V_i \mathcal{E}_1 \Big/ (\Delta V/\Delta R)_i$$

whereupon (4-52) becomes:

$$(4\text{-}56)\quad \Delta I_i = I_o \alpha \mathcal{E}_1 N_{g_i} V_i \Big/ (\Delta V/\Delta R)_i$$

Due to the nature of α equation (4-56) describes the absorption arising from a particular outflow velocity and hence from a particular integration step. Assuming that $I_o(\nu_i)$ remains constant over the frequency range of interest and letting N_{go}, V_o be assigned to the location of maximum absorption one may write an expression for a normalized line profile in the following way.

$$(4\text{-}57a)\quad \frac{\Delta I(\lambda)}{\Delta I_{max}} = \frac{N_{g_i} V_i}{(\Delta V/\Delta R)_i} \Big/ \frac{N_{g_o} V_o}{(\Delta V/\Delta R)_o}$$

$$(4\text{-}57b)\quad \lambda = \lambda_o (1 - V_i/c)$$

where $\lambda_o \equiv$ rest wavelength and the sign indicates that the motion is toward the observer.

The appearance of an optically thick gas line will not be considered since it requires a detailed solution of the transfer equation and the equations of statistical equilibrium.

In the case of emission from the grain field one may have an optically thick or an optically thin situation depending on the frequency

range considered. For the optically thick case it will be assumed that the emergent flux is given by the Eddington-Barbier relation, viz:

$$(4\text{-}58)\quad F_\nu(o) = \pi S_\nu(\tau_\nu = 2/3)$$

where S_ν is assumed to be $B_\nu(T_{gr})$. Using (4-58) the monochromatic luminosity may be written as:

$$(4\text{-}59)\quad L_\nu = 4\pi^2 R_{2/3} B_\nu(T_{gr})$$

where $R_{2/3}$ is the radial position of the $\tau = 2/3$ level. Employing equation (3-31) and substituting for $B_\nu(T_{gr})$ the luminosity emitted over a frequency interval $\Delta\nu$ may be expressed as:

$$(4\text{-}60)\quad L_{\nu,\,\nu+\Delta\nu} = 2h\nu^3 \left(\frac{2\pi R_{2/3}}{c}\right)^2 \left(\mathrm{EXP}\left(\frac{\sqrt{2h\nu}}{\mathcal{R}^{\frac{1}{2}} T_*}\right) - 1\right)^{-1} \Delta\nu$$

For purposes of calculation $\frac{\Delta\nu}{\nu}$ will be set equal to .02 in order to allow comparison between the author's results and those of Gillett, Low, and Stein (1968). The value of $R_{2/3}$ may be found in the following way.

By definition:

$$(4\text{-}61)\quad \tau \equiv \int_{\mathcal{R}_1}^{\mathcal{R}_2} N(R) Q_{EXT}\, a_o\, dR$$

which may be approximated as:

$$(4\text{-}62a)\quad \tau_i = Q_{EXT} a_o \sum_i N_{gr}(R_i)\Delta R_i$$

with the augmenting relation

$$(4\text{-}62b)\quad R(\tau_i) = R(o) - \sum \Delta R_i$$

where the summation begins at the flow's outer boundary (R (o)) and progresses inward. At $\tau = 2/3$ one may write (4-61) as:

$$(4\text{-}63)\quad 2/3 = Q_{EXT} a_o \sum N_{gr}(R_i)\,\Delta R_i$$

and $R_{2/3}$ is then given by the corresponding value of (4-62b). It should be noted that due to the uncertainties in the exact nature of circumstellar grains and hence in their Q's (Woolf 1971) computation will be carried out with the following expression:

$$(4\text{-}64)\quad \tau/Q_{EXT} = a_o \sum N_{gr}(R_i)\,\Delta R_i$$

which may be solved in the fashion of equation (4-63) for various values of Q_{EXT}.

At frequencies where the grain field is optically thin the luminosity emitted may be written as:

$$(4\text{-}65)\quad L_\nu = \oint j_\nu dV$$

where j_ν is the volume emission coefficient. The formal expression for j_ν may be derived in the following manner. The amount of power radiated by a particle at temperature T_{gr} is:

$$(4\text{-}66)\quad 4 Q_{\nu ABS} a_o \left(\pi B_\nu(T_{gr})\right)$$

whereupon one may immediately write:

$$(4\text{-}67)\quad j_\nu(R_i) = 4 Q^{\pi}_{\nu ABS} a_o N_{gr}(R_i) B_\nu(T_{gr})$$

This in turn may be employed to yield an equation for the luminosity emanating from a shell of thickness dR_i, centered on R_i, viz.:

$$(4\text{-}68)\quad dL_{\nu_i} = j_\nu(R_i)\,dV_i = 16\pi^2 Q_{\nu\,ABS} a_o N_{gr}(R_i) B_\nu(T_{gr}(R_i))\, R_i^2\, dR_i$$

Approximating the integral of equation (4-65) by a summation and substituting explicitly for $B_\nu(T_{gr})$ the total luminosity emitted over a frequency interval $\Delta\nu$ takes the form:

$$(4\text{-}69)\quad L_{\nu,\nu+\Delta\nu} = \frac{32\pi^2 h\nu^3 Q_{ABS} a_o \Delta\nu}{c^2} \sum_i N(R_i)\left(EXP\left(\frac{\sqrt{2}h\nu}{R_i^{\frac{1}{2}} T_*}\right) - 1\right)^{-1} R_i^2 \Delta R_i$$

Again $\frac{\Delta\nu}{\nu}$ will be set equal to .02 and calculations will be made in terms of a variable Q, i.e., (L_{thin}/Q).

Results and Discussion

In order to investigate the various facets of grain induced mass loss two series of models have been created. Series 1 considers the consequences of varying grain size, initial gas to grain mass ratio, initial gas temperature, and the size of the basal isothermal zone (BIZ) for a star of type MO I. The models of series 2 explore the behavior of the mass loss rate in the H-R diagram for fixed values of grain radius and gas to grain mass ratio. Specification of the initial gas temperature and size of the BIZ is unnecessary since it will be shown in the subsequent discussion that the mass loss rate does not depend on these quantities.

The Models of Series 1

The salient quantities of the models of series 1 are presented in Table 4-2. Column one contains the model number, while column two lists the size of grain used. The third and fourth columns contain the initial gas to grain mass ratio and the initial gas temperature respectively. Columns five, six, and seven, display the size of the BIZ, the position of the transsonic point, and the location of the point where the gas velocity exceeds the escape velocity, all in units of the stellar radius. The eighth column contains the terminal gas velocity in km-sec^{-1} while the ninth column presents the logarithm of the mass loss rate in $M_{\odot}$-yr^{-1}. The tenth column gives the average of the logarithm of the grain to gas number ratio in a zone of one stellar radius above the surface of the star. The final three columns contain, respectively, the logarithmic values of Q_{EXT}, Q_{SCA}, and the value of $\langle COS\theta \rangle$ evaluated at 1μ, the wavelength of maximum radiation for a 3000K black body.

The grain radius was varied over the range $.1\mu \geq a \geq .05\mu$ as these values are consistent with the polarization observations (Dyck 1971), suggested models of the interstellar medium (Wickramasinghe 1970) and theoretical calculations (Fix 1971). The variation of the gas to grain mass ratio from 100 to 1000 was set arbitrarily. The lower limit may be justified on the basis of the elemental composition of normal stellar material, but neither theoretical nor observational

TABLE 4-2. Data for the Models of Series 1.

Model	a_μ	$\frac{\rho_g}{\rho_{gr}}$	$T_{initial}$	$\frac{R_{15}}{R_*}$	$\frac{R_{sonic}}{R_*}$	$\frac{R_{esc}}{R_*}$	V_g final km/sec	$\mathrm{Log}\left(\frac{dM_*}{dt}\right)\frac{M_\odot}{yr}$	$\left\langle \mathrm{Log}\frac{N_{gr}}{N_g} \right\rangle$ $1 \leq \frac{R}{R_*} \leq 2$	$\mathrm{Log}\,Q_{EXT}$	$\mathrm{Log}\,Q_{SCA}$	$\langle \cos\theta \rangle$
1	.07	250	2056	10^{-3}	1.06	3.88	70	-4.68	-11.44	-1.86	-1.86	.059
2	.07	250	10000	10^{-3}	2.7	12	40	-4.66	-11.50	-1.86	-1.86	.059
3	.07	250	2056	0.1	5.5	30.2	26	-4.65	-11.49	-1.86	-1.86	.059
4	.07	250	10000	0.1	14.4	71.5	18	-4.67	-11.50	-1.86	-1.86	.059
5	.07	250	2056	1.0	14.6	67	18	-4.69	-11.50	-1.86	-1.86	.059
6	.07	250	10000	1.0	53.0	273	12	-4.67	-11.52	-1.86	-1.86	.059
7	.07	250	2056	5.0	40	210	12	-4.68	-11.50	-1.86	-1.86	.059
8	.07	250	10000	5.0	126	650	10	-4.64	-11.52	-1.86	-1.86	.059
9	.07	250	2056	10^{-3}	-	-	$10^{-5.03}$	-4.82	*	-1.86	-1.86	.059
10	.07	250	10000	10^{-3}	-	-	$10^{-4.99}$	-4.82	*	-1.86	-1.86	.059
11	.07	100	2056	1.0	1.12	31.4	25	-3.54	*	-1.86	-1.86	.059
12	.07	1000	2056	1.0	3.30	14.5	36	-5.43	-11.80	-1.86	-1.86	.059
13	.07	1000	10000	1.0	8.5	168	14	-5.38	-11.52	-1.86	-1.86	.059
14	.1	250	2056	1.0	10.7	207	13	-2.82	*	-1.23	-1.23	.120
15	.05	250	2056	1.0	11.5	43.5	23	-5.5	*	-2.49	-2.49	.033

* Has not been evaluated

evidence exists concerning the upper limit and thus it should be kept in mind that values substantially larger than this may occur. The initial temperature of 2056K which corresponds to the gas temperature at the top of the convection layer in the atmosphere model by Carbon (1970), represents a situation of low turbulence and/or a minimal residual chromosphere. The 10000K starting temperature, on the other hand, corresponds to those cases where turbulence and/or chromospheric activity are important. The range of the BIZ from $10^{-3}R_*$ to $5R_*$ was arbitrarily imposed, but should encompass the range over which turbulence and/or a residual chromosphere might be sustained.

Supersonic Flow Characteristics

Figure 4-1 displays a plot of the logarithm of the physical flow parameters, i.e. V_g, V_{gr}, N_g, T_g, versus the logarithm of the radial position for model 3. The grain number density was not plotted since by comparing the gas and grain velocity profiles and invoking continuity it obviously has the same form as the gas number density. The most interesting feature of the figure is the isovelocity zone, $(\overline{AB})$, preceding the sonic point. The answer to the question of the reality of this region seems to be affirmative since it appears in all models and cannot be expunged by adjusting the flow within the limits allowed by the sonic condition. Physically it may be understood in

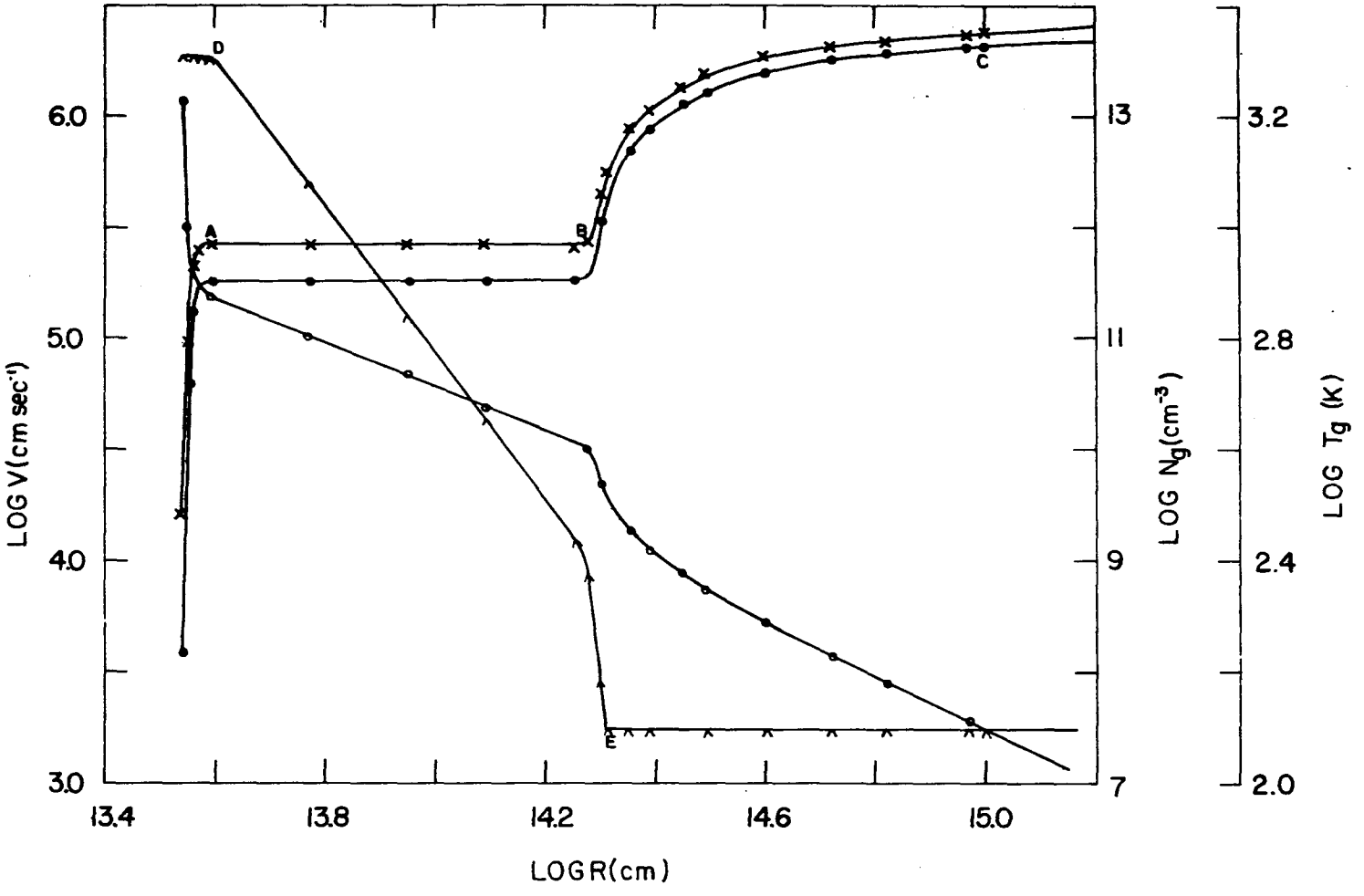

Fig. 4-1. Flow Characteristics for Model 3.

X = Grain Velocity
O = Gas Velocity
O = Gas Density
^ = Gas Temperature

the following way. At the outset of an allowed flow the gravity term holds sway over the grains (the far right term of (4-50a)), which results in an acceleration since the left hand side of (4-50a) is negative. As the flow gains speed the grain term grows and finally surpasses the gravity term. Unless this event coincides with the sonic point, a deceleration results until the gravity again dominates, precipitating another round of acceleration and a cycling of the above process. Thus the flow arrives at a state of constant velocity (point A) with the grains attempting to pass through the velocity ceiling and gravity rebuffing those attempts. This situation continues until the temperature drops to where the sound velocity equals the flow velocity. At this point, (B), the sign of the left hand term of (4-50a) changes, the flow becomes unstable to positive velocity perturbations, and the grain term and hence the velocities grow. It should be noted that this phenomenon depends on the double component nature of the flow and hence cannot be understood within the framework of the single component flows discussed by Parker (1958, 1960a, b). Consideration of the importance of the isovelocity zone will be deferred until later.

Other features of interest in the figure are C, the position at which the gas velocity exceeds the escape velocity, thereby satisfying the outer boundary condition, D, the end of the BIZ, and E, the onset of the 125K isothermal region. It is also noted that the functional behavior of the velocities at large distances agrees with the expression

derived by Gehrz and Woolf (1971) viz.:

$$(4\text{-}70)\quad V_g \alpha (\text{const.} - \frac{1}{R})$$

but that gross deviations from this relation occur near the base of the flow. A more complete comparison of the author's results with those of Gerhz and Woolf will be deferred until the end of the discussion of series 1. Since all flows, except models 9 and 10, have the same basic form as that shown in Figure 4-1 they will not be presented individually.

Subsonic Flow Characteristics

Figure 4-2 exhibits a plot of the logarithm of the gas velocity versus the logarithm of the radial position for model 10. Here one sees the behavior of flows which remain subsonic for all R. The isovelocity region is entered at point A, as in a supersonic flow, but in this case the isovelocity lies below the sound velocity of the imposed temperature minimum, which occurs at point B. Immediately downstream from (B) the gravity and grain terms decrease as R^{-2} while the temperature term, $(n+1)\frac{2kT}{\mu_g R}$ falls off as R^{-1} and thus soon becomes dominant. Since the temperature term remains positive and the left hand side of (4-50a) stays negative a monotonic deceleration results. Model 9 has the same form as ten and will not be presented separately.

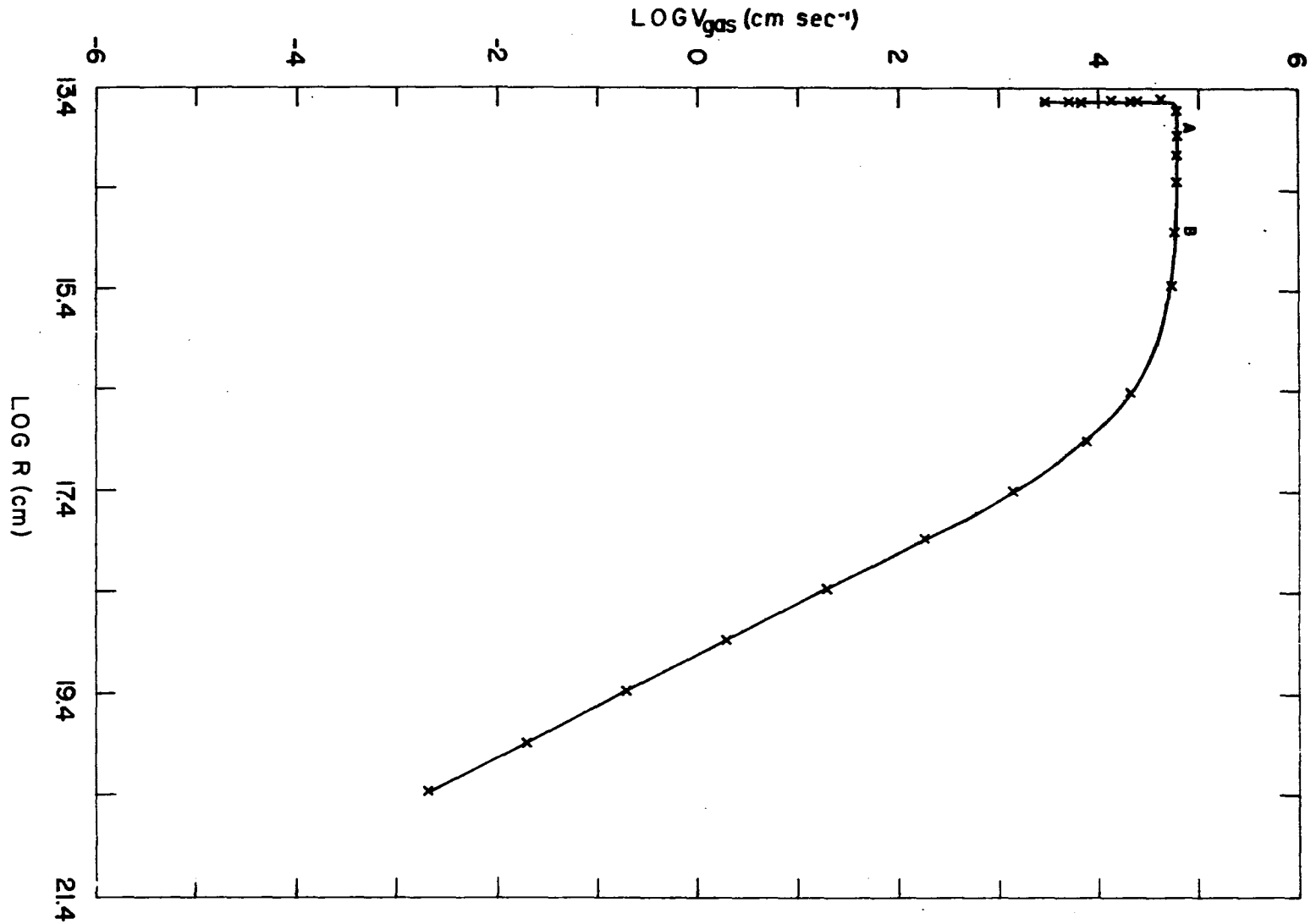

Fig. 4-2. Gas Velocity versus Radial Distance for Model 9.

Two component subsonic flows may be dismissed as unacceptable on the basis of high gas pressures at large distances, the same criterion used by Parker (1960a). In the outer regions of the flow the gas pressure of model 10 equals 7×10^{-9} dynes/cm^2, which far exceeds reasonable values of the intergalactic magnetic pressure (4×10^{-12} dynes/cm^2) or the interstellar medium pressure (1.4×10^{-14} dynes/cm^2), given by Parker (1960a).

Detailed Behavior of Supersonic Flows

Considering models one through eight, which differ only in the initial gas temperature and the size of the BIZ, one sees virtually identical mass loss rates in all cases. This verifies the assumption used in obtaining equation (4-49): viz. that the flow rate satisfying the sonic condition depends on the gross stellar characteristics and not the details of the flow's temperature structure. In addition one sees that the loss rate falls in the upper range of observed rates for supergiants given by Gehrz and Woolf (1971). Caution should be exercised, however, in the sense that while good agreement seems to exist between calculations and the observations considered as a whole, the uncertainties in empirically determined loss rates (Deutsch 1960) and the lack of complete knowledge regarding grain parameters would inhibit any attempt at precise matching of calculated rates with individual stars.

Examining columns four, five, and seven of models one to eight one notes that the terminal velocity depends strongly on the thermal details of the flow in the sense that the higher the initial temperature and/or the larger the BIZ the lower the velocity. This result may be understood by considering the effect of the initial temperature and the size of the BIZ on the isovelocity zone and, in turn, its role in determining the terminal velocity. Since cases 1 through 8 have the same mass loss, and hence initial velocities, they all enter the isovelocity zone at approximately the same radial position. The point at which the zone ends, however, depends on the distance the flow must progress before the temperature drops sufficiently for the flow to go supersonic, and this distance will obviously be larger for those cases where the initial temperature is high or where the BIZ is large. Since no acceleration occurs while the flow remains in the isovelocity zone, a longer zone results in less total acceleration and a lower terminal velocity. This may be seen graphically in Figure 4-3, which plots the logarithm of the size of the isovelocity zone versus the logarithm of the terminal velocity. The number to the side of each point is the product of the initial temperature and the size of the BIZ in stellar radii. From the previous discussion one expects the number to correlate directly with the size of the isovelocity zone, which one finds to be the case. The dependence of the final velocity on the size of the isovelocity zone is readily seen. Most of scatter arises

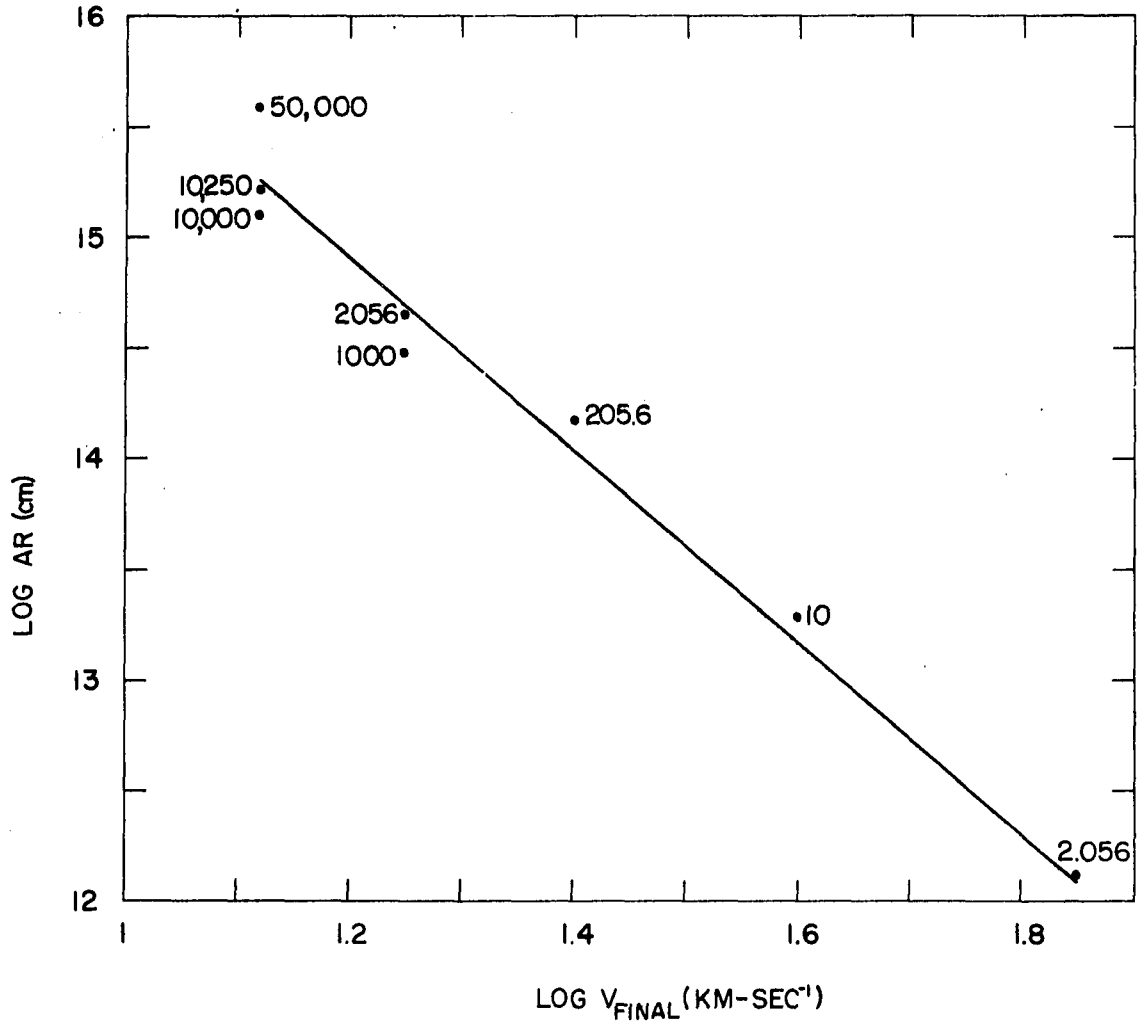

Fig. 4-3. The Size of the Isovelocity Zone versus the Terminal Velocity.

from the fact that the integration proceeds in finite steps and that the results are printed out only every ten steps. Assuming the empirically drawn line to give the correct relation one finds:

$$(4\text{-}71)\quad V_{g\ final} = R_{isovel}^{-.23},\ \text{at a constant mass loss rate}$$

Models 11 to 13 explore the effects of varying the gas to grain mass ratio. Considering all three models one sees that the mass loss rate depends strongly on the gas to grain ratio. Indeed while the ratio varies through a decade the loss rate changes by a factor of 145. This puts rather stringent limits on the range of mass ratios one may have without doing violence to the observations. It is notable that Fix's (1971) calculations yield ratios within this range. The extremely large loss rate of model 11, which corresponds to the lower limit of ρ_g/ρ_{gr}, would seem to preclude models of this type since no observational evidence exists for rates of this magnitude. It should be noted, however, that since significant mass loss occurs on the short time scale of 10^4 yrs. and such flows, if they exist, might be identified with phenomena other than quiescent mass loss. The twelfth and thirteenth models are seen to give loss rates falling in the middle of the observed range and, hence, indicate that gas to grain mass ratios somewhat below 250 are probably the rule.

The two final models, 14 and 15, examine the consequences of varying grain size. Again a strong dependence is seen; as the grain

size increases by a factor of two the loss rate grows 480 fold. However, this result depends not so much on the grain's physical size as on its associated radiation cross section, Q_{PR}, which changes by a factor of 16.7 while the grains are doubling in size. The large loss rate occasioned by .1μ particles precludes their being associated with quiescent mass loss for gas to grain mass ratios as small as those considered here. The .05μ particles, however, produce quite acceptable loss rates and when combined with an increased gas to grain ratio could account for the lower range of observed loss rates. Again it is noteworthy that grain characteristics required by polarization, and indicated by theoretical considerations (Fix 1971) are able to reproduce the observed loss rates.

Grain Cooling

Inspection of the tenth column of Table 4-1 reveals that the average of the grain to gas number ratio over the first stellar radius of the flow maintains a fairly constant value of 3×10^{-12} for all models. Recalling the results displayed in Figure 3-2 one finds that the cooling mechanism of Chapter 3 results in a temperature reduction of approximately 40 per cent. Though significant, this value is too small to permit an unequivocal statement to the effect that grain cooling will explain the perturbed chromospheres indicated by the results of Chapter 2. Only a detailed consideration of the structure and

transfer of radiation within a late type chromosphere can provide a definitive answer, and this lies beyond the scope of this dissertation. On the basis of the dynamical calculation, however, further arguments can be made in favor of an altered chromosphere. Referring to Figure 4-1 one sees that immediately above the base of the flow the rapid increase in velocity, coupled with the continuity relation, results in the density dropping off as $\mathcal{R}^{-30}$ and that from $.015 \leq \mathcal{R} \leq 5.5$ the density declines as $\mathcal{R}^{-2}$ due to the isovelocity zone. Using the sun for a crude comparison one finds that at $\mathcal{R} = .02$ the density decreases as $\mathcal{R}^{-500}$(Allen 1963). If heating takes place via hydrodynamic processes it can be argued that such an enormous difference in density structure will result in deviations in the energy dissipation process from that expected in the static case. In addition the tendency of the flow to cool adiabatically will provide an additional sink in which to absorb energy. In summary, while it is not possible at this time to make detailed predictions regarding the effect of the flow on an ambient chromosphere, one may make a reasonable prima facia case for a perturbed situation by invoking grain cooling, the altered density structure, and the expansive nature of the flow.

Line Profiles

Employing expressions (4-57a, b) a normalized profile for a fictitious line of rest wavelength $\lambda 5000$ has been computed for eight

series 1 models. Some of these are plotted in Figure 4-4. The number below each line indicates the position of maximum absorption in stellar radii, while the error bar displays the maximum resolution element of a $10\overset{*}{A}\text{-mm}^{-1}$ spectrum taken on a plate with a 10μ grain emulsion. The photospheric portion of the line has not been included for the sake of simplicity. On the basis of this data flows of the type associated with model 1, i.e., low initial temperature and small BIZ, may be excluded since observations fail to show stars with diffuse and/or high velocity (i.e., greater than 30 km-sec^{-1}) circumstellar lines. This in turn may be interpreted as possible evidence for the existence of residual chromospheric activity in view of the initial temperature, BIZ versus terminal velocity correlation. The fact that the maximum absorption of acceptable lines occurs at large distances from the star agrees with the observation that the circumstellar lines of α Ori are unaffected by its periodic pulsations (Weymann 1962a). Although not shown by the graph, it has been found that flows with similar terminal velocities have similar line profiles. Relative to the following discussion one should note that the velocities of the profiles for models 3 and 4 correspond approximately to those observed for μ Cep and α Ori respectively. However, it should be pointed out that model 3 has a somewhat higher velocity than has been observed for μ Cep.

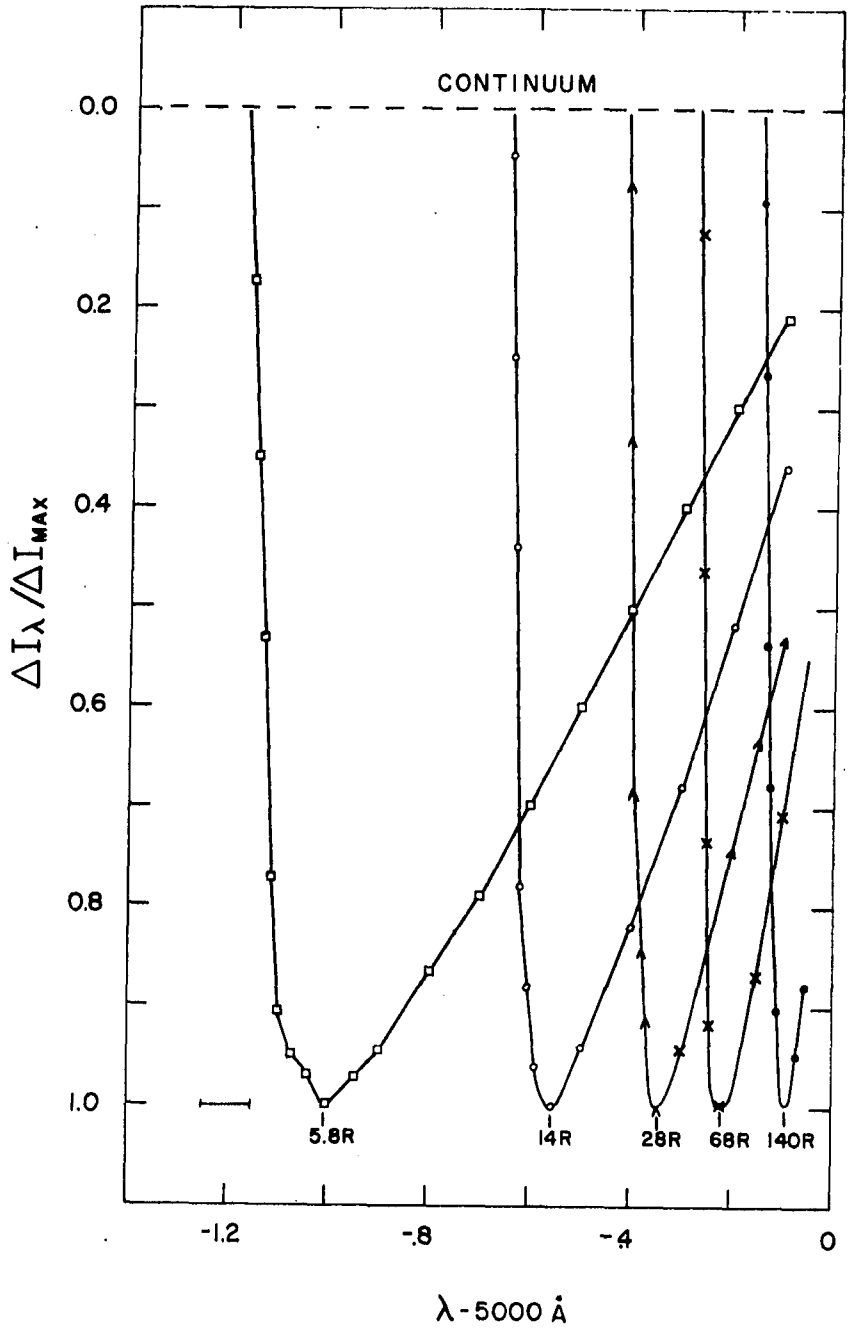

Fig. 4-4. Normalized Absorption Line Profiles.

□ Model 1
○ Model 2
^ Model 3
X Model 4
● Model 6

Figure 4-5 augments Figure 4-4 by showing the normalized profile of model 4 with the contribution from the base of the flow included. Since this portion of the line may be identified with the normal photospheric component it has been convolved with a gaussian profile of a half width of 20 km-sec^{-1}, which corresponds to the magnitude of turbulent velocities observed in late type supergiants (Biermann and Lüst 1960, Deutsch 1960). It should be remember that since the turbulent temperature has been assumed to obey the same adiabatic relation as the thermal temperature and since the lines are formed at a large distance from the star the question of the effect of turbulence on the circumstellar component does not arise. Again the error bar indicates the resolution element. Since it has been noted that model 4 might correspond to α Ori the plot was compared with intensity tracings of optically thin lines given by Weymann (1962a). The general correspondence in shape is remarkably good, and indeed the half-width of the calculated circumstellar line corresponds to that given by the tracing. While the agreement in the case of α Ori may be in part fortuitous, it appears that on the basis of Figures 4-4 and 4-5 one may conclude that the essential features of circumstellar lines, as regards shape, displacement from the line center, and required formation at large distances from the star, are satisfied by the theory at hand.

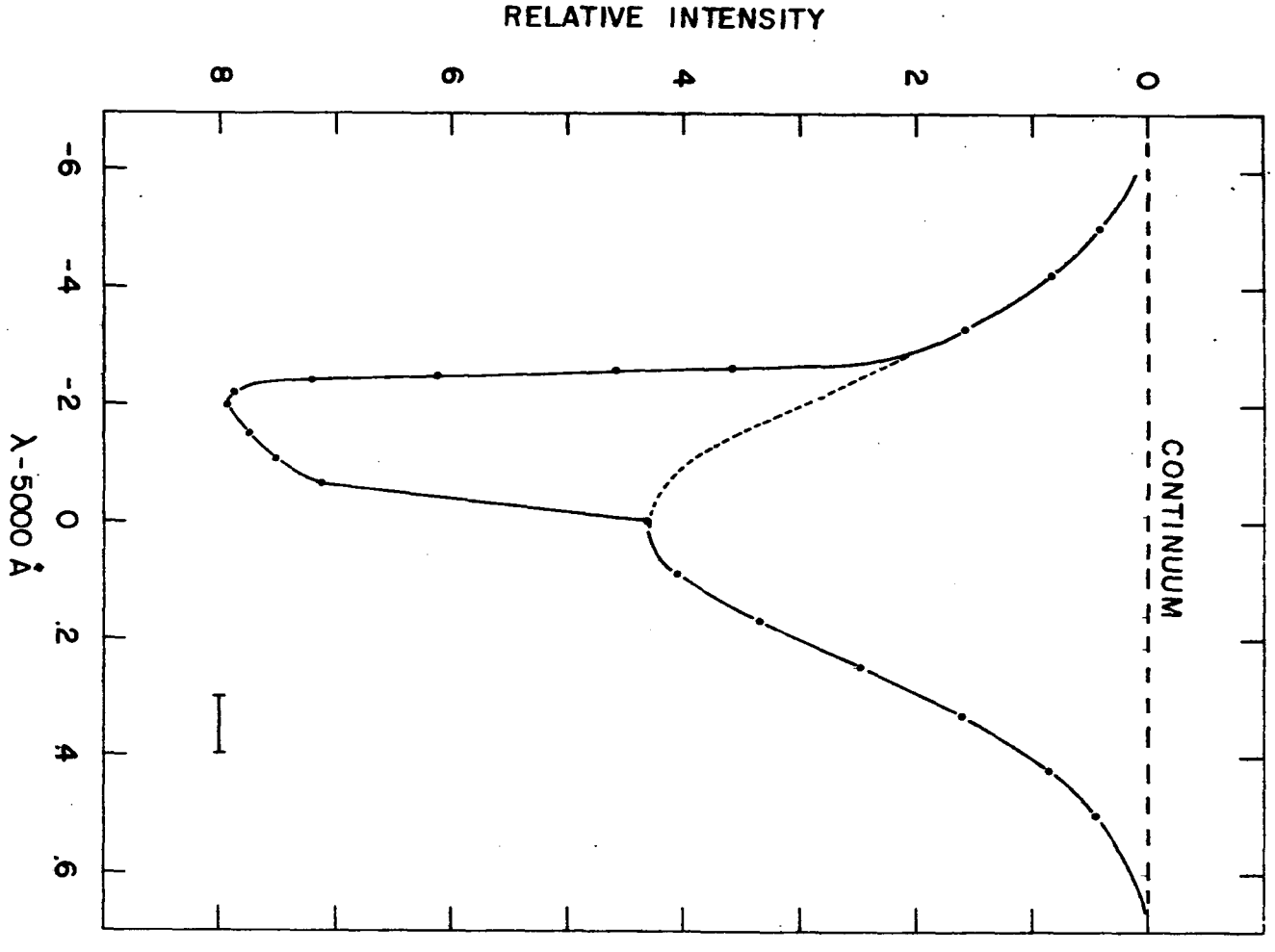

Fig. 4-5. Normalized Line Profile for the Model Corresponding to α Orionis.

Infrared Excesses

Figure 4-6 displays a plot of the infrared luminosity expected from the $\tau = 2/3$ level of an optically thick grain flow (equation (4-60)) versus the parameter τ/Q (equation (4-62a)) for models 3 and 4. Results for other models have not been plotted since they are all of the same basic form. The point designated (S) corresponds to the base of the flow in each case; points ($A_{1,2}$) and (B) will be discussed later. From the plot one sees that for models of the same gas to grain mass ratio, those with higher terminal velocities (e.g. 3) produce a higher luminosity at a given value of τ/Q in the outer region of the flow. This may be readily understood by recalling that as the velocity at a given point increases the density must decrease to satisfy continuity. Thus the faster the flow, the physically nearer to the star one must look to arrive at the same value of τ/Q, and this in turn means looking to a region of higher luminosity. A similar relation may be seen by considering Table 4-3, column one of which lists the models for which the optical properties of the grains have been examined and the logarithm of τ/Q at the base of the flow in column two. The third column contains the logarithm of the optically thin luminosity divided by Q (equation (4-69)) while column four presents the terminal velocity in $km\text{-}sec^{-1}$. For models one to eight, one finds that as the velocity increases the optical depth at the base of the star decreases in agreement with the above discussion. The same effect is noted for L/Q

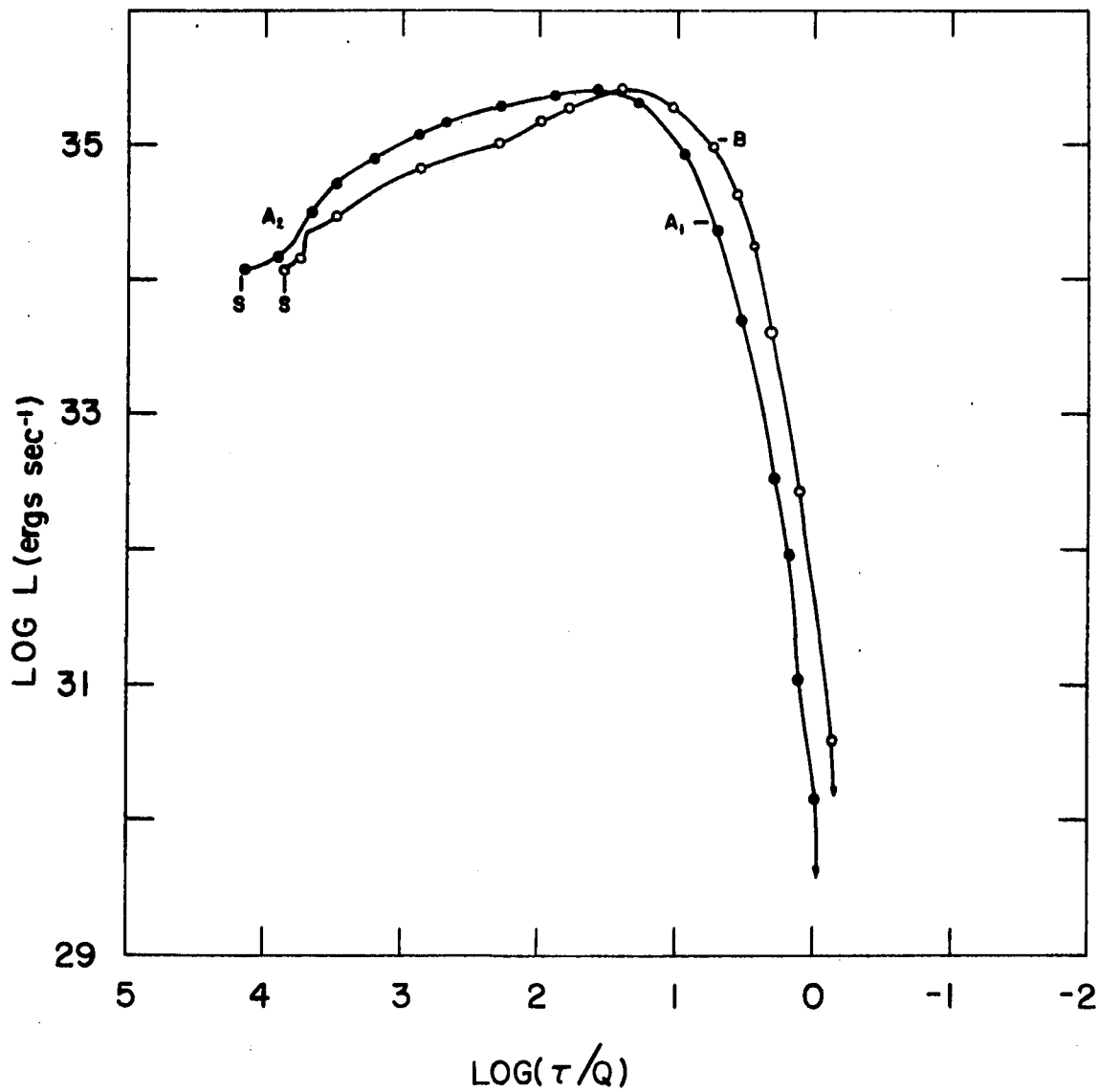

Fig. 4-6. Black Body Luminosity versus τ/Q.

O Model 9
● Model 16

TABLE 4-3. Optical Data for the Models of Series 1.

Model	$\text{Log}\left(\frac{\tau}{Q}\right)$	$\text{Log}\left(\frac{L_{thn}}{Q}\right)$	V_{term}
1	3.28	39.13	70
2	3.98	39.87	40
3	3.89	39.81	26
4	4.16	40.04	18
5	3.96	39.85	18
6	4.23	40.11	12
7	3.94	39.81	12
8	4.22	40.08	10
12	2.84	38.74	36
13	3.20	39.05	14

which also depends on the number of particles in the line of sight. Models 12 and 13 display this same behavior, but here an additional scale factor must be included to account for the change in gas to grain ratio.

Since values of Q_{ABS} for the grains are unknown the calculated results cannot be used directly to discuss infrared excesses, however, the results can be combined with observational data to produce an expected value of Q_{ABS}, which in turn may then be checked for consistency by comparison with other observations. From Gillett, Low, and Stein (1968) one finds that α Ori shows excess radiation at 10μ equal to 1.85 times the stellar flux. Assuming the central star to have a temperature of 3000K and considering a band pass of $\Delta\nu = .02\nu$ this corresponds to a 10μ luminosity of 3.42×10^{34} ergs-sec^{-1}. The question of whether this radiation emanates from an optically thin or thick region may be answered by appealing to the data of Table 4-3. Considering model 4, one sees that were the flow field thin one must have $Q_{ABS} \simeq 3 \times 10^{-6}$ to satisfy the observations. A Q_{ABS} this small is highly unlikely since at 10μ silicates absorb due to fundamental lattice vibrations which are known to give large values of Q_{ABS} (Huffman 1971). Thus it appears that one is dealing with an optically thick situation in all cases. One should note that this conflicts with Woolf's (1971) suggestion that α Ori is optically thin at 10μ. Referring

to model 4 of Figure 4-6 one finds that there are two possible values of τ/Q which will produce a flux of 3.42×10^{34}. These are denoted by A_1 and A_2. Solving for the value of Q necessary to make A_1 the $\tau = 2/3$ level one obtains $Q_{ABS} = .115$, which is of the order of magnitude expected (Huffman 1971). It is interesting to note that the $\tau = 2/3$ level occurs at a distance of 7×10^{15} cm or $200R_*$ thus raising the possibility of an observational test via long wavelength interferometry. This distance also corresponds to those which have been observed for the OH sources surrounding some stars of the type considered here (Herbig 1970). Recalling that model 3 approximated μ Cep and using the Q_{ABS} derived above one finds a predicted 10μ flux of 1.05×10^{35} ergs-sec^{-1} or 5.6 times the stellar flux, again assuming a stellar temperature of 3000K. This is to be compared with the value of 4.5 times the stellar flux given by Gillett, Low, and Stein (1968). Remembering that model 3 yields a terminal velocity which is somewhat too high for μ Cep and that the slower the flow the lower the excess, one expects a more accurate fit to μ Cep to produce an excess deviating from observations by less than that derived here. Point A_2 may be discounted as a possible solution on the grounds of a required value of Q_{ABS} much less than expected, and the fact the excess derived for μ Cep would disagree strongly with observation. One should note that while the velocity-luminosity relation allows a 10μ absorption feature for those flow which are sufficiently slow none

has been observed. The explanation of this would seem to be that if flows exist they proceed rapidly enough or begin with sufficiently large gas to grain mass ratios to preclude arriving in such a state.

Returning to columns 2 and 3 of Table 4-3 and noting that one expects Q_{ABS} at 3μ to have a value on the order of 10^{-6} to 10^{-5} (Huffman 1971) one finds the grain field optically thin to absorption in all cases and the luminosity due to grains at 3μ, over a band pass $\Delta\nu = .02\nu$, to be much smaller than the stellar luminosity (3.6×10^{35} ergs-sec^{-1}) in most cases and never to exceed 35 percent of the stellar value. This agrees with observational results by Gillett, Low, and Stein (1968) and Gehrz and Woolf (1971) to the effect that the absorption properties of grains are unimportant at 3μ. Also since $Q_{ABS} \sim 10^{-5}$ for the visual wavelength this spectral region should also be optically thin to absorption which is obviously the case.

In summary, the theory adequately explains the observed infrared excesses as arising from an optically thick cloud, with the strength of the excess depending on the details of the flow. The near infrared and visual wavelengths are found to be optically thin to absorption.

Scattering by Grains

Consider the situation in the case of scattering opacity. Over the wavelength region $1\mu \geq \lambda \geq .5\mu$ one finds $.014 \leq Q_{SCA} \leq .22$ (Shawl

1972). Combined with the data of column 2 of Table 4-3 this indicates that all models are optically thick to scattering over the entire wavelength range with τ varying between approximately 10 and 1000 depending on the wavelength and model. Since this is at first sight quite surprising, it is of interest to see if varying the parameters of the problem will significantly alter the situation. While there are certainly errors in the values of the stellar physical characteristics of Table 4-1 a disucssion of their nature and magnitude lies beyond the scope of this work. It may be said, however, that were gross adjustments to be made the good agreement between observation and theory obtained thus far would be seriously jeopardized. Variation of the gas to grain mass ratio by a factor large enough to enter the optically thin regime would make it impossible to produce the observed rates of mass loss. Indeed for a fast flow with $\rho_g/\rho_{gr} = 1000$ (model 12) the optical depth at $.5\mu$ is on the order of 1000 and hence values of ρ_g/ρ_{gr} substantially larger than this are needed. However, in view of the strong dependence of the loss rate on this ratio, one would then be unable to reproduce the observed rates. Since the exact nature of the grains remains unknown the index of refraction and hence Q_{PR} are open to question. One finds that for m, the real part of the index of refraction, > 1.65, Q_{PR} increases whereupon the loss rate increases thereby aggrevating the situation. Values much less than m = 1.65 are unlikely since one rapidly arrives at the value of 1.3 corresponding

to pure ice, the material of lowest index commonly suggested for grains. Even in this case $Q_{SCA}{}_{.5\mu} = 5.4 \times 10^{-2}$ with τ still $>> 1$. The physical size of the particles cannot be significantly changed without doing violence to the polarization data (Dyck 1971) and any change toward larger sizes worsens the problem. Thus we are driven to seriously consider the fact that we are dealing with envelopes which are optically thick to scattering.

Assuming that the theory is correct and that the true case is one of optical thickness in the visible spectrum, one may proceed to ascertain the observational consequences of this situation and determine whether these conflict with observation. The most obvious effect will be the fact that were the star resolved one would not see the photosphere but some layer in the purely scattering envelope. Observations of apparent stellar size have been performed interferometrically by Michelson and Pease (Brown 1968) and more recently by Gezari, Labeyrie, and Stachnik (1972), but before comparing these results with the calculated predictions one must examine what one measures in the case of an extended scattering envelope.

While a detailed solution of the transfer problem in the envelope lies beyond the scope of this work, it seems certain that even in the case of isotropic scattering the $\tau = 2/3$ layer will be limb darkened. In addition, the strongly forward throwing nature of the grain phase function (van de Hulst 1957) would be expected to introduce further

darkening. The occurrence of limb darkening would mean that one sees an effective, flux weighted, diameter rather than the full $\tau = 2/3$ diameter when one performs an interferometric measure.

For the purpose of further discussion it will be assumed that this effective diameter is 40 percent of the true diameter and hence the latter may be expressed as:

$$(4\text{-}72)\quad \alpha''_{true} = 2.7\alpha''_{meas.}$$

Consider the interferometric data concerning α Ori. Michelson and Pease working in integrated light found an angular diameter of $.034''$. In view of the effective temperature of α Ori and the form of the spectral response function of the eye it will be assumed that this diameter corresponds to an effective wavelength of $\lambda 6500$. For a $.07\mu$ particle of m = 1.65, $Q_{SCA} = 8 \times 10^{-2}$, and letting $\tau = 2/3$ be the effective radiation depth one derives a τ/Q of 8.25. In model 4 this level occurs at a radius of 5×10^{15}cm or a diameter of 10^{16}cm. Correcting the measured diameter via equation (4-72) yields $\alpha_{true} = .092''$. Combining the radius and the angular size allows one to calculate the distance: viz.,

$$R = 10^{16}/4.45 \times 10^{-7} = 2.2 \times 10^{22}\text{cm} = 7.3\text{kpc.}$$

which is certainly too large. However, by letting the particle index of refraction be m = 1.5 and employing model 13 which has a gas to grain ratio of 1000 and correcting linearly for the small velocity

difference between it and model 4 one arrives at a distance of R = 970pc. While this is still a factor of 6.4 greater than the currently accepted distance (i.e., R = 150pc.) it may be considered a much more reasonable value. In addition Brown (1968) estimates the error of the Michelson-Pease determination at $\pm$ 20 percent which converts to an error of $\pm$ 195pc. Of greater interest than the exact size of the discrepancy, however, is the fact that the calculation depends strongly on the precise details of the model used as witness the reduction in distance by a factor of 7.5 achieved by only minor changes in the nature of the flow. Indeed, this test is probably too sensitive for the crude nature of the models. A property does exist, however, which is virtually independent of the exact nature of the flow: the ratio of the apparent size at various wavelengths due to the variation of Q_{SCA}. For both models 4 and 13 the ratio of the radii at 1μ to those at $.65\mu$ and $.5\mu$ is 1:4.35:10.9. While no interferometric measures exist at 1μ, a determination for α Ori at $.5\mu$ has been made by Geazri, Labeyrie, and Stachnik (1972) who find a diameter of $.072'' \pm .022''$. Thus one finds that the observed ratio at $.5\mu$ and $.65\mu$ to be 2.1 while the calculated value is 2.5. In view of the model independence of this ratio it appears to be a more useful test at present and one may conclude the comparison with observation to be affirmative.

By virtue of the motion of the grain field transmitted light will suffer a displacement relative to its photospheric wavelength. This may be expressed quantitatively by considering Figure 4-7 which exhibits the necessary geometry. A grain may be completely described by specifying its spatial coordinates (R, θ, ϕ) where the polar axis is the direction of the observer. A particle at R sees a photon of initial frequency ν_o red shifted by an amount $\nu_o \frac{V(R)}{c}$ and thus in a scattering situation the grain can be thought of as emitting radiation of frequency

$$(4\text{-}73)\quad \nu_p = \nu_o\left(1 - \frac{V(R)}{c}\right)$$

The component of the particle's motion in the direction of the observer may be written as:

$$(4\text{-}74)\quad V_{RAD} = V(R)\,\mathrm{COS}\phi\mathrm{COS}\theta$$

Therefore the observer sees a frequency shift given by:

$$(4\text{-}75)\quad \Delta\nu_p = \frac{V(R)\mathrm{COS}\phi\mathrm{COS}\theta}{c}$$

or a frequency

$$(4\text{-}76)\quad \nu_{OBS} = \nu_p\left(1 + \frac{V(R)\mathrm{COS}\phi\mathrm{COS}\theta}{c}\right)$$

Combining (4-73) and (4-76) and neglecting the term in $(V/c)^2$ yields:

$$(4\text{-}77)\quad \nu_{OBS} = \nu_o\left(1 - \frac{V(R)}{c}\,(1 - \mathrm{COS}\phi\mathrm{COS}\theta)\right)$$

From this one sees that only red shifts are possible and hence one would expect an originally symmetric line to be observed with a profile

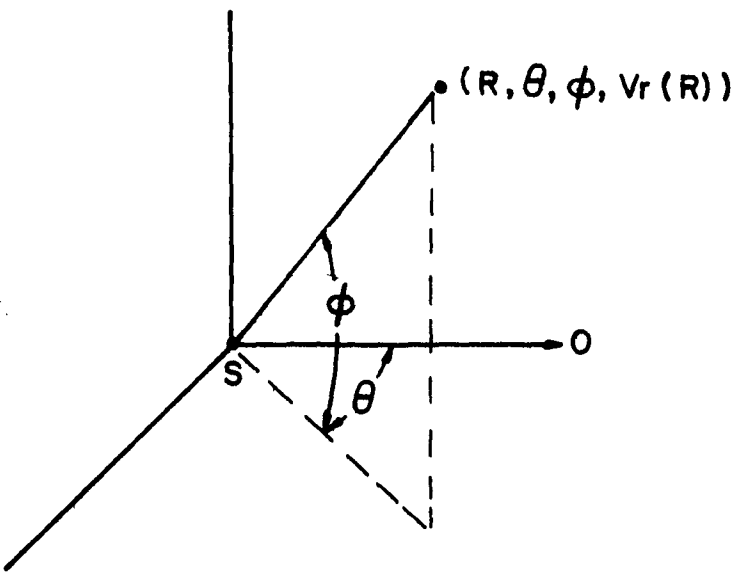

Fig. 4-7. Geometry Relevant to Doppler Shifting by Scattering.

skewed to the red. The exact shape of such a line would depend in a complicated way on the particle number and velocity distribution, and the form of the limb darkening. It should be noted that in the optically thick situation the range of observable θ is confined to $(\pi/_2+\omega) \geq \theta \geq -(\pi/_2+\omega)$ where $\omega << \pi/_2$. Only in the case of a disk shaped flow of the kind discussed by Herbig (1970) would one be able to see the far side of the envelope. The restriction on θ limits the amount of redward displacement to a value not exceeding V (R)/c. The conclusion that the lines are deformed toward the red remains valid in the case of multiple scattering since a given grain either has a zero (in the isovelocity zone) or positive relative velocity with respect to all other grains.

In view of the predicted line asymmetry it is interesting to note that a number of mass loss stars are observed to have abnormally diffuse lines (Herbig 1970, Deutsch 1960, 1961) and that for α Ori Weymann (1962a) notes a strong asymmetry in H_α, a weaker asymmetry in H_β and red "shoulders" on the Na I D lines. He further notes that a portion of the H_α line appears to arise in a region undisturbed by the star's pulsations, which implies a zone well removed from the photosphere. One should note that the D line observations may be explained by interstellar absorption (Weymann 1962a) and that the reason for an appreciably weaker asymmetry in H_β as compared to H_α is not clear. With H_β being the weaker line, however, the possibility

exists that the full asymmetry has not been detected. Deutsch (1960) has noted that the FeI lines λλ4046, 4064, and 4072 of α Ori show marked redward asymmetry. While this has usually been interpreted as indicative of appreciable flow velocities in the vicinity of the photosphere, such velocities are not indicated by the results of this work (see Figure 4-1), but the line profiles may be explained by a combination of absorption at larger distances and broadening by scattering.

If the flow deviates at all from spherical symmetry an additional consequence of scattering by a moving envelope will be found in the nature of the polarization observed as a function of wavelength within a spectral line. Consider Figure 4-8 which displays the geometry of the final scattering as viewed along the short axis of a grain distribution in the form of an oblate spheroid. For simplicity it has been assumed that the radiation is unpolarized prior to the last scattering and that the phase function is pure Rayleigh (i.e., dipole). Resolving the incident radiation into components in the plane of the page (⟷) and perpendicular to it (•) one sees that the light from $\theta = 0$ remains unpolarized while at $\theta = \pi/2$, the maximum θ in the optically thick case, the radiation is composed solely of the perpendicular component. The intermediate case of $\theta = \theta_o$ emits a combination of both polarizations. Since various values of θ correspond to different radial velocities relative to O the various polarizations will appear resolved across a line broadened by scattering. This may be seen in Figure 4-9

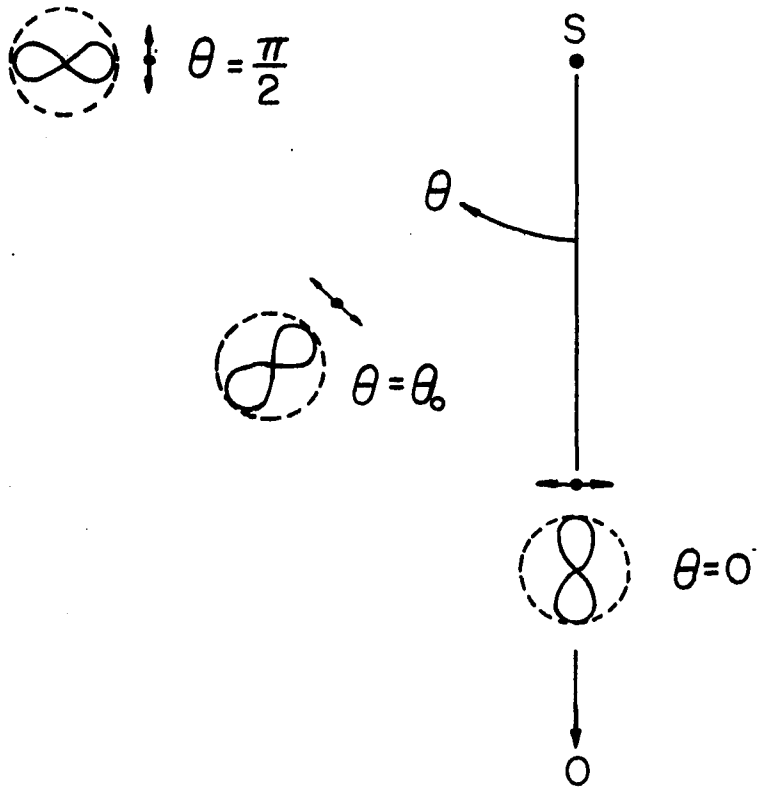

Fig. 4-8. Scattering Polarization Geometry.

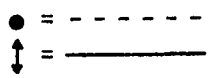

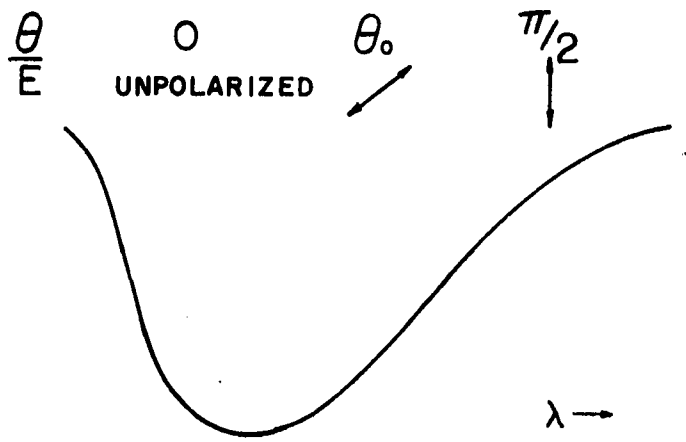

Fig. 4-9. Expected Polarization Across a Line Broadened by Scattering.

which displays an asymmetric line and the polarization angle expected in various parts of that line. While the real situation is not this simple due to the fact that the light arriving at the final scattering will already be polarized because of previous scattering, and that the details of the geometry may vary the basic conclusion that the plane of polarization should rotate across the line seems firm. Thus were this observed it would validate the prediction of an optically thick scattering region surrounding mass loss supergiants.

For the assumptions of this model, i.e., a spherically symmetric flow, a large scattering envelope has no effect on the apparent color of the star. However, it should be realized that were appreciable asymmetry to exist an aspect effect would result with a given star appearing bluer when viewed along the short axis of the envelope. The fact that no obvious color anomalies have been observed for these stars may be taken as evidence favoring a generally spherical grain distribution. While the discussion of scattering envelopes has been formally carried on for the supergiants, the same basic conclusions hold in the case of the giants, albeit with appropriate scaling. The giants will be discussed more fully in connection with the series 2 models.

At this point it is of interest to compare the results of this work with those of the other existing grain driven mass loss theory, that of Gehrz and Woolf (1971). Their model considers only the

effect of radiation pressure while neglecting the following points: gravity, imperfect gas-grain coupling, and pressure effects, including the sonic point condition. Thus they arrive at an equation of motion for particles with the density of the gas component and the radiation cross section of the grain component. Solving this expression (their equation 3) for the conditions of model 4 one obtains a terminal velocity of 63km/sec. It has been demonstrated, however, that velocities of this size are somewhat larger than observed. Thus it appears that the greater detail of the models presented here represents an improvement upon Gerhz and Woolf's simplified theory.

Mass Loss in the H-R Diagram

The results for the models of series 2 may be seen in Table 4-4. Column one lists the MK class of the model, while columns two and three present the logarithm of the mass loss rate in solar masses per year for the gas and grains respectively. On the basis of the evidence of series 1 all models of this series were calculated with the gas to grain mass ratio equal to 1000. One immediately notes that for all the giants except M5 the loss of mass in the form of grains far exceeds the loss in gas. Thus rates calculated in the usual way via the circumstellar line profile are grossly underestimated. As a function of luminosity class one finds the super-giants lose mass at a substantially higher rate than the giants, in agreement with observation

TABLE 4-4. Gas and Grain Mass Loss Rates for the Models of Series 2.

Model	Log (dM/dt) $M_\odot$/yr GAS	Log (dM/dt) $M_\odot$/yr GRAINS
KO I	-6.99	-7.78
K5 I	-6.03	-7.32
MO I	-5.38	-7.12
KO III	-10.76	-9.20
K5 III	-9.55	-8.68
MO III	-10.71	-8.96
M5 III	-6.84	-7.38

(Gehrz and Woolf 1971). Considering spectral type as the variable, one sees that among the supergiants the loss rate increases monotonically with decreasing temperature. This also holds for the giants except between K5 and MO where a decrease in the loss rate occurs. This deviation results from the lower luminosity of the M star relative to the K star as can be seen from both columns two and seven of Table 4-1. The MO III and M5 III loss rates of -10.71 and -6.84 respectively may be compared with the M1 III and M5 III average rates of -11.4 and -7.3, respectively, given by Deutsch (1960). Again one finds good agreement between theory and observation.

Figure 4-10 displays the location of the series 2 models in the H-R diagram. Each data point is accompanied by its spectral type and the logarithm of its gas and grain loss rates which are the upper and lower numbers respectively. The dashed line represents one of the possible lines of constant gas mass loss and shows the strong dependence of the loss rate on luminosity. The solid line depicts the line of constant grain loss, which is less sensitive to luminosity. The broken line represents the tentative blue envelope of intrinsic polarization as derived by Dyck and Jennings (1971a). One immediately notes the close agreement in slope between this line and that of constant grain loss rate. This suggests that the domain of polarization in the late H-R diagram may be understood in terms of the grain ejection in the sense that for polarization to be detected one must have

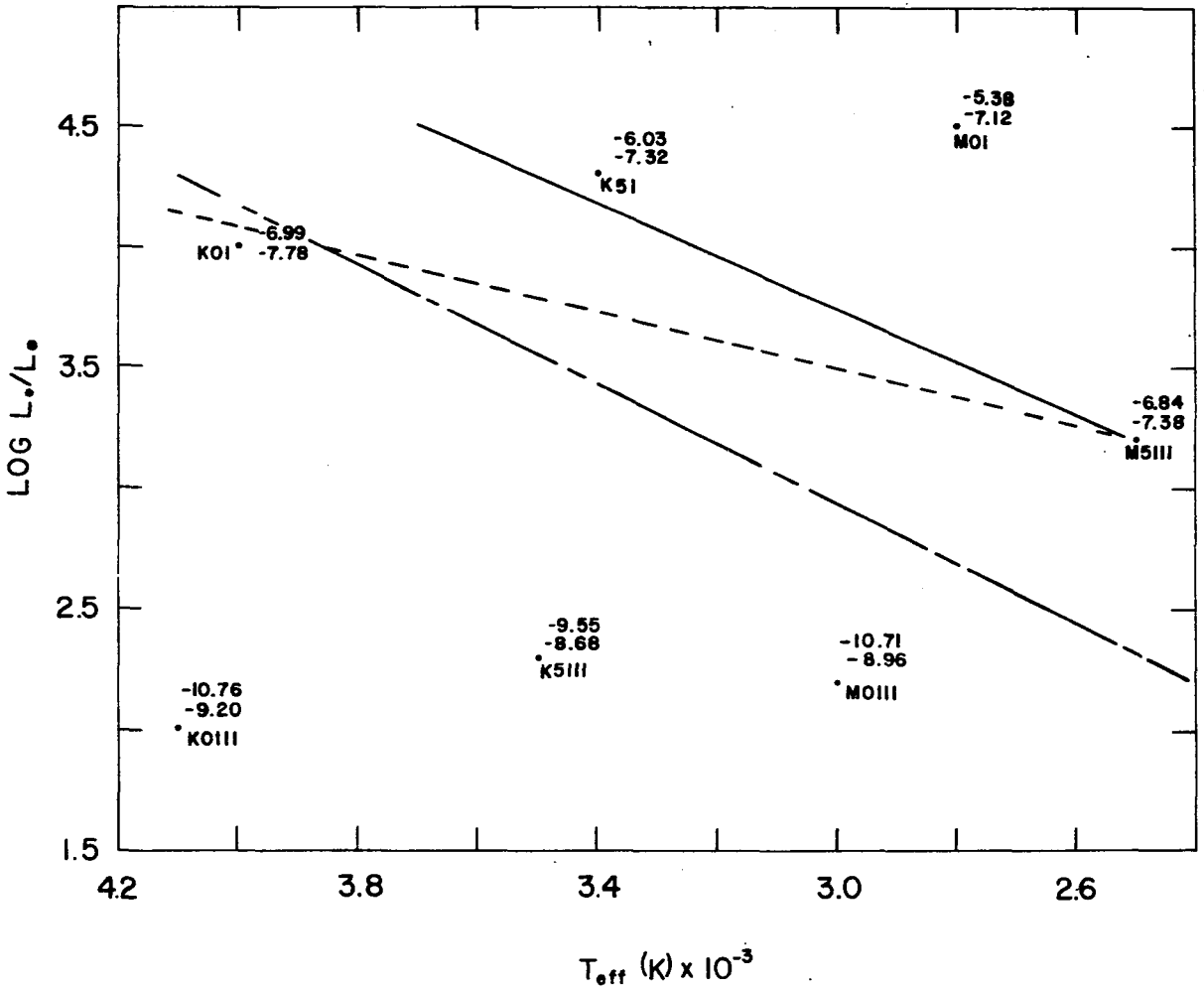

Fig. 4-10. Mass Loss in the Late H-R Diagram.

a certain minimum density of grains exterior to the photosphere and hence a minimum grain loss rate. From the figure the threshold value seems to be on the order of $\log \frac{dM_{gr}}{dt} = -7.8 M_\odot/yr$. This value should be considered as tentative, however, due to the fact the blue envelope is not well determined observationally, and that its shape and/or slope may be due in part to a cut on in allowed grain production.

While line profiles, τ/Q, L_{thin}/Q, L_{thick} have not been calculated for most of the models of series 2 a consistency check has been made using the K5111 star. In this case one finds the following results. The circumstellar line has a narrow profile centered at 2km-sec^{-1}. τ/Q is found to be 10^2 at the base of the flow while the $\tau = 2/3$ level at $.65\mu$ for particles of refractive index $m = 1.5$ occur at 1.1×10^{13}cm or $6.3R_*$. Thus while the flow remains optically thick to scattering the size of the apparent disk has decreased substantially. L_{thin}/Q takes a value of 3.67×10^{35} ergs per second, which when combined with a Q_{ABS} at 3μ of 10^{-6} to 10^{-5} produces no excess relative to the stellar flux of 1×10^{33} ergs per second. Using the value of Q_{ABS} at 10μ derived previously, one obtains an excess equal to approximately 5 times the 10μ stellar flux. In summary, it appears that the results obtained for the supergiants are also applicable to the giants upon allowance for scaling.

From the foregoing analysis the following conclusions can be drawn. One may explain the known observational features of quiescent mass loss from irregular and semi-regular variables without appealing to any agency other than refractory grains produced in the atmospheres of these stars. The veracity of this statement rests on the following points:

1. The model gives mass loss rates of the magnitude observed and reproduces their behavior as a function of spectral and luminosity class.
2. The observed shape and velocity range of circumstellar lines is recovered from the details of the flow.
3. Infrared excesses of the magnitude observed are predicted for the 10μ region while for the 3μ and optical regions excess radiation is neither predicted nor observed.

The fitting of these three basic observed quantities is based on, or results in the following conclusions.

1. Assuming the physical parameters of the stars to be essentially correct, the proper loss rates are recovered for gas to grain mass ratios greater than 250, with the best value being approximately 1000, and grains of radius $.07\mu \leq a \leq .05\mu$ and refractive index $1.4 \leq m \leq 1.65$. Having specified the physical parameters, one finds that the sonic condition determines the actual mass loss rate and that

such rates automatically satisfy the requirement of zero pressure at infinity. Subsonic flows are unacceptable due to their high pressures at large distances.

2. The velocity and width of a circumstellar line profile, as well as the gas terminal velocity, are negatively correlated with the size of the pre-sonic isovelocity zone, a feature occasioned by the two component nature of the flow. The size of this zone is in turn directly related to the initial temperature and length of the basal isothermal zone. Thus the low velocity of the observed profiles indicates some residual chromospheric activity and/or a region of turbulence surrounding the star. The line profiles are formed at large distances from the star.

3. The infrared excess at 10μ may be reproduced if and only if the grain field is optically thick with Q_{ABS} on the order of 0.1. Further the amount of the excess correlates directly with the magnitude of the terminal velocity. The lack of 10μ absorption features seems to indicate that all allowed flows proceed at a velocity large enough to avoid this situation. The radius of the effective radiation level at 10μ corresponds to that observed for the OH emission sources observed around a number of late type stars.

4. For both giants and supergiants the magnitude of the grain loss rate combined with the values of Q_{SCA} associated with the required grains parameters produces an optically thick situation at

all visible wavelengths and in the near infrared. This in turn results in apparent radii substantially larger than the photosphere of the star with the radius changing as a function of wavelength due to the wavelength dependence of Q_{SCA}. The theory predicts the apparent radii at 1μ, $.65\mu$, and $.5\mu$ to be in the ratio of 1:4.35:10.9 which is supported by the available data. For supergiants radii on the order of 5×10^{15} cm at $.65\mu$ are expected while giants exhibit radii of approximately 10^{13}cm. The optically thick nature of the flow also results in a broadening of transmitted stellar spectral lines due to doppler shifting. The broadening is found to be in the form of a skewing of the lines to the red, and indeed such asymmetry has been observed in a number of mass loss stars. It is noted that one expects a scattering induced rotation of the polarization vector across any line broadened by grains with an asymmetric distribution.

5. For giant stars earlier than approximately M3 mass loss rates obtained via the analysis of circumstellar gas line profiles seriously underestimate the true rate, which arises mainly from the grains.

6. Lines of constant grain loss rate in the H-R diagram have the same slope as the blue envelope of intrinsically polarized stars and hence indicate the possibility of a threshold grain density below which polarization is not detected with present accuracy.

7. The average grain to gas number ratio in the base of the flow seems to be sufficient to reduce the temperature of any ambient chromosphere to approximately 60% of its initial value via collisional cooling. In addition to this the altered density structure and the expansive nature of the flow may precipitate further cooling. While no definitive statement can be made, the results of this work are consistent with the idea of an altered chromosphere.

In view of the scope of the predictions of this theory, ample opportunity appears to be available for future work both observationally and theoretically. The most definitive checks of the theory seem to involve the large scattering envelope. Interferometric measures should be made to see if such large envelopes are reasonable and especially to test the predicted variation in apparent size as a function of wavelength. Since rotation of the polarization vector across a scattered line seems probable this would be another critical test. Assuming that these tests are affirmative the next step should be the solution of the transfer problem in the envelope including polarization, for this will depend strongly on the precise nature of the grains and their micro- and macrogeometry, and hence would serve as a powerful tool with which to probe their exact nature. High dispersion spectroscopic work, especially to examine the suggested circumstellar line velocity versus infrared excess correlation would be useful. The apparent power of this theory in explaining the known

properties of irregular and semi-regular variables indicates that it may be fruitful to try to extend it to encompass the carbon stars and Miras.

APPENDIX A

GAS-GAS AND GAS-GRAIN COLLISIONAL RATES

The question of whether gas particles can maintain a maxwellian velocity distribution in the presence of grains may be answered by comparing the intra-gas collisional rates with the gas-grain collisional rate. It will be assumed that all particles except electrons may be considered fixed. This will be verified a posteriori.

The collisional rate of the average electron with an uncharged grain may be written in the following way:

$$(A\text{-}1)\quad \mathcal{N}_{e\text{-}gr} = N_{gr} a_o \langle v \rangle;\ \langle v \rangle \equiv \left(\frac{3kT_e}{\mu_e} \right)^{\frac{1}{2}}$$

For particles of radius $.1\mu$ (A-1) becomes:

$$(A\text{-}2)\quad \mathcal{N}_{e\text{-}gr} = 3.14 \times 10^{-10} N_{gr} \langle v \rangle$$

Intra-gas collisional rates may be expressed in the following forms employing results given by Allen (1963).

electron and electron or ion:

$$(A\text{-}3)\quad \mathcal{N}_{e\text{-}e,i} = 2.96 \times 10^{-6} \frac{N_e \langle v \rangle}{T_e^{\,2}}$$

The electron-electron and electron-ion rates are equal due to the assumption of a pure hydrogen gas.

electron-neutral:

$$(A\text{-}4)\quad \mathcal{N}_{e\text{-}N} = 6.13 \times 10^{-13} \frac{N_N \langle v \rangle}{T_e^{\frac{1}{2}}}$$

Evaluating (A-3, 4) for a temperature of 10000K and letting $N_e = .5N$ one has:

$$(A\text{-}5)\quad a\ \mathcal{N}_{e\text{-}e,i}\ 1.48 \times 10^{-14} N \langle v \rangle$$

$$b\ \mathcal{N}_{e\text{-}N} = 3.06 \times 10^{-15} N \langle v \rangle$$

Forming the ratios of gas interaction rates to the gas-grain interaction rate produces the following:

$$(A\text{-}6)\quad a\ \mathcal{N}_{e\text{-}e,i} / \mathcal{N}_{e\text{-}gr} = 4.7 \times 10^{-5} (N/N_{gr})$$

$$b\ \mathcal{N}_{e\text{-}N} / \mathcal{N}_{e\text{-}gr} = 9.75 \times 10^{-6} (N/N_{gr})$$

Letting $N/N_{gr} = 10^{9.4}$ one has

$$(A\text{-}7)\quad a\ \mathcal{N}_{e\text{-}e,i} / \mathcal{N}_{e\text{-}gr} = 1.2 \times 10^{5}$$

$$b\ \mathcal{N}_{e\text{-}N} / \mathcal{N}_{e\text{-}gr} = 2.4 \times 10^{4}$$

One sees that intra-gas collisions are far more numerous than gas-grain collisions and therefore a maxwellian distribution will be maintained. It is also noted the rate ratios increase as temperature decreases. The high collision rate between electrons and the other gas species assures equipartition of energy and validates the assumption that heavy particles may be viewed as fixed.

APPENDIX B

DETERMINATION OF THE AMBIENT ELECTRON NUMBER DENSITY

The number density of electrons in the ambient gas may be ascertained in a manner consistent with the assumed processes of the model by considering equation (3-41) in a steady state, i.e.:

$$(B\text{-}1)\quad \frac{N_o N_e (N-N_e)}{T_o^{\frac{1}{2}}(N-N_o)} - \frac{N_e^2}{T_e^{\frac{1}{2}}} = 0$$

Defining N_e and T_e to be equilibrium values other than N_o and T_o which are to be specified, and letting

$$\Gamma \equiv \frac{N_o}{T_o^{\frac{1}{2}}(N-N_o)}, \text{ and } \chi = N_e/N$$

(B-1) may be rewritten as:

$$(B\text{-}2)\quad \Gamma\chi(1-\chi) = \chi^2/T_e^{\frac{1}{2}}$$

Rearranging:

$$(B\text{-}3)\quad \chi^2\left(\frac{1+T_e^{\frac{1}{2}}\Gamma}{T_e^{\frac{1}{2}}}\right) - \Gamma\chi = 0$$

or upon substitution for Γ and subsequent cancellation:

$$(B\text{-}4)\quad \chi = \left(\left(\frac{T_o}{T_e}\right)^{\frac{1}{2}}\left(\frac{1}{\chi_o} - 1\right) + 1\right)^{-1} \qquad \text{where } \chi_o = N_o/N$$

From this one may immediately write

$$N_e = \chi N$$

The values of T_o and χ_o needed to calibrate (B-4) were taken from the model of the solar chromosphere given by Allen (1963).

APPENDIX C

GLOSSARY OF SYMBOLS

a	grain radius
a_o	grain cross section, πa^2
a_1	radiative ionization cross section of the first level of hydrogen
$B_\nu(T)$	Planck function
c	speed of light
c_1	$4\pi(L\text{-}GM)\mu_{gr}/a_o\lambda_g$
f	body force
$f(v)dv$	maxwellian velocity distribution
F	radiative flux, $\oint I\mu d\Omega$
G	gravitational constant
h	Planck's constant
H_ν	monochromatic first moment of the specific intensity, $\frac{1}{2}\oint I\mu d\mu$
I_ν	monochromatic specific radiation intensity
j_ν	monochromatic volume emission coefficient
J_ν	monochromatic mean specific intensity, $\frac{1}{2}\oint I d\mu$
k	Boltzman constant
K_ν	monochromatic second moment of the specific intensity, $\frac{1}{2}\oint I\mu^2 d\mu$
L	$L_* Q a_o / 4\pi c \mu_{gr}$
L_ν	$\chi_\nu / (\chi_\nu + \sigma_\nu)$
L_*	stellar luminosity
M	stellar mass

n	γ-1, $\gamma \equiv$ ratio of gas specific heats
N	proton and hydrogen atom number density
N_i	number density of the $i^{\underline{th}}$ species
P	gas pressure
Q_i	radiation cross section of the $i^{\underline{th}}$ type in units of the physical cross section
r	radial position
R	radial position
$R_{2/3}$	radial position of the $\tau = 2/3$ level
$\mathcal{R}$	radial position in units of stellar radii
S	adiabatic sound velocity
S_ν	monochromatic source function
t	time
T	temperature
T_e	gas kinetic temperature
T_G	internal grain temperature
T_o	a constant temperature
T_T	turbulent temperature, $\left(\frac{\mu_g V_T}{3k}\right)^{\frac{1}{2}}$
T_*	stellar effective temperature
V_i	velocity of particles of the $i^{\underline{th}}$ species
V_R	gas-grain relative velocity, $(V_{gr}-V_g)$
V_T	isotropic turbulent velocity
α	atomic absorption cross section
β_i	$4\pi\left(\frac{\mu_i}{2\pi k T_e}\right)^{3/2}$
δ	grain velocity correction distance
$\mathcal{E}$	average energy supplied to the gas per collisional ionization
$\mathcal{E}_o, \mathcal{E}_1$	integration step amplitude control coefficient
ζ	$1 - \frac{T}{\mu_g}\frac{d\mu_g}{dT}$

η	$6L_\nu h\nu^3/c^2$
θ	angular coordinate
κ_ν	monochromatic absorption opacity
λ	$\sqrt{3L}$
λ_o	rest wavelength
λ_i	mass loss rate of the $i^{\underline{th}}$ species
μ	COSθ
μ_i	mass of particles of the $i^{\underline{th}}$ species
μ_{go}	constant gas particle mass
ν	frequency
ν_o	rest frequency
ν_1	ionization frequency of the first hydrogen level, 1 Ryd/h
ν_p	frequency of a grain scattered photon
ν_{OBS}	frequency seen by an observer
ξ	$h\nu/kT_o$
ρ_i	mass density of the $i^{\underline{th}}$ species
ρ_{go}	constant gas density
σ	Stefan-Boltzman constant
σ_ν	monochromatic scattering opacity
σ_{Rn}	recombination cross section to level n
τ_ν	monochromatic optical depth, $\int N\alpha\, dR$
ϕ	constant
ϕ	angular coordinate
χ	percent ionization
ψ	constant
Ψ	$\frac{16\pi a_o}{c^2}\left(\frac{k^{1/3}}{2\pi\mu_e}\right)h\nu_1$
ω	incremental angle

REFERENCES

Abt, H. A., Dukes, R. J., and Weaver, B. W. 1969, Ap. J., 157, 717.

Adams, W. S., and MacCormack, E. 1935, Ap. J., 81, 119.

Allen, C. W. 1963, Astrophysical Quantities (London: University of London, The Athlone Press).

Athay, R. G., and Skumanich, A. 1968, Ap. J., 152, 141.

Athay, R. G., and Skumanich, A. 1968, The Structure of the Quiet Photosphere and Low Chromosphere, ed. C. de Jager (Cambridge: M.I.T. Press), Chap. 11.

Athay, R. G., and Thomas, R. N. 1956, Ap. J., 124, 586.

Athay, R. G., and Thomas, R. N. 1957, Ap. J. 125, 804.

Barlow, M. J. 1971, Nature, 232, 152.

Bidelman, W. D. 1954, Ap. J. Suppl., 1, 175.

Bidelman, W. D. 1964, Ap. J., 139, 405.

Bidelman, W. D., and Pyper, D. M. 1963, P.A.S.P., 75, 389.

Biermann, L., and Lüst, R. 1960, Stellar Atmospheres, ed. J. L. Greenstein (Chicago: University of Chicago Press), Chap. 6.

Brown, R. H. 1968, Annual Review of Astronomy and Astrophysics, 6, 13.

Capriotti, E. R. 1970, University of Ohio, Columbus (private communication).

Carbon, D. F. 1969, Theory and Observation of Normal Stellar Atmospheres, ed. O. Gingerich (Cambridge: M.I.T. Press).

Carbon, D. F. 1970, Smithsonian Institute, Cambridge (private communication).

Chaffee, F. H., and Rosendahl, J. D. 1967, K.P.N.O. 84-inch telescope coudé spectrograph user's manual.

Clerke, A., and Shane, R. 1948, M. N., 108, 117.

Deutsch, A. J. 1956, Ap. J., 123, 210.

Deutsch, A. J. 1960, Stellar Atmospheres, ed. J. L. Greenstein (Chicago: University of Chicago).

Deutsch, A. J. 1961, Sky and Telescope, 21, 261.

Dyck, H. M. 1970, 1971, Kitt Peak Nat'l Obs., Tucson (private communication).

Dyck, H. M., Forrest, W. J., Gillett, F. C., Stein, W. A., Gehrz, R. D., Woolf, N. J., and Shawl, S. J. 1971, Ap. J., 165, 57.

Dyck, H. M., and Jennings, M. C. 1971a, A. J., 76, 431.

Dyck, H. M., and Jennings, M. C. 1971b, Kitt Peak Nat'l. Obs., Tucson (unpublished data).

Dyck, H. M., and Johnson, H. R. 1969, Ap. J., 156, 389.

Dyck, H. M., Sandford, M. T., and Jennings, M. C. 1971, K.P.N.O. Contr., No. 554, 127.

Fix, J. D. 1970, Ap. J., 161, 359.

Fix, J. D. 1971, K.P.N.O. Contr., No. 554, 213.

Gaustad, J. E. 1963, Ap. J., 138, 1050.

Gehrz, R. D., Ney, E. P., and Strecker, D. W. 1970, Ap. J., 161, L219.

Gehrz, R. D., and Woolf, N. J. 1971, Ap. J., 165, 285.

Gehrz, R. D., Woolf, N. J., and Shawl, S. J. 1971, Ap. J., 165, 57.

Geisel, S. L. 1970, Ap. J. Letters, 161, L105.

Gezari, D. Y., Labeyrie, A., and Stachnik, R. V. 1972, Ap. J. Letters (to be published).

Gillett, F. C., Low, F. J., and Stein, W. A. 1968, Ap. J., 154, 677.

Gilman, R. C. 1969, Ap. J., 155, L185.

Giovanelli, R. G. 1948, Australian J. Sci. Res., 1, 275, 289, 305, 360.

Giovanelli, R. G. 1949, M. N., 109, 298.

Giovanelli, R. G. 1967, Solar Physics, ed. J. N. Xanthakils (New York: John Wiley and Sons).

Gratton, L. 1950, Ap. J., 111, 31.

Grigoryan, K. A. 1958, Soobshch. Byurakanskoi Observ., 25, 45.

Grigoryan, K. A. 1959a, Soobshch. Byurakanskoi Observ., 27, 43.

Grigoryan, K. A. 1959b, Soobshch. Byurakanskoi Observ., 27, 55.

Harris III, D. L., Strand, K. Aa., and Worley, C. E. 1963, Basic Astronomical Data, ed. K. Aa. Strand (Chicago: University of Chicago Press), Chap. 15.

Herbig, G. H. 1970, Mem. Soc. Roy. Sci. Liège, 19, 16.

Hoyle, F., and Wickramashinge, N. C. 1962, M.N.R.A.S., 124, 417.

Hossack, W. R. 1954, J.R.A.S.C., 48, 211.

Huang, S.-S., and Struve, O. 1960, Stellar Atmospheres, ed. J. L. Greenstein (Chicago: University of Chicago Press), Chap. 8.

Huffman, D. R. 1970, 1971, University of Arizona, Tucson (private communication).

Jefferies, J. T., and Thomas, R. N. 1959, Ap. J., 129, 401.

Jennings, M. C. 1969, 1970, University of Arizona, Tucson (unpublished data).

Jennings, M. C., and Abt, H. A. 1970, University of Arizona, Tucson (unpublished data).

Jennings, M. C., and Dyck, H. M. 1971a, A. J., 76, 40.

Jennings, M. C., and Dyck, H. M. 1971b, K.P.N.O. Contr., No. 554, 203.

Joy, A. H. 1942, Ap. J., 96, 344.

Joy, A. H. 1947, Ap. J., 106, 288.

Joy, A. H., and Wilson, R. E. 1949, Ap. J., 109, 141.

Kippenhahn, R., and Temesváry, S. 1958, Max Planck Institute, Munich (unpublished data).

Kruszewski, A., Gehrels, T., and Serkowski, K. 1968, A. J., 73, 677.

Low, F. J. 1965, I.A.U. Circ., No. 1884-5.

Low, F. J., and Johnson, H. L. 1964, Ap. J., 139, 435.

Mathews, W. G. 1969, Ap. J., 157, 583.

Matsushima, S. 1952, Ap. J., 115, 544.

Menzel, D. H. 1937, Ap. J., 85, 330.

Merrill, P. W. 1941, Ap. J., 93, 380.

Merrill, P. W. 1945, P.A.S.P., 57, 178.

Ney, E. P., and Allen, D. A. 1969, Ap. J., 155, L193.

Oster, L. 1971, Ap. J., 169, 57.

Osterbrock, D. 1961, Ap. J., 134, 347.

Parker, E. N. 1958, Ap. J., 128, 664.

Parker, E. N. 1960a, Ap. J., 132, 175.

Parker, E. N. 1960b, Ap. J., 132, 821.

Pease, F. G. 1931, Ergebn. Exacten. Naturwissen., 10, 84.

Roman, N. G. 1955, Ap. J. Suppl., 2, 195.

Roman, N. G. 1965, Galactic Structure, eds. A. Blaauw and Maarten Schmidt (Chicago: University of Chicago Press), Chap. 16.

Rubbra, F. T., and Cowling, T. G. 1959, Ninth International Astrophysical Symposium, Liège, p. 274.

Sabersky, R. H., and Acosta, A. J. 1964, Fluid Flow (New York: The Macmillan Company).

Schmidt-Kaler, Th. 1965, Landolt-Börnstein, ed. H. H. Voight (Berlin: Springer-Verlag).

Serkowski, K. 1965, Acta Astro., 15, 79.

Serkowski, K. 1966, Ap. J., 144, 857.

Serkowski, K. 1968, A. J., 73, 677.

Serkowski, K. 1969a, Ap. J. Letters, 156, L139.

Serkowski, K. 1969b, Ap. J. Letters, 158, L107.

Shakhovskoi, N. M. 1963, Astron. Zh., 40, 1055.

Shawl, S. J. 1972, unpublished dissertation, University of Texas.

Spitzer, Jr., L. 1948, Ap. J., 107, 6.

Stein, W. A., and Gillett, F. C. 1969, Ap. J., 155, L197.

Thomas, R. N. 1948, Ap. J., 108, 142.

Thomas, R. N. 1949, Ap. J., 109, 480, 500.

Underhill, A. B. 1971 (announcement of the Goddard Space Flight Center Conference on Stellar Chromospheres).

Van de Hulst, H. C. 1957, Light Scattering by Small Particles (New York: John Wiley and Sons).

Vardanyan, R. A. 1960, Soobshch. Byurakanskoi Observ., 28, 9.

Weymann, R. 1960, Ap. J., 132, 380.

Weymann, R. 1962a, Ap. J., 136, 844.

Weymann, R. 1962b, Ap. J., 136, 476.

Weymann, R. 1971, University of Arizona, Tucson (private communication).

Weymann, R., and Chapman, G. 1965, Ap. J., 142, 1268.

Wickramashinge, N. C. 1970, Publ. Astr. Soc. Japan, 22, 85.

Wildey, R. L., and Murray, B. C. 1964, Ap. J., 139, 435.

Williams, R. E. 1970, University of Arizona, Tucson (unpublished lecture notes).

Wilson, O. C., and Bappu, M.K.V. 1957, Ap. J., 125, 661.

Woolf, N. J., and Ney, E. P. 1969, Ap. J., Letters, 155, L181.

Woolf, N. J. 1971, K.P.N.O. Contr. No. 554, 187.

Zappala, R. R. 1969, P.A.S.P., 81, 433.